# CARBIDE FORMATION ON CARBON STEELS IN $CO_2$ CORROSION BY USE OF APPLIED ANODIC CURRENT

Master Thesis

by

Nushjarin Laethaisong

University of Stavanger

June, 2011

University of Stavanger

**Faculty of Science and Technology**

# MASTER'S THESIS

| | |
|---|---|
| Study program/ Specialization:<br>MSc in environmental technology/<br>Specialization in offshore environmental engineering | Spring semester, 2011<br><br>Open / ~~Restricted access~~ |
| Writer: Nushjarin Laethaisong | ……<br>(Writer's signature) |
| Faculty supervisor: Tor Hemmingsen<br><br>External supervisor(s): | |
| Title of thesis: Carbide formation on carbon steels in $CO_2$ corrosion by use of applied anodic current | |
| Credits (ECTS): 30 | |
| Key words:<br>carbide, carbon steel, X-65, St52, Steel33, anodic current, $CO_2$ corrosion | Pages: ……86……<br><br>+ enclosure: …2CDs.……<br><br>Stavanger, 15.06.11<br>Date/year |

## ABSTRACT

The present study aims to validate the method in enriching of iron carbide surface from carbon steels in $CO_2$ corrosion. Applying an anodic current to carbon steel electrodes by galvanostatic measurement was a selected approach. Influence of magnitude of the applied current and exposure time on the corrosion process was studied. The experiments were conducted with $CO_2$-saturated-0.5M NaCl solution as an electrolyte at room temperature and atmospheric pressure. Three different steels, X-65, St52 and Steel33, are used as materials. The corrosion behavior is monitored by weight loss measurement and potentiodynamic sweep, while steel surfaces are examined by SEM/EDS technique. The results show that carbide formation as the weight losses increased with the applied currents and the exposure time. The iron carbide was detected on steel surfaces and iron carbonate was observed on the steel surface which was applied with the highest current density. However, the effect of steel's microstructure and composition on the corrosion cannot be identified clearly.

## ACKNOWLEDGEMENT

My master thesis could not be completed without my supervisor, Tor Hemmingsen, who gave me an opportunity to do this study. I wish to thank him for his great contribution and motivation since the beginning until the end of the project.

A very special recognition is given to Marion Seiersten and Tonje Bernsten for valuable advices and support throughout the study.

My thanks also go to all laboratory staffs that provided me necessary assistance, equipment and materials. I also would like to thank Institute for Energy Technology (IFE) for carbon steels used in the experiments and conducting SEM analysis of my samples.

I am grateful to all labmates who shared their experience and assisted me in any respect during the whole process of the study. I would also like to express my warmest thanks to all my friends in Thailand and Norway for their moral support and standing by my side.

Lastly, I owe my deepest gratitude to my father and mother for their unconditional love and powerful encouragement.

Nushjarin Laethaisong

## TABLE OF CONTENTS

## LIST OF FIGURES

## LIST OF TABLES

# 1 INTRODUCTION

Corrosion issues have been concerned for many decades since they have been important causes of failure in equipment and structure made of metal. In oil and gas industry, the corrosion problems are generally found in pipelines, storage tanks and other equipment which have to operate with corrosive materials. Due to large effects on the operation, therefore, there are many studies and researches dedicating to these problems. Their investigations aim to uncover mechanisms and factors associating in the corrosion process. Many models have been developed in order to predict the most accurate corrosion mechanisms [1-3]. The main objectives are not only to understand the phenomenon, but also to formulate effective countermeasure and protection.

Carbon steel is a material that has been widely used in various engineering applications due to its low cost, good mechanical properties, and simple fabrication. Thanks to large applications, the corrosion of carbon steels under different conditions has been continuously studied by many researchers and working groups. One condition of interest is the corrosion in $CO_2$ environment, which is also called sweet corrosion. It is one of major and costly corrosion problem in oil and gas industry in which fluids containing dissolved $CO_2$ are dealt with.

In the process of $CO_2$ corrosion, one of very important subjects is corrosion products or corrosion films. The corrosion films have significant effects on the corrosion mechanisms once they are formed. For carbon steel, iron carbide ($Fe_3C$) and iron carbonate ($FeCO_3$) are key compounds in the corrosion layers. Their mixed films possess different properties which depend on many factors, e.g. temperature, composition and micro structure of the metal substrate. The combination of the iron carbide and the iron carbonate films significantly influence corrosion rate in both positive and negative ways. This leads to difficulties in prediction of the mechanisms of corrosion. Thus, the characteristics of $CO_2$ corrosion films of the carbon steel are currently one of attractive area for corrosion researchers.

However, many studies focus on the formation of iron carbonate film and combination film of the iron carbide and the iron carbonate, not only the carbide layer. Some investigate the carbide film as pre-corrosion for further study on corrosion inhibitor performance [4, 5]. Therefore, iron carbide is of interest in the current study as it is the main corrosion product and, moreover, the carbide has an

important role in enhancing the protectiveness of the corrosion films under $CO_2$ environment even though the carbide itself is found non-protective [1, 2, 4-6].

In the present study, accelerating the corrosion process to obtain iron carbide is of interest. It is initiated from the real condition where the process forming $Fe_3C$ layer on the corroded surface consumes some time. Hence, provoking the corrosion will reduce the time in corrosion researches. Consequently, it could be a supplement for studying the corrosion films and also other investigation where the corroded carbon steel surface is required.

## 2 LITERATURE REVIEW

In $CO_2$-containing environment, corrosion process of carbon steels produces corrosion layers on steel surface. These corrosion films have major effects on corrosion mechanisms. Depending on composition, location and structure of the films, they can increase or decrease corrosion rate. Complication in film properties results in difficulties of the corrosion rate prediction. Moreover, many other environmental factors, e.g. temperature, metal composition, $CO_2$ partial pressure, flowrate and pH of electrolyte, could also affect the formation of corrosion product layers [6, 7].

### 2.1 $CO_2$ Corrosion Mechanism

The process of corrosion consists of many electrochemical reactions at the metal surface and transportation of chemical species in the system [2]. The reactions include transportation of mass and charge [8]. The mass transportation occurs between metal surface and an electrolyte while the charge is transferred between atoms and ions.

In $CO_2$ Corrosion, carbonic acid is produced when dissolved $CO_2$ combines with water as shown in the reaction below.

$$CO_2 + H_2O = H_2CO_3 \quad (1)$$

The process then is governed by the following cathodic and anodic reactions [1]. In the electrolyte, the cathodic reactions are from dissociation of the carbonic acid:

$$2H_2CO_3 + 2e^- = H_2 + 2HCO_3^- \quad (2)$$

$$2HCO_3^- + 2e^- = H_2 + 2CO_3^{2-} \quad (3)$$

The anodic reaction at the metal surface generates $Fe^{2+}$ and $e^-$ from an electrochemical dissolution:

$$Fe = Fe^{2+} + 2e^- \quad (4)$$

Hydrogen gas is produced by hydrogen evolution reaction.

$$2H^+ + 2e^- = H_2 \quad (5)$$

Thus, the overall reaction of $CO_2$ corrosion is:

$$Fe + H_2CO_3 = FeCO_3 + H_2 \quad (6)$$

## 2.2 Corrosion Product Film

One important process in $CO_2$ corrosion is the corrosion film formation since it governs the corrosion mechanisms and the corrosion rate. There are four types of main corrosion product layers formed in $CO_2$ corrosion at temperature ranging from $5^oC$ to $150^oC$. Four types of the mentioned layers are (1) transparent films, (2) iron carbide film, (3) iron carbonate film, and (4) iron carbonate plus iron carbide film [9].

### 2.2.1 Transparent Film

Transparent film can be observed at around room temperature. Without carbonate, it consists of iron and oxygen ions and has thickness less than 1 μm. Its protectiveness is improved by increasing concentration of the ferrous ions. However, this layer is not important and normally ignored. It has not been identified clearly whether it affects on the formation of the other type of the corrosion films [9].

### 2.2.2 Iron Carbide Film($Fe_3C$)

Iron carbide, which is also known as “cementite”, contains 6.67%C (by weight) and has chemical composition of $Fe_3C$. Like austenite, ferrite, and perlite, iron carbide is one of constituents in the carbon steels. This microstructure is obtained during heat treatment in steel manufacture. In the corrosion process, the iron carbide

is simply generated by the anodic dissolution when the dissolved ferrous ions are dissociated and the uncorroded iron carbide is left remaining on steel surfaces. Figure 2.1 is a scheme of the corrosion reactions of carbon steels in acid. The letter “A” and “C” in the figure denotes to anode and cathode, respectively.

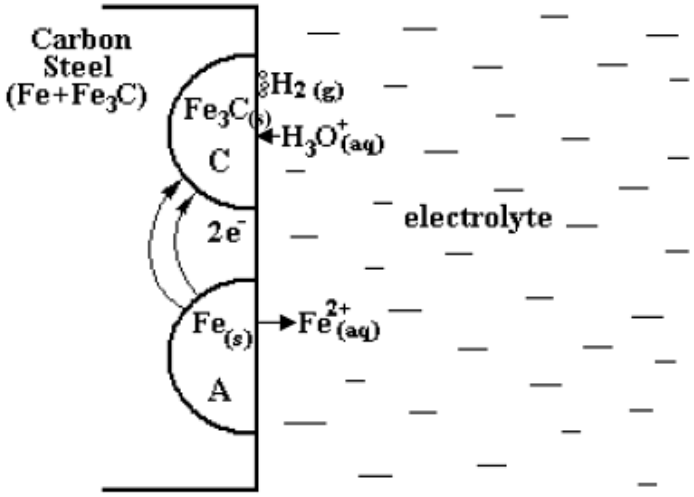


**FIGURE 2.1** Corrosion of carbon steel in acidic solutions [10]

Once the carbon steels are corroded in acid, black deposit can be observed on the steel surfaces. The carbon powder is generated following a reaction in equation (7) shown below [10]. Figure 2.2 also shows a high-resolution image of the carbide layer.

$$Fe_3C_{(s)} + 6H_3O^+_{(aq)} = 3Fe^{2+}_{(aq)} + C_{(s)} + 3H_{2(g)} + 6H_2O_{(l)} \qquad (7)$$

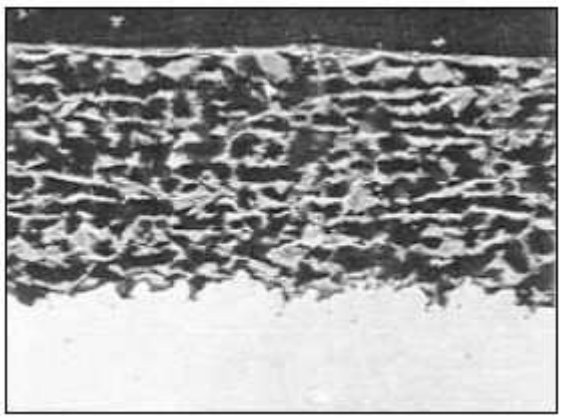

**FIGURE 2.2** A pure iron carbide layer formed at 60°C and 1 to 3 times supersaturation [9]

The iron carbide is stable structure which is uncorroded and undeformable. It is porous and brittle, however, it can form a strong network on the steel surface [9]. The iron carbide structure depends upon chemical composition and microstructure of carbon steel. Ueda and Takabe [11] found that after ferritic-pearlitic microstructure steel is corroded lamellar cementite is left behind while dispersed-cementite is found in martensitic microstructure steel. The difference of carbide structures varies the anchor property of the corrosion product. The carbon steel with dispersed-carbide undergoes more severe corrosion when compared to the carbon steel with lamellar carbide structure. It is because the structure of lamellar carbide has the cavities, which more efficiently carry the corrosion products. This characteristic of the carbide layer, thus, enhances stability of the corrosion film.

However, the cementite is found metallic conductive, therefore, it is considered non-protective when it attaches directly to the metal surface. There are many studies working on the effects of the iron carbide on the corrosion rate [4, 9, 11-13]. It was found that iron carbide film formed on the steel surface promotes the corrosion process by following approaches [9]:

- Galvanic effect: The $Fe_3C$ structure provides cathodic area to the steel surfaces due to lower overpotential of $Fe_3C$ compared to the carbon steel structure or ferrite. As shown in Figure 2.1, an iron acts as an anode while $Fe_3C$ is a cathode. This condition enhances further iron dissolution by accelerating the cathodic reactions.
- Local acidification: When the cathodic reactions take place, water composition at cathodic and anodic regions will become more alkaline and acidic, respectively. As a sequence, internal localized acidification will occur at the steel surface and accelerate the corrosion process.

Apart from the increase in the corrosion rate, the iron carbide also has an effect on performance of corrosion inhibitor applied to the carbon steels. It was reported that the longer precorrosion time results in the thicker of iron carbide layer. Consequently, the thickness of iron carbide scales impaired the inhibitor performance

[4, 5]. The reason is that the iron carbide layer acts as a barrier preventing the transportation of the inhibitor to the active steel surfaces.

### 2.2.3 Iron Carbonate Film ($FeCO_3$)

Iron carbonate or siderite film is formed by $FeCO_3$ precipitation when $Fe^{2+}$ and $CO_3^{2-}$ concentrations are higher than solubility limit. As a result, the products from the cathodic (2), (3) and anodic (4) reactions form the iron carbonate film by precipitation. The chemical reactions forming the carbonate film follows.

$$Fe^{2+} + CO_3^{2-} = FeCO_3 \quad (8)$$

$$Fe^{2+} + 2HCO_3^{-} = Fe(HCO_3)_2 \quad (9)$$

$$Fe(HCO_3)_2 = FeCO_3 + CO_2 + H_2O \quad (10)$$

The film is developed by two processes; nucleation and crystallization or partial growth [1]. Firstly, the nucleation process occurs on the metal surface or in the microstructure of an existing layer. Then the film thickness increases by the crystallization process. During the precipitation of iron carbonate scale, the corrosion process still carries on simultaneously. If the precipitation rate is equal or higher than the corrosion rate, the corrosion film will be compact and have the protective property. On the other hand, if the precipitation is slower than the corrosion, the film will be porous and found unprotective [3].

Precipitation of $FeCO_3$ is influenced by many factors such as temperature, pH, $Fe^{2+}$ concentration, $CO_2$ partial pressure, and $H_2S$ effect [3, 5, 9].

- Temperature: Temperature has an effect on the film formation since kinetics of the precipitation is accelerated by increasing the temperature. The results of many studies show that precipitation of iron carbonate increases with temperature at higher than $60^oC$. Furthermore, the protection level of the film

is also improved at this temperature. In addition, morphology of the film is also affected by the temperature.

- pH: Solubility of iron carbonate is greatly affected by pH. The $FeCO_3$ solubility decreases with increasing pH. Therefore, at high pH of the electrolyte, the precipitation occurs easier and the protective film can be formed.
- $Fe^{2+}$ concentration: Ferrous ions concentration affects the precipitation as mentioned earlier that $FeCO_3$ is formed by precipitation of $Fe^{2+}$ and $CO_3^{2-}$ when their concentrations exceeds the solubility limit. Low level of $Fe^{2+}$ concentration will prevent the iron carbonate formation and sometimes dissolve the existing film.
- $CO_2$ partial pressure: In the beginning of the corrosion, when there is no film formed, corrosion rate increases with $CO_2$ partial pressure. Nevertheless, the film is produced faster at higher $CO_2$ partial pressure.
- $H_2S$ effect: FeS and $Fe_2S$ are produced if the corrosion environment contains both $H_2S$ and $CO_2$ and it also depends on the $H_2S$ partial pressure. Some studies have reported that the sulfide layer is more protective than the carbonate. Conversely, less protective is found at low $H_2S$ concentration when a combination has the $FeCO_3$ at the inner part while the outer is sulfide.

As mentioned above, the formation of iron carbonate film consists of main two processes, nucleation and crystal growth. It was discovered by Gao M. et al [6] that the crystal growth step controls the formation of the films when the relative supersaturation of $FeCO_3$ is low in the initial stage. On the other hand, nucleation is dominant at high supersaturation of the $FeCO_3$. This condition develops the dense films which improve the protectiveness of the corrosion films.

The iron carbonate is adherent, protective and non-conductive. Its protectiveness is affected by the temperature and pH [9]. Increasing temperature and/or pH will improve the protection characteristic and also adhesion and hardness of the iron carbonate film. At higher temperature, the more protective film is obtained.

Nevertheless, there is a proper temperature range reported, for instance, the films are protective when the temperature is higher than 70$^{o}$C, and the performance and adhesion are improved when $CO_2$ partial pressure exceeds 10 bar. The protection level of the iron carbonate increases proportionally to the exposure time. Beside, the adhesion property and thickness is also influenced by the metal composition and microstructure [7, 9]. The large crystal structures provide the dense film which improves the film adherence.

After $FeCO_3$ precipitation carries on the surface of the steels, and then the protective film is formed. This layer acts as a barrier between the steel surfaces and the corrosive species. This barrier prevents any substances associated in the corrosion reactions transporting to the active metal surfaces. Once this film covers the active area on the surface, the electrochemical activities are limited. Thus, this mechanism leads to decrease in corrosion rate.

### 2.2.4 Iron Carbonate plus Iron Carbide Film

Many studies of corrosion layers [9, 12] discovered that the uncorroded cementite formed the non-protective film if it directly attached to the metal surfaces. Nevertheless, if the pores in its porous structure were sealed with the iron carbonate, it could form the protective film.

As mentioned previously, when the condition in $CO_2$ corrosion is proper, the iron carbide and iron carbonate scales will be generated. They can settle on the steel surfaces as separate layers or they could be partially combined. The approach that the mixed films are constructed depends on where and when the iron carbonate is formed [9]. The structure of the mixed film greatly influences the properties, particularly the protectiveness of the films.

For the first case, the iron carbide accumulates forming the layer directly on the steel surface and followed by precipitation of carbonate scales on the top. This structure leads to the formation of non-protective layer. The second case is when the porous iron carbide is filled up with the iron carbonate scales. This kind of film is still able to keep its protectiveness. Figure 2.3 shows the morphologies of the protective and non-protective films.

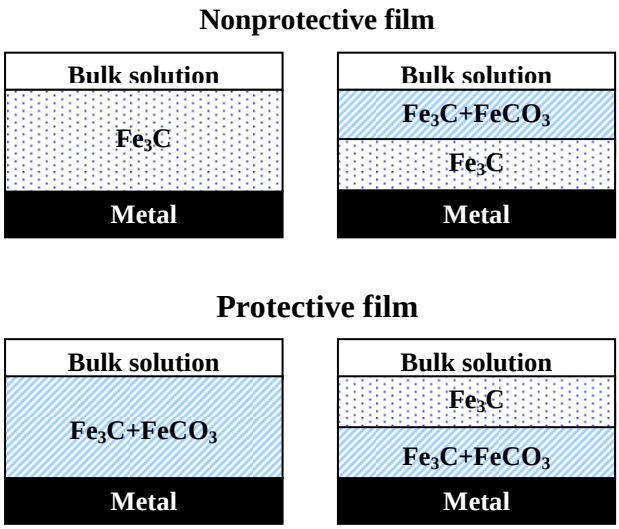


**FIGURE 2.3** Morphologies of protective and non-protective corrosion layers [12]

Development and breakdown of carbonate film are affected by the structure of the $Fe_3C$ and $FeCO_3$ combination. A important factor is the microstructure of the carbon steel which is influenced by carbon content and distribution of cementite [11].

To improve the protectiveness of the corrosion product films, the carbide is one important part. Even though the $Fe_3C$ is non-protective, but it physically enhances the adhesion of the carbonate film to the steel surface by the anchor effect. The anchoring by the iron carbide helps the iron carbonate to resist shear force under high-flowrate condition. Beside, the iron dissolution under the carbide layer provides high $Fe^{2+}$ concentration gradient at the metal surface. This high concentration gradient increases the supersaturation of $Fe^{2+}$ on the surface and leads to generating more protective iron carbonate film [9].

## 2.3 Accelerating Corrosion Process

It is apparently seen that the iron carbide plays an important role in the $CO_2$ corrosion. It particularly affects on the protectiveness of the corrosion film. However, there are only few researches focusing on the iron carbide formation in the corrosion process. Corroding the carbon steel to gain the iron carbide is often carried as a precorrosion step prior to studying the formation of protective films. In other case, it was conducted to provide partially corroded surface for a particular test, which

requires the surface with some scales as exists in the real situation. Some studies contributed to an investigation of inhibitor performance on the steel surface which is covered by the corrosion scales. For instance, Gulbrandsen E. et al. investigated the effects of precorrosion on the film formation and inhibition [4]. Nevertheless, those studies have not focused on the process of the iron carbide layer is generated.

As described previously, the iron carbide can be simply obtained by allowing the carbon steel to be corroded, though; this process consumes quite long time. In the experiments of Gulbrandsen E. et al [4], they precorroded X-65 and St52 without applying external current density for 14 days and no iron carbonate was observed. Therefore, it will be more practical to prepare the precorroded steel in shorter period by accelerating the corrosion process to gain the iron carbide scales for further study. There are many factors are found able to accelerate the corrosion mechanisms i.e. pH and temperature. However, in the present study, the influence of applied current density, exposure time and steel composition are focused on.

### 2.3.1 Effects of Applied Current on the Corrosion

In order to accelerate the corrosion, applying anodic current density is considered as one alternative rather than changing the corrosion environment. According to Pourbaix diagram, pH and potential correlation of iron-water system provides a region where the iron dissolution or corrosion can take place.

Pourbaix diagram, also called pH-potential diagram, in Figure2.4 shows the dominant species in the domains of iron-water system at 25$^{o}$C. Following the solid curves on the left hand-side, ferrous ions can be generated or the corrosion takes place. Iron in the immunity area (Fe) will be dissolved and generate ferrous ions in corrosion area ($Fe^{2+}$) by increasing potential at pH below 9. Even though the diagram can provide conception of kinetic process, but it does not give the information about the corrosion rate of the iron. In addition, the other limitation of Pourbaix diagram is that the other ionic species in the solution are not covered in the diagram. However, this principle introduces to the stimulation of corrosion mechanism by increasing the applied potential. Alternatively, the anodic current could be applied so as to accelerate the iron dissolution.

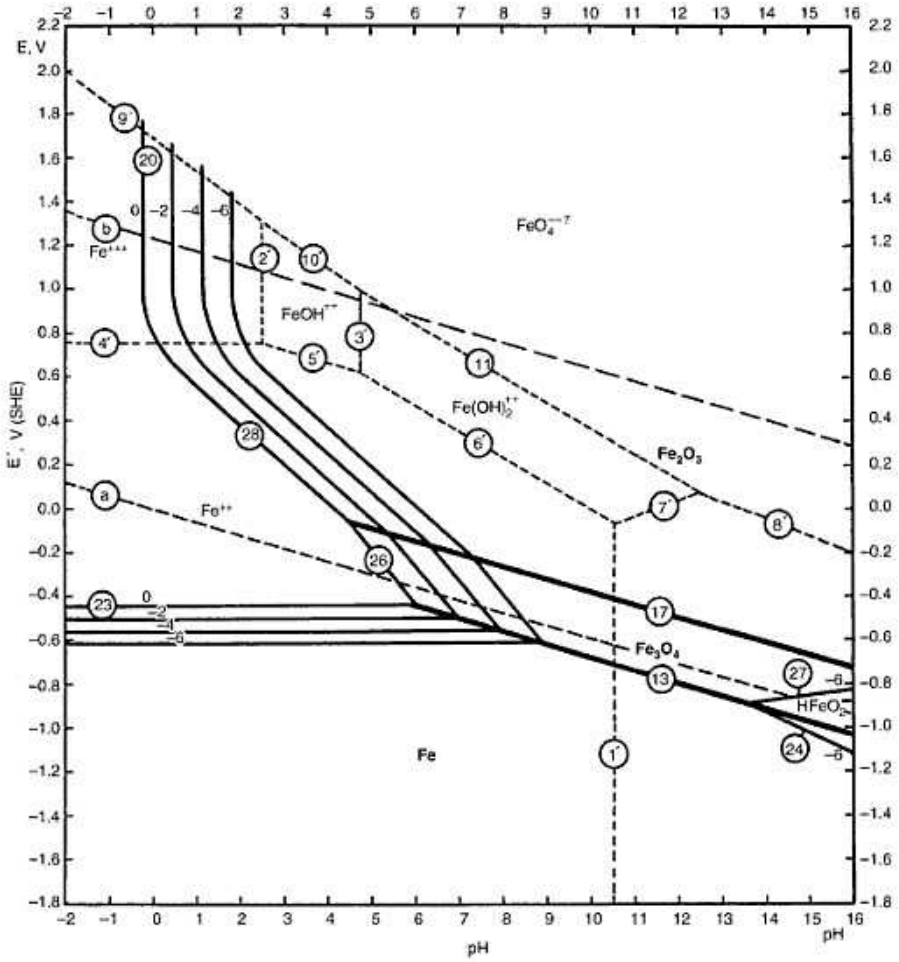


**FIGURE 2.4** Potential-pH Equilibrium Diagram for the System Iron-Water, at 25°C (considering as solid substances only Fe, $Fe_3O_4$ and $Fe_2O_3$)[14]

With this approach, Muralidharan, et al. [15] studied the effects of applying currents on the corrosion rate of mild steel. The investigation was conducted by applying alternating (AC), direct (DC) and superimposed alternating and direct (AC+DC) currents to the steels. The results revealed that applying the currents to the mild steel in marine environments caused an increase in the corrosion rates. They also found that the highest corrosion rate of the steel was obtained when the superimposed current was applied. The lower and the lowest corrosion rate were observed when applying DC and AC, respectively.

Focusing on the DC source, the study of Muralidharan, et al. found that the DC current is able to accelerate the corrosion at low current density even lower than $i_{corr}$. There are two approaches to accelerate the corrosion process as shown in the following equations [15].

First mechanism:

$$Fe + H_2O = Fe.H_2O_{ads} \quad (11)$$

$$Fe.H_2O_{ads} + Cl^- = FeCl^-_{ads} + H_2O \quad (12)$$

$$FeCl^-_{ads} + OH^- = FeOH^+ + Cl^- + 2e^- \quad (13)$$

$$FeOH^+ + H^+ = Fe^{2+} + 2e^- \quad (14)$$

Second mechanism:

$$Fe + Cl^- = FeCl^-_{ads} \quad (15)$$

$$FeCl^-_{ads} + H_2O = FeOH^-_{ads} + H^+ + Cl^- \quad (16)$$

$$FeOH^-_{ads} = FeOH_{ads} + e^- \quad (17)$$

$$FeOH_{ads} = FeOH^+_{ads} + e^- \quad (18)$$

$$FeOH^+_{ads} = Fe^{2+} + OH^- \quad (19)$$

### 2.3.2 Effect of Exposure Time on the Corrosion

In Gulbrandsen E. et al. [4] , it reported that the corrosion rate of the carbon steels increased proportionally to the exposure period during the pre-corrosion. This increasing corrosion rate can be explained by many reasons which are (1) protective oxide film removal (2) galvanic coupling between cementite and steel surface (3) true surface area of the specimen increase (4) acidification under the corrosion film. These conditions can be promoted by the accumulation of the iron carbide on the steel surfaces. The accumulation increases the area of $Fe_3C$ resulting to increasing the corrosion rate [16].

### 2.3.3 Effect of Composition and Structure of Carbon Steel on $CO_2$ Corrosion

The effects of composition and microstructure on $CO_2$ corrosion are found in many researches. However, it is surprising that the general conclusion cannot be drawn as many studies still have conflicts in results [17]. Some carbon steels have the same composition, but their microstructure is different. In contrast, the steels with the same microstructure can be gained from different composition. Furthermore, large variation in corrosion behavior could be observed from the carbon steels that have the same composition and microstructure under the same corrosive conditions.

*Composition of Steel*

Carbon steels are defined as low-alloy steels. An alloying elements added, as a definition of carbon steel, should not be more than 2%wt of the total additions [10, 18]. This results to insignificant difference in corrosion rate of the most grades of the carbon steels [18, 19]. However, alloying elements are found to have effects and make some changes in steel properties. The elements which are generally added and affect the corrosion behavior on the carbon steels are chromium, copper, nickel, sulfur, phosphorus and manganese. Here below are briefs of the effects of some alloying elements on the corrosion performance.

- Carbon: Carbon is added to an iron in order to improve the mechanical properties. It is dissolved and mixed with the iron, forming iron carbide. Gulbrandsen E. et al. [4] found that during the precorrosion without applying current at room temperature, the corrosion rate of the carbon steel increased due to the increase in cathodic sites. Those increasing active areas were from the remaining of iron carbide layer after the steel corroded. In addition, more amount of cementite was observed on St52 steel surface than X-65 which has lower carbon content. The other research also found that the corrosion rate in CO2 corrosion of the carbon steels increased with the carbon content [20]. Figure 2.5 below shows the effect of carbon content on the corrosion rates.

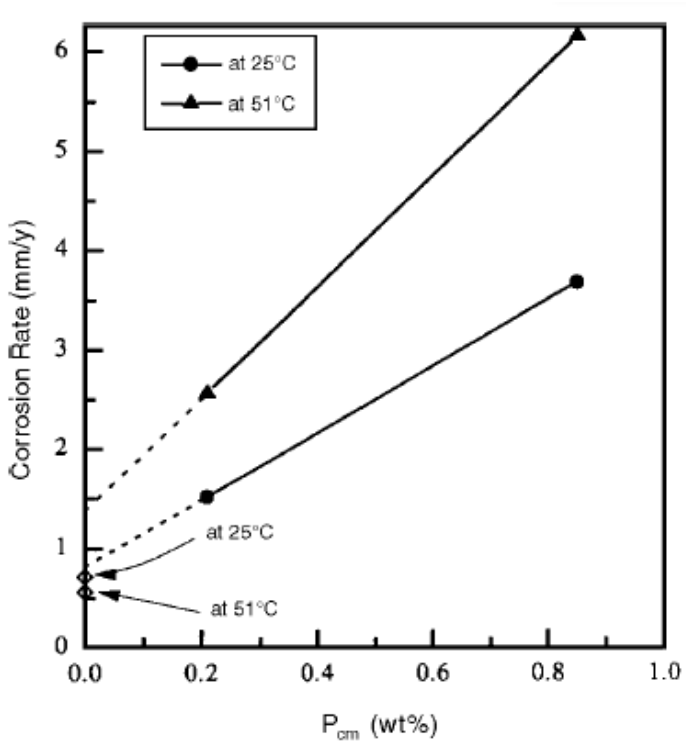


**FIGURE 2.5** Effect of carbon content on corrosion rates [20]

- Chromium: Chromium is a very important alloying element used to improve corrosion resistance by increasing protectiveness of the corrosion film [13]. It is a major element which is focused to reduce the corrosion rate in many studies. Depending on the amount added to the steel, chromium can combine with iron and form double carbide [$Fe.Cr_3)_3C$] or carbide of chromium ($Cr_7C_3$ or $Cr_{23}C_6$). Chromium carbide has properties in amend for hardness, tensile strength, wear resistance and heat resistance [21]. The corrosion rate can be reduced by the addition of chromium since it forms the passive film and decrease the anodic dissolution rate. Moreover, the chromium lowered the corrosion rate by protecting the alloy and preventing $Fe_3C$ formation [20]. It is found in many studies that the corrosion rate decreased with the addition of chromium [13, 20, 22]. The effect of Cr can be seen in Figure 2.6.

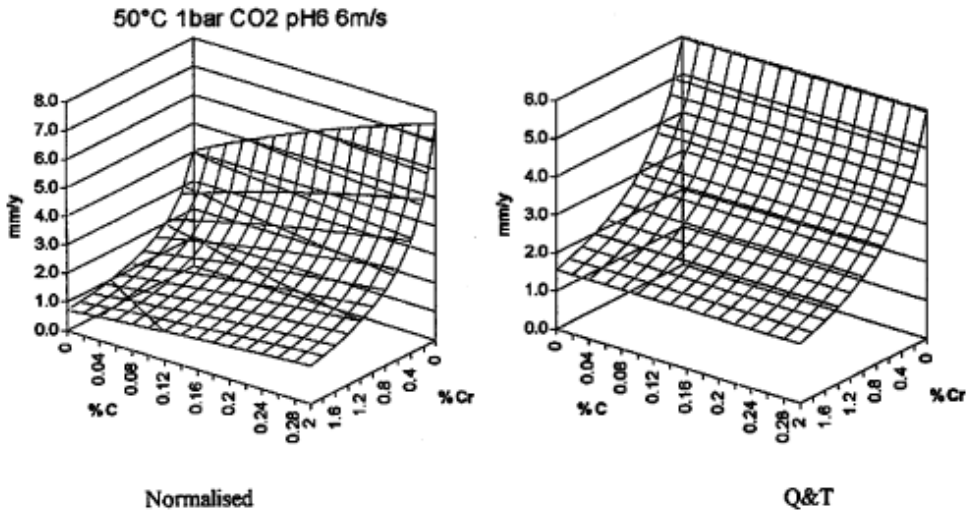


**FIGURE 2.6** Effect of composition of low alloy steels on corrosion rate [17]

- Copper: Copper is added in order to improve atmospheric-corrosion resistance. It is normally added to structural steels. Copper will not affect the mechanical properties if it is added not more than 0.6% [21] .
- Nickel: Nickel is also normally added to the structural steels because it enhances the mechanical properties without decrease in ductility. Furthermore, the corrosion and oxidation resistances are improved by adding nickel higher than 5% [21].

  However, there is a study that reported disagreement on addition of Cu and Ni. It was found that mesa attack and general corrosion can be accelerated by increasing the content of Cu and Ni [22].
- Sulfur and Phosphorus: Sulfur and phosphorus are normal components in commercial steels. They increase the rate of the corrosion, particularly in acidic solutions. It is because they form compounds with low potentials. For mild steels at neutral pH, sulfide compound also serves as a site for pitting corrosion to initiate. However, there is no marked effects from sulfur content noticed when the steels contains copper more than 0.01% [23].
- Manganese: The corrosion rate in acid can be reduced by adding manganese to the steels containing low sulfur content. Manganese recovers the anodic

polarization lowered by the sulfur since MnS has lower electrical conductivity than FeS [23].

Other alloying elements and their effects on the corrosion rate are shown in Figure 2.7.

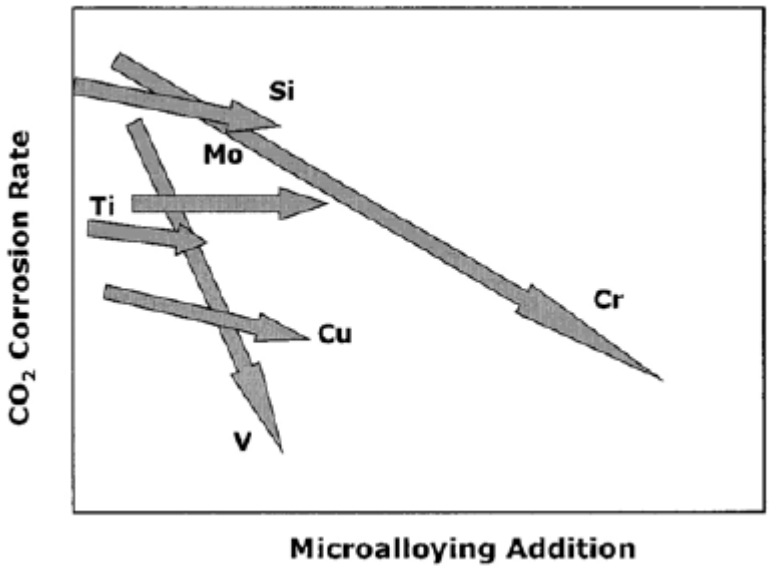


**FIGURE 2.7** Effects of alloying elements on corrosion rate of 3%Cr Steels [22]

However, it cannot be clearly identified that how corrosion behavior of carbon steels changes by adding the alloying element. It is because the effects of alloying also depend on the corrosion environments and the combination effects of all elements. The corrosion performance can not be concluded as a function of only one added element.

*Structure*

Apart of compositions, structure of the steels also affects on the $CO_2$ corrosion, particularly the morphology of the corrosion product films [13]. Difference in microstructure of the steels is obtained from steel manufacturing by different heat treatments. For instance, cooling slowly will combine the cementite with the ferrite and form a mixture called pearlite [19].

The structure of carbide layers strongly depends on the microstructure of the parental steels. It is reported by Ueda M. and Takabe H. that the steel with ferritic-

pearlitic structure gave the lamellar carbide layer. On the other hand, the martensitic-structure steels provided disperse-cementite after they were corroded [11].

The adhesion of the mixed films, iron carbide and iron carbonate inclusion, is also influenced by the microstructure of the steels. For example, ferritic-pearlitic steels provided porous carbide on the corroded steel surface [24]. This structure helps anchoring the iron carbonate to the steel surface forming protective corrosion films.

Considering the corrosion rate, there are some researches studying the corrosion reactions of different steel microstucture. Some reported that the ferritic-pearlitic aturcture is more resistant to the corrosion than martensitic [17], however, the opposite results of the ferritic-pearlitic are also found [25]

Nevertheless, the effects of microstructure and composition sometimes depend on certain condition. It was found that the effect microstructure is significant at high temperature. St52 microstructure effect increased with temperature from 25$^{o}$C to 51$^{o}$C [20]. In addition, the literature revealed that chromium addition improved the corrosion performance rather than the microstructure [17]. Therefore, the influence of microstructure and composition of the carbon steels on the corrosion process still remains complicated and should be investigated in more detail.

## 2.4 Corrosion Testing and Monitoring

Nowadays many techniques are established to investigate the corrosion behavior including the characteristics of corrosion product films and the corrosion rate. The commonly used, for example, are corrosion potential, weight loss measurement, potentidynamic polarization and scanning electron microscope (SEM), While SEM is the method to observe the corrosion products appearance, weight loss measurement and potentiodynamic sweep are the electrochemical techniques used to monitor and determine the corrosion rate for many studies[4-7, 26]. In addition, for the present study, galvanostatic polarization is used to stimulate the corrosion process by applying the anodic current to the tested electrodes.

### 2.4.1 Corrosion Potential Measurement

Corrosion potential ($E_{corr}$) technique is the measurement of the voltage of corroding metal surface with respect to the reference electrode at open circuit. Corrosion potential, on the other hand, is the potential where the oxidation and the reduction reactions have the same rates without applying external current. Corrosion potential is an important indicator of corrosion status since it shows the changes of free-corrosion potential over time; however, it doesn't provide any information about the corrosion rate. Nevertheless, it is suggestive that specimen having more negative potential is more sensitive to corrosion or has more corrosivity. In addition, corrosion potential measurement can be conducted in order to ensure that the potential reaches steady-state condition.

### 2.4.2 Galvanostatic Polarization

In galvanostatic polarization, current density applied to working electrode is controlled while responding potential is measured with time. This technique can be performed in order to determine Tafel curve and linear polarization, which are related to the corrosion rate [19].

However, in the current study, the galvanostatic technique is not used to determine the corrosion rate. It is used to accelerate the corrosion process by applying the constant anodic current density to the specimens. In this measurement, the applied current and exposure time will be specified. The potential corresponding to the current then will be shown as a result.

### 2.4.3 Determination of Corrosion Rate

Two methods are selected to determine corrosion rate in the present study. They are weight loss measurement and potentiodynamic polarization.

*Weight Loss Measurement*

Measuring mass of metal loss is a common method to determine the corrosion rate. This technique provides the constant corrosion rate based on average rates over the exposure time. In reality, linear corrosion with time is rarely found, especially in sweet corrosion where film formation significantly affects the corrosion rates. Even

though this measurement is valid for linear corrosion process, however, it is the exception and the result is acceptable. This method is simply performed by measuring the weight of specimens before and after the exposure to the corrosive solutions. Then the weight losses over the corrosion period can be calculated. However, this method is not applicable when applied to the industry scale due to size and location of the metal needing to be investigated. The corrosion rate can be determined by the weight loss using the equation below.

$$CR = \frac{K_1 \bullet W}{A \bullet T \bullet D} \tag{20}$$

where

CR = the corrosion rate (mm/y)

$K_1$ = the constant ($8.76 \times 10^4$ for the corrosion rate unit of mm/y)

T = the exposure time (hour)

A = the exposure area ($cm^2$)

W = the mass loss (g), and

D = the metal density ($g/cm^3$)

*Potentiodynamic Polarization Measurement*

Potentiodynamic sweep is one of the polarization techniques. It is the common method in the corrosion studies [27, 28]. For the potentiodynamic polarization, the correlation of potential and current is observed by varying potential applied to the working electrode and recording the generated current. In this measurement, reaction rate or the response current is measured when the potential is shifted away from the free-corrosion potential at a constant rate.

In the current study, the potentiodynamic sweep is used for two objectives. First, it is performed in order to activate the surface of the working electrode. Being polarized for several minutes, the electrode will oxidize or reduce all the deposits on its surface [29].

Another objective is to determine the corrosion rate. Potentiodynamic measurement consists of cathodic and anodic polarization. Cathodic polarization is to make the working electrode become a cathode. The potential is swept in more negative direction from the free-corrosion potential. In contrast, the potential is

changed in more positive direction to make working electrode as an anode in anodic polarization.

This technique provides the data for plotting a polarization curve between the corrosion cell potential versus the current as depicted in Figure 2.8 below.

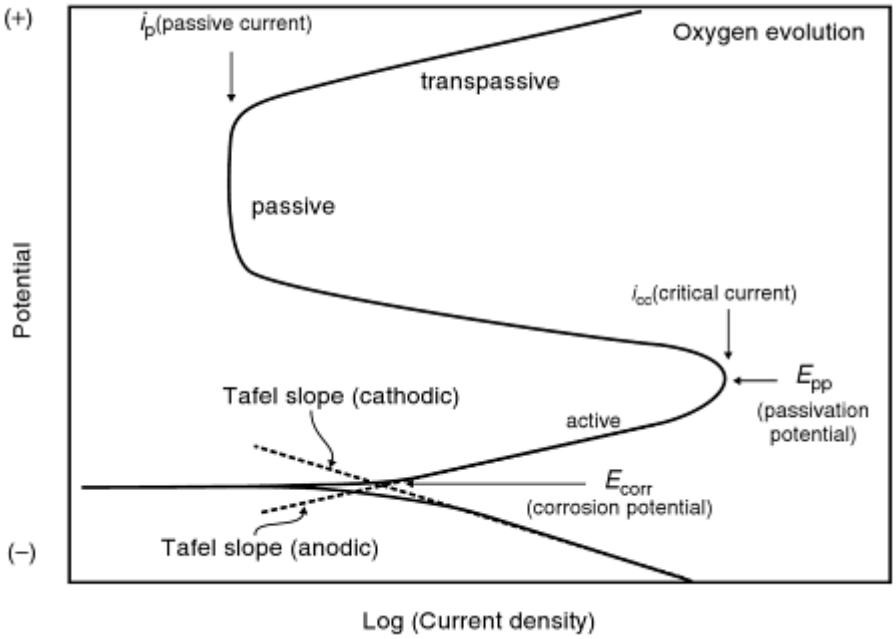


**FIGURE 2.8** General polarization diagram of a passivable metal [29]

Beside, the curve in E-logI plot can be used to determine Tafel constants and corrosion current. The Tafel constants are acquired from slopes of anodic and cathodic currents. In addition, the interception of the anodic and the cathodic currents extrapolation is a position of the corrosion currents. Figure 2.9 illustrates the variables that are obtained from the polarization plot.

However, there are many factors that might have effects on the polarization measurement [29].

- Scan rate: The scan rate should be slow enough to minimize surface capacitance charging. If the sweep rate is too high, some currents can be generated and they will charge the surface capacitance. It results in measuring the greater currents than the actual current from lone corrosion.

- Solution resistance: The distance between the reference electrode and the working electrode should be minimized in order to avoid the effect of solution resistance. However, this effect is significant in high-resistive electrolyte, e.g. concrete, soils, and organic solutions.
- Surface conditions: Since a surface of corroded metal is changed by the corrosion process, therefore, the different polarization curves could be obtained.

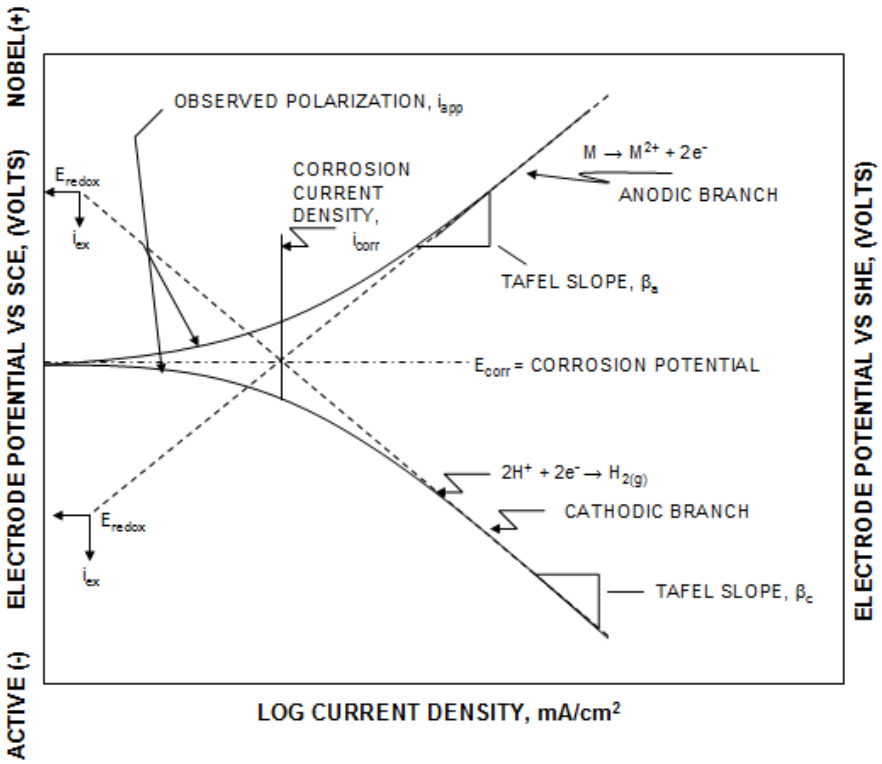


**FIGURE 2.9** Polarization curve showing Tafel constants and corrosion current [30]

Regarding to ASTM G102 standard [31], the corrosion current is normally obtained from the linear Tafel extrapolation of anodic and cathodic currents near the corrosion potential. The common value is ±5 and ±20 mV from the corrosion potential.

The variables from the polarization curve are simply applied to calculate the corrosion rate which is directly proportional to the corrosion current. The corrosion rate and the corrosion current have a relationship as shown in equation below [31].

$$CR = \frac{i_{corr} \cdot K_2 \cdot EW}{D} \quad (21)$$

where

CR = the corrosion rate (mm/y)

$i_{corr}$ = the corrosion current density ($\mu A/cm^2$)

$K_2$ = the constant ($3.27 \times 10^{-3}$ mm g/$\mu$A cm y)

EW = the equivalent weight

D = the metal density ($g/cm^3$), and

**2.5 Corrosion Film Examination**

To investigate the corrosion product films, scanning electron microscope with energy dispersive X-Ray spectroscopy (SEM/EDS) is widely used. SEM technique is normally used to examine the cross section of specimens with the corrosion films on top. EDS is performed in order to analysis chemical components contained in the films.

Scanning Electron Microscope (SEM) is widely used to make a high-resolution image especially in an analytical work. For the corrosion investigation, SEM is commonly used to examine corroded surfaces and corrosion product films [3]. SEM is capable of providing the image of the corroded metal surfaces and external morphologies of the films. Furthermore, with an additional instrument, it also provides chemical composition of the selected area of the samples.

SEM operates by scanning the solid surface with an electron beam. The selected area of the examined surface is bombarded by electrons with certain amount of kinetic energy. A detector records backscattered and secondary electrons after the beam strikes the surface. After that signals are collected above the surface and stored in a computer before using in generating an image [32].

As mentioned earlier, the current technology also provides qualitative and quantitative analysis with SEM by attaching the additional instrument. In the present study, the energy-dispersive instrument with an X-ray source is used. It is briefly called as SEM/EDS technique, where EDS stands for Energy Dispersive X-Ray Spectroscopy. In this technique, the emitted X-ray lines are detected with their energy

and the signals are converted to produce an energy-dispersive spectrum for further analysis. Beside, EDS provides chemical composition of each element present in the sample. Base on these data, the compound contained in the selected area can be identified.

The limitation of this technique which decreases the efficiency is the accelerating of microscope beam. The voltage applied to the electrons should be in the proper level. Too low voltage is not able to generate the characteristic radiation. On the other hand, too high energy results in excessive absorption when the lower-energy X-rays are needed. This can cause the less accuracy in the result.

In summary, corrosion films are very important issue since they markedly affects on the mechanisms in $CO_2$ corrosion. The mixed films consist of iron carbide and iron carbonate as key components. Protectiveness of the films depends on their composition and structure. Even though the iron carbide is found metallic conductive, but it plays an important role in enhancing the adhesion of the protective iron carbonate to the steel surfaces. Moreover, studying in the carbide layer is needed in establishing the accurate model of the protective films. Nevertheless, many studies and researches have not clearly indicated the factors which affect the formation of iron carbide.

In the current study, the formation of carbide layer is focused on. The iron carbide scales are basically formed by having carbon steels corroded. After the steels are corroded and ferrous ions are generated, the iron carbide is then left behind on the steel surfaces. However, this process consumes quite long time. Hence, the experiment in this study is proposed mainly to accelerate the corrosion by applying the anodic current to the steels. In addition the effects of exposure time and steel composition are also observed.

# 3 EXPERIMENTAL

## 3.1 Experimental Settings

Since the main objective of the study is to gain the iron carbide from carbon steels in $CO_2$ environment by applying anodic current. Thus, the effect of the applied current on the corrosion reactions is mainly focused on. In addition, effects of exposure time and steel's composition and microstructure are also studied. The experiments are set up in three series which are denoted as A, B and C.

**Series A**: It is to study the effect of applied current on the carbide formation. The corrosion behaviors with different applied current densities are of interest. The experiments are conducted by applying different currents to working electrodes for a fixed duration of 24-hours.

**Series B:** With the same amount of the current applied to the specimens, the exposure time is varied in order to investigate the corrosion performance over time of the steels. In these experiments, the working electrodes are applied with the fixed current density (0.25 $mA/cm^2$) for different durations.

**Series C:** In this series, both current density and exposure time are varied in the opposite way. The applied current is reduced while the exposure time is increased.

The applied current density and exposure time for each series are established as shown in Table 3.1.

**TABLE 3.1**

Applied current density and exposure time used in the experiments

| | | | | | |
|---|---|---|---|---|---|
| Series A | i ($mA/cm^2$) | 0.125 | 0.25 | 0.5 | 1.0 |
| | t (h) | 24 | 24 | 24 | 24 |
| Series B | i ($mA/cm^2$) | 0.25 | 0.25 | 0.25 | 0.25 |
| | t (h) | 12 | 24 | 48 | 96 |
| Series C | i ($mA/cm^2$) | 1.0 | 0.5 | 0.25 | 0.125 |
| | t (h) | 6 | 12 | 24 | 48 |

Apart from applied current and exposure time, different composition and microstructure of carbon steels are also studied. The experiments are done on three different carbon steels. The specimens made of X-65, St52 and steel 33 are received from Institute for Energy Technology (IFE). The composition of the steels is listed in Table 3.2 and the microstructure is given in Table 3.3.

**TABLE 3.2**

Chemical composition of carbon steels from material certificates

| | **C** | **Si** | **Mn** | **S** | **P** | **Cr** | **Ni** | **Mo** | **Cu** | **Al** |
|---|---|---|---|---|---|---|---|---|---|---|
| X-65 | 0.08 | 0.25 | 1.54 | 0.001 | 0.019 | 0.04 | 0.03 | 0.01 | 0.02 | 0.038 |
| St52 | 0.13 | 0.38 | 1.29 | 0.008 | 0.015 | 0.07 | 0.09 | 0.01 | 0.34 | 0.05 |
| Steel33 | 0.07 | 0.19 | 0.87 | 0.004 | 0.012 | 0.56 | 0.01 | 0.01 | 0.01 | 0.035 |

**TABLE 3.3**

Microstructure of carbon steels from material certificates

| | **Structure** |
|---|---|
| X-65 | Ferrite - pearlite |
| St52 | Ferrite - some pearlite |
| Steel33 | Coarse ferrite - some Widmanstätten ferrite |

$CO_2$ saturated environment is developed by purging $CO_2$ gas into an electrolyte before and during the experiments at atmospheric pressure. $CO_2$ gas is supplied from Yara Praxair as a cylinder. The physical properties of $CO_2$ gas are molecular weight 44.0 g/mol, density (1 bar, 15$^{o}$C) 1.53, boiling point -78.5$^{o}$C. The experiments are conducted in a condition shown in Table 3.4.

**TABLE 3.4**

Experimental Conditions

| | |
|---|---|
| Electrolyte | saturated $CO_2$, 1 g/kg NaCl |
| Temperature | 20$^{o}$C (room temperature) |
| pH | ~ 4 |

## 3.2 Equipment

Three-electrode system is used as a corrosion cell for all experiments. The configuration is shown in Figure 3.1.

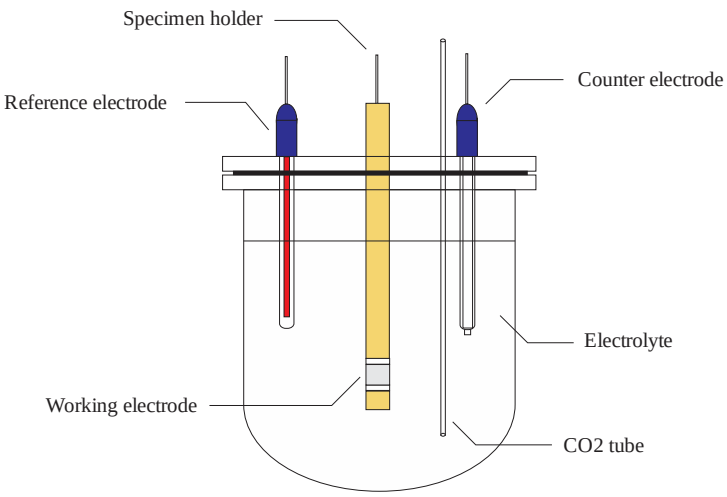


**FIGURE 3.1** Schematic of three-electrode configuration used in the experiments

The equipment and materials needed in the experiment are a working electrode, a reference electrode, a counter electrode, a glass cell, an electrolyte, a potentiostat, a pH meter and a balance. Following below is description and set up method of the equipment.

- Working Electrode (WE): After the specimen is treated as mentioned in the instruction in 3.3, it is sandwiched by Teflon rings and mounted on the holder. The electrode contacts to the metal inside the holder which is connected to a potentiostat. The Teflon rings prevent the electrolyte get into a gap between the electrode and the holder. In case the electrolyte contacts to the metal part of the holder, the corrosion could occur inside the holder in addition to the electrode surface, which is not desirable.

Therefore, the electrode should be tightened properly to the holder.

- Reference Electrode (RE): Saturated Calomel Electrode, Radiometer Red rod (REF201) electrode, is used as a reference electrode. The electrode has to be filled up with saturated KCl solution. KCl crystals should be observed when used as it indicates supersaturation of the solution. Before and after the experiments, the electrode is calibrated by measuring potential deviation compared to a dedicated standard reference electrode.
- Counter Electrode (CE): Radiometer Pt100 electrode is selected. The electrode is made from platinum plate and connected to sensing elements.
- Glass cell: The glass cell is added with 1800 ml of the NaCl solution. The glass is covered with a plastic lid with holes for three electrodes, pH electrode and $CO_2$ supplying tube. The electrolyte is deaerated by bubbling $CO_2$ for two hours before starting and throughout the experiments. In order to allow the reactions in $CO_2$ corrosion mechanisms proceed effectively. The cell and the cover plate are well sealed with a rubber ring and silicone to prevent air ingress. Moreover, they are secured tightly by two clamps with a cell holder.
- Electrolyte: The electrolyte in this experiment is 1g/kg NaCl in ion-exchanged water which is the typical salinity. The solution is prepared by mixing distilled water and sodium chloride. The electrolyte should be transparent throughout the experiment, which indicates that there is no oxygen getting into the cell. The electrolyte will turn yellowish if $Fe^{2+}$ is oxidized by the oxygen.
- Potentiostat: Gamry's PC4/750 potentiostat is connected to three electrodes by cables. The potentiostat is installed in CPU of a personal computer which processes data and provides information for further analysis.

- pH meter: pH of the electrolyte is measured by pH meter immediately before running the measurement. The pH meter has to be calibrated periodically for reliable results.
- Balance: Sartorius 4-digit electronic balance (BP310S) is used to measure the weight of the specimens before and after the exposure. The maximum capacity of the balance is 310g with d = 0.001g.

The equipment is set up as shown in Figure 3.2. The three-electrode system is mounted on the metal glass holder by the wooden plate and clamps. The electrodes are then connected to the potentiostat by cables. To avoid the short circuit to the glass holder which causes the error to the result, the metal parts of the cables should be insulated by non-conductive material e.g. paper.

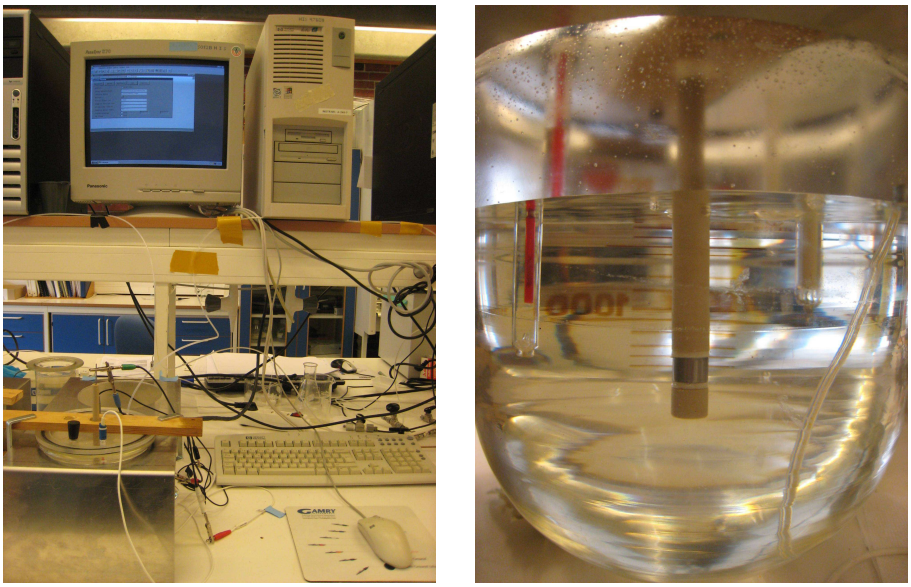

**FIGURE 3.2** Three-electrode corrosion cell used in the experiments

### 3.3 Specimen Preparation

A specimen used in the experiment is cylindrical steel with 1 cm in diameter and 1 cm long. Thus, the exposure area of the specimen is 3.14 $cm^2$. In order to have

homogeneously clean surface, all working electrode is treated as described in the following instruction.

a. Polish the specimen by grinding its surface with 1000 mesh silicon carbide paper with rotation rate of 300 rpm until homogeneous surface is obtained. After polishing, the specimen should not be touched directly by hand to avoid any grease or contaminant left on the surface.

b. Degrease the specimen by rinsing with isopropanol and let it dry in a chemical fume hood.

c. Weight the specimen.

d. Mount the specimen on a holder carefully and tightly enough. The specimen with the holder is immersed to the electrolyte immediately before starting the experiment.

## 3.4 Procedure

The electrochemical measurements used in this study are listed orderly below. There are four steps excluding the examination of the surface by SEM.

### 3.4.1 Corrosion Potential Measurement

After finishing equipment setup, deaeration and pH measurement, corrosion potential ($E_{corr}$) test is conducted to measure the open-circuit potential of the electrode for 15 minutes. Parameters set up is shown in the below table.

**TABLE 3.5**

Parameter setting for measuring corrosion potential

| | |
|---|---|
| Total times (s) | 900 |
| Sample period (s) | 5 |
| Sample area ($cm^2$) | 1 |

### 3.4.2 Cathodic Polarization

Before applying anodic current, the specimen surface is activated by cathodic polarization with the parameters given in Table 3.6. This is a technique to clean the surface by removing air formed films.

**TABLE 3.6**

Parameter setting for activating electrode surface

| | |
|---|---|
| Initial E (mV vs. Ecorr) | 5 |
| Final E (mV vs. Ecorr) | -300 |
| Scan rate (mV/s) | 0.5 |
| Sample period (s) | 1 |
| Sample area ($cm^2$) | 1 |
| Density ($g/cm^3$) | 7.87 |
| Equivalent weight | 27.92 |

### 3.4.3 Galvanostatic measurement

Anodic current is applied to the working electrode in order to provoke the corrosion of the specimen by using galvanostatic mode following the parameters in Table 3.7.

**TABLE 3.7**

Parameter setting for galvanostaticscan

| | |
|---|---|
| Initial I ($mA/cm^2$) | see Table 3.1 |
| Final I ($mA/cm^2$) | same as initial I |
| Initial time (s) | 0 |
| Final time (s) | See Table 3.1 |
| Sample period (s) | 3 |
| Sample area ($cm^2$) | 1 |
| Density ($g/cm^3$) | 7.87 |
| Equivalent weight | 27.92 |

### 3.4.4 Potentiodynamic Polarization

After applying the current, the working electrode is cathodically polarized with the parameters shown in Table 3.8. The anodic sweep is not conducted to preserve the steel surface for analysis by SEM technique.

**TABLE 3.8**

Parameter setting for potentiodynamic polarization

| | |
|---|---|
| Initial E (mV vs. Ecorr) | 5 |
| Final E (mV vs. Ecorr) | -300 |
| Scan rate (mV/s) | 0.2 |
| Sample period (s) | 1 |
| Sample area ($cm^2$) | 1 |
| Density ($g/cm^3$) | 7.87 |
| Equivalent weight | 27.92 |

### 3.5 Sample Preservation

After finishing the electrochemical measurements, the specimen is removed from the electrolyte. It has to be handled very carefully in order to preserve the corrosion film on the surface. The preservation including mounting of the specimen is done by the following steps.

a. Immerse the specimen with the holder into isopropanol.
b. Remove the specimen from the holder and let it completely dry.
c. Weigh the specimen.
d. Store the specimen in a decicator in case that sample does not need to do SEM analysis

For the specimen that needs to do SEM analysis, it has to be mounted by epoxy following an instruction below.

e. Mix the epoxy with the hardener by the ratio of 7:1
f. Apply vacuum to the mix in order to remove any air trapped
g. Pour the mixed epoxy throughout the surface of the specimen
h. Minimize air entrapment by applying vacuum to the epoxy-coated specimen
i. Dry the mount in the oven at $50^oC$ overnight
j. Store the mount in a decicator

### 3.6 Scanning Electron Microscopy (SEM)

Preserved samples are sent for SEM analysis performed by IFE. The samples sent to IFE are listed below.

**TABLE 3.9**

List of samples for SEM analysis

| Steel | Applied current density ($mA/cm^2$) | Exposure time (h) |
|---|---|---|
| X-65 | 0.125 | 24 |
| X-65 | 1.0 | 24 |
| St52 | 1.0 | 24 |
| Steel33 | 1.0 | 24 |

SEM instrument used in IFE is an ultra-high resolution Hitachi S-4800. It is also attached with a Noran System Six energy dispersive spectrometer (EDS) for element analysis. Figure 3.3 shows the picture of SEM instrument.

**FIGURE 3.3** IFE's Scanning electron microscope (www.ife.no)

The SEM is a conventional semi-in-lens. It can be used for large sample accommodation while achieving ultra-high resolution (UHR). Specifications of SEM used in the experiments are listed in Table 3.10.

**TABLE 3.10**

Specification of IFE's scanning electron microscope

| | |
|---|---|
| Secondary electron image resolution | 1.0 nm (at 15 kV) |
| Electron optics | Electron gun |
| Cold field emission electron source | |
| Acc. voltage | 0.5 ~ 30 kV (variable at 0.1 kV/step) |
| Magnification | x30 ~ x800,000 |
| Detector | Secondary electron detector |
| | (upper/lower/upper+lower), |
| | Energy dispersive X-ray detector |
| Specimen stage | PC-controlled 5 axis motor drive |
| | Traverse X: 0-110 mm |
| | Y: 0-110 mm |
| | Z: 1.5-40 mm |
| | R: 0-360$^{o}$ |
| | T: -5~+70 degrees (depends on Z) |

The chemical composition analysis uses Noran System Six energy dispersive spectrometer; the specifications are shown in Table 3.11.

**TABLE 3.11**

Specifications of Noran System Six energy dispersive spectrometer

| | |
|---|---|
| Crystal area | 30 mm$^2$ |
| Mn resolution | 134 eV |
| F resolution | 65 eV |
| Light element detection | down to Beryllium |

# 4 RESULT AND DISSCUSSION

The results of the experiments discussed below are categorized by the effects of each parameter following the study objectives. The corrosion reactions are represented by weight loss measurements and corrosion rates. The corrosion rates are determined by two methods which are from weight loss conversion and Tafel's linear extrapolation. An example of corrosion rate calculation following the equation (20) and (21) is explained in Appendix A. For the results of SEM/EDS analysis, only main alloy elements, C and Cr, which directly affect the corrosion, will be discussed. The other trace elements can be found from the results in Appendix B.

However, the results of the corrosion rates are only used as guidance of the corrosion behavior since the methods in the experiments have some limitations as follows:

- The error of the results could be from the specimen handling. Less carefully handling can damage the surface of the specimen. It was found that after the corrosion the deposit on the surface of some specimens is easily to peel off.
- As the corrosion is simulated at low temperature, the process will proceed with low rate. Hence, the weight loss will be very low and the error could occur as the capacity of the balance used in the weight measurement is not in the proper scale and sensitive enough.
- The potentiodynamic sweep is done when there is no current applied (after finishing galvanostatic mode). Therefore, it is not the corrosion rate of the steel with the applied current, but the free-corrosion rate of the steel after the corrosion. However, the results can be used to indicate the change and difference of the steel's surface.

*Electrolyte pH*

After bubbling with $CO_2$ for two hours, pH values of electrolytes were measured immediately before starting electrochemical measurements. The results show that the average value was 3.92 with allowance of ±0.3. It should be noted that $CO_2$ flows were kept constant throughout the experiments.

*Corrosion Potential*

Corrosion potential measurements were performed as the first sequence of all experiments. In theory, $E_{corr}$ obtained from the experiments of the same material should ideally be equal since freshly-prepared specimens were measured at open circuit condition. However, the results show some variations which are acceptable. The variations could be from many reasons e.g. the difference in microstructure of different electrodes, or there is some noise in the experiments. The corrosion potentials of three different steels are shown in Figure 4.1 (a) through (c) and the values at the end of the measurement are also listed in Table 4.1.

It is obvious that the allowances of $E_{corr}$ for all steels are quite broad which are possibly from the reasons mentioned above. In Figure 4.1 (a), some specimens had significant higher values than the others. This could be from an error of reading from the reference electrode. However, their values seemed to reach the average values of the others after some time. Nevertheless, these variations can generally happen in $E_{corr}$ measurements which are acceptable and do not make significant effects to the experiments. In addition, the values are used as "0" point for later potential measurement. The figures also showed that the electrodes can be stabilized within 15 minutes, or even in 10 minutes.

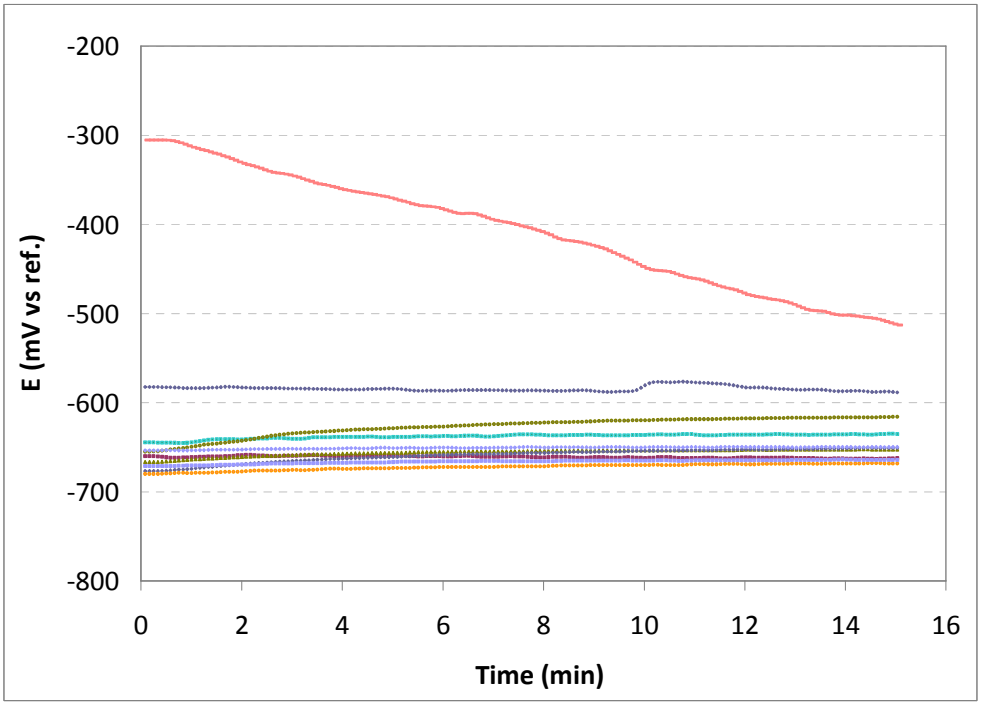


(a) X-65

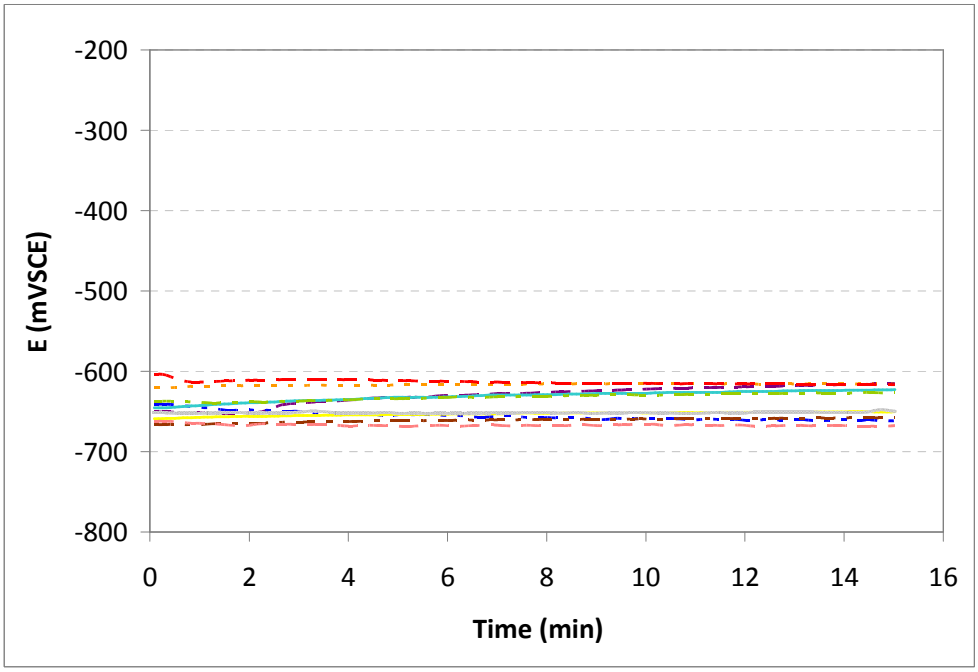


(b) St52

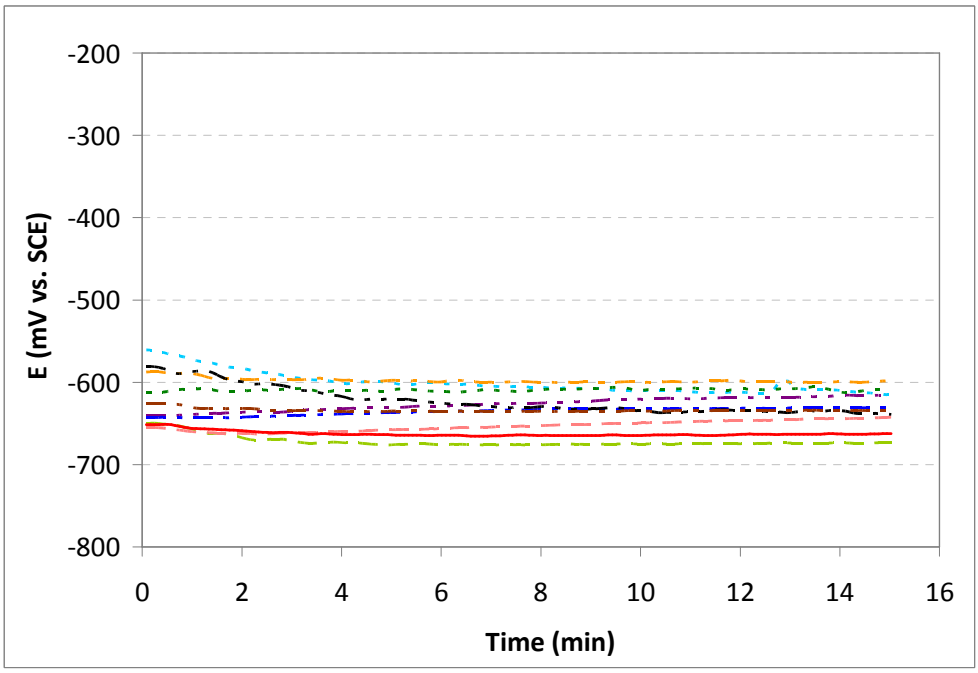


(c) Steel33

**FIGURE 4.1** Corrosion potentials ($E_{corr}$) of three different steels

**TABLE 4.1**

Corrosion potentials of the three steels used in the experiments

| | $E_{corr}$ (mV vs ref.) |
|---|---|
| X-65 | -640 ±27 |
| St52 | -629 ±34 |
| Steel33 | -637 ±36 |

## 4.1 Effect of Applied Anodic Current

After activating the electrode surfaces by cathodic polarization, anodic currents were applied to the working electrodes by galvanostatic method. Figure 4.2 shows the trend lines of potential response with different applied current densities for 24 hours.

From Figure 4.2 (a), X-65 specimens took around 15 hours to reach the equilibrium condition. It is unexpected that the responding potentials of electrodes applied with 0.25 and 0.5 $mA/cm^2$ overlapped. St52 specimens, as shown in Figure 4.2 (b), spent less than five hours to adapt to the equilibrium. Furthermore, the potentials are more consistent than another two steels. In Figure 4.2 (c), Steel33 had the responding potentials with small oscillations and the potential seemed not steady when the measurement finished.

The potentials at the end of the measurements are shown in Figure 4.3. It shows that the potentials of the electrodes increases with increasing applied anodic currents. At low applied currents (0.125 and 0.25 $mA/cm^2$), X-65 had the highest potentials followed by Steel33 and St52, respectively, but the reversed order showed at high applied currents (0.5 and 1.0 $mA/cm^2$).

However, it is seen that the higher currents applied to the working electrode shifted the potentials in a positive direction. According to the Pourbaix diagram, increase in potential at $pH < 4$ will force the iron to dissolute to $Fe^{2+}$. Therefore, the corrosion of the steels is accelerated.

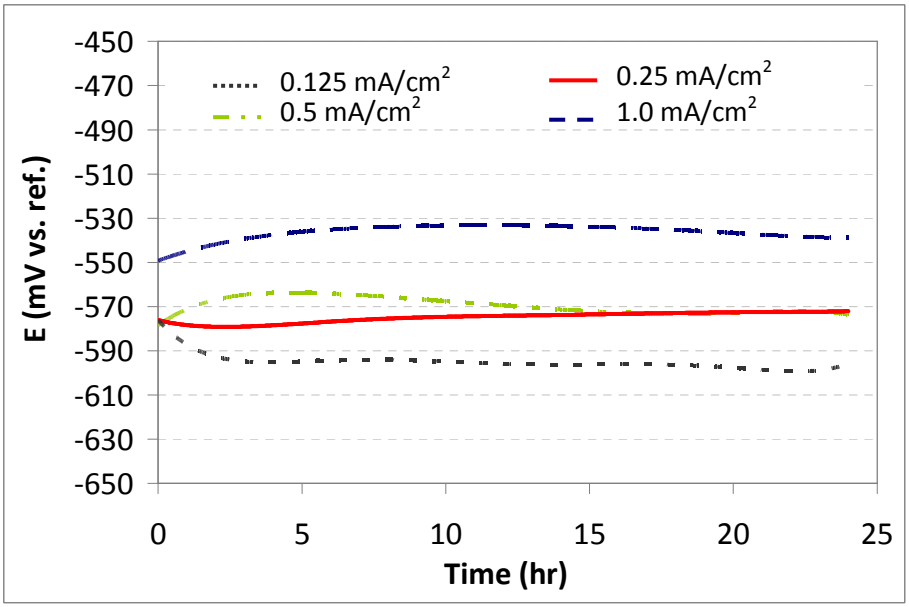
-450
-470
-490
-510
-530
-550
-570
-590
-610
-630
-650
E (mV vs. ref.)
0.125 mA/cm2
0.5 mA/cm2
0.25 mA/cm2
1.0 mA/cm2
0
5
10
15
20
25
Time (hr)

(a) X-65

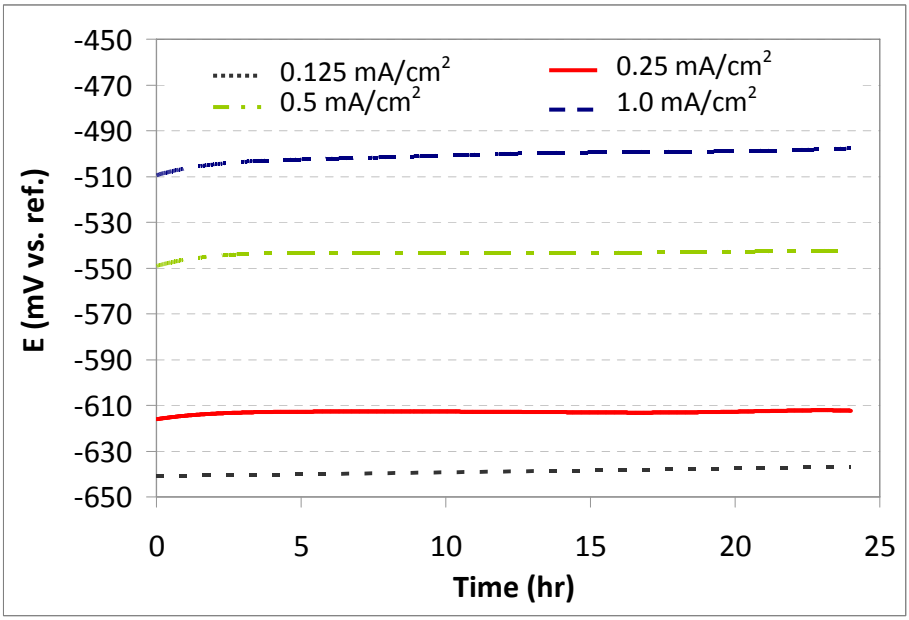
-450
-470
-490
-510
-530
-550
-570
-590
-610
-630
-650
E (mV vs. ref.)
0.125 mA/cm2
0.5 mA/cm2
0.25 mA/cm2
1.0 mA/cm2
0
5
10
15
20
25
Time (hr)

(b) St52

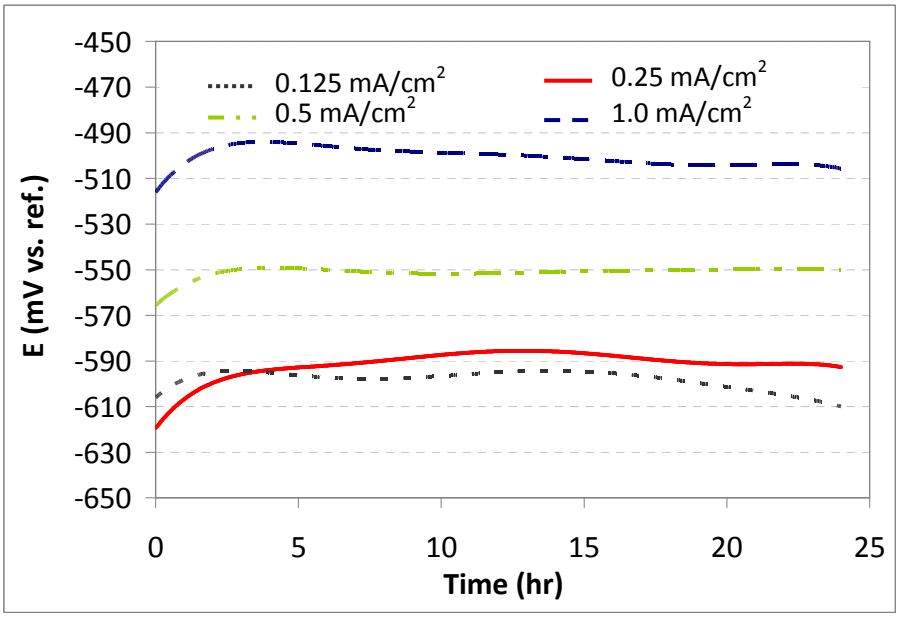


(c) Steel33

**FIGURE 4.2** Responding potentials of the working electrodes which are applied with various applied current densities and 24-hour exposure time

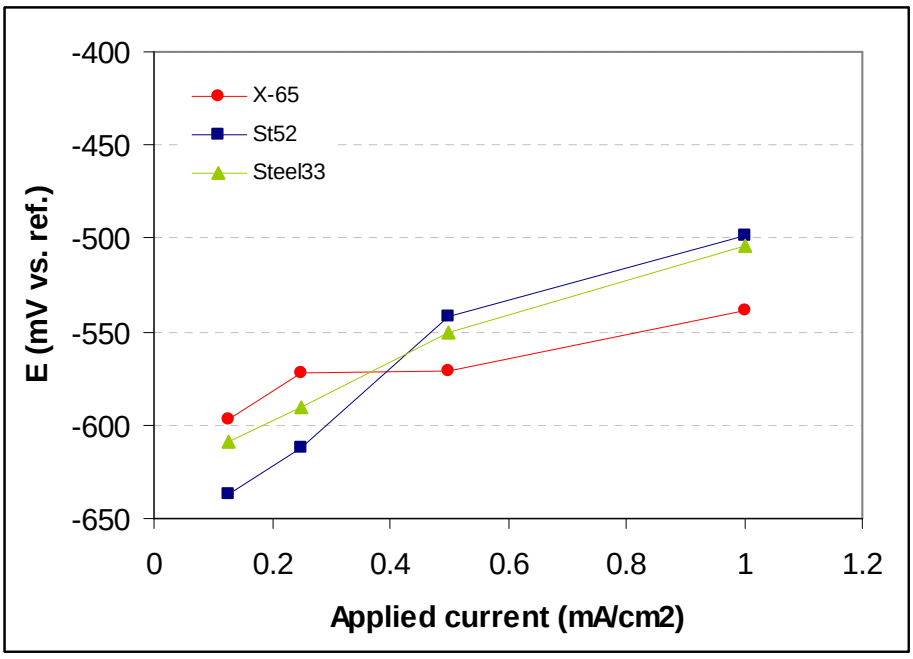


**FIGURE 4.3** Potentials at the end of galvanostatic measurement with different applied anodic currents for 24-hour exposure time

After the exposure, the specimens were removed from the solutions and black powder was observed on the surfaces. Figure 4.4 is the pictures of a specimen before and after the exposure to the corrosion which are taken by an optical microscope. The black deposit indicates the corrosion and presence of iron carbide according to eq. (7)

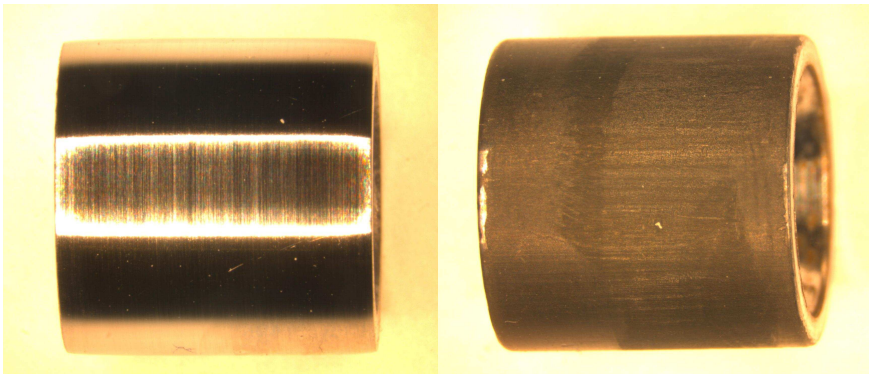

Before After

**FIGURE 4.4** Picture of the specimen before and after the corrosion exposure

The weight losses of the specimens are shown in Figure 4.5 and Table 4.2. Figure 4.5 shows that the weight loss increased with increasing applied anodic current. This means that the steels are more corroded when applying higher current density. Therefore, more amount of carbide should be found when applying high current density. At the lowest applied current (0.125 $mA/cm^2$), X-65 and Steel33 had the same weight loss lower than St52. When increased the applied current to 0.25 $mA/cm^2$, St52 still got the highest value followed by Steel33 and X-65. The weight loss of X-65 increased rapidly and reached the highest among the others when applying the current at 0.5 $mA/cm^2$. However, these weight losses are not different significantly when compared to each other at the same applied current density.

In term of corrosion rate, as mentioned earlier, the rates are determined by two methods. The comparison of the results is shown in Figure 4.6 (a) through (c). By means of weight loss calculation, it is evident that all three steels corroded at faster rates with higher applied anodic currents. The corrosion rates from Tafel's linear extrapolation are far lower than the corrosion rates from weight loss. The weight losses gave the larger corrosion rates than polarization around one order of magnitude.

As mentioned in the beginning, the corrosion rate from polarization cannot represent the actual corrosion rate of the specimen during the external current is applied. However, the values can be used as an indicator of the changes occurring on the steel surfaces. In Figure 4.6, the general trend of the corrosion rates from polarization showed some small decrease. It can be explained in the way that the surface of the specimen applied with high current density got more corrosion leaving more iron carbide on the steel surface. As the iron carbide is uncorroded, therefore it is not active for further corrosion resulting to low corrosion rate. On the other hand, the steel with low applied current density is less corroded providing more general iron surface available for corrosion. Hence, high corrosion rate of the steel was observed. In that way, however, the carbide content on the carbon steel surface will reach the maximum level and the corrosion rate then is not changed.

The values from polarization were very low; thus, they even can be considered indifferent since the difference could be from the error in equipment or reading data. It can be seen that the available data still could not make a clear conclusion for the corrosion rate.

**TABLE 4.2**

Weight losses, corrosion currents and corrosion rates of the specimens which are applied with different anodic currents for 24 hours

| **Applied Current Density ($mA/cm^2$)** | **X-65** | | | | **St52** | | | | **Steel33** | | | |
|---|---|---|---|---|---|---|---|---|---|---|---|---|
| | **Weight loss method** | | **Polarization method** | | **Weight loss method** | | **Polarization method** | | **Weight loss method** | | **Polarization method** | |
| | WL (g) | CR* (mm/y) | $i_{corr}$ ($mA/cm^2$) | CR** (mm/y) | WL (g) | CR* (mm/y) | $i_{corr}$ ($mA/cm^2$) | CR** (mm/y) | WL (g) | CR* (mm/y) | $i_{corr}$ ($mA/cm^2$) | CR** (mm/y) |
| 0.125 | 0.010 | 1.48 | 0.0095 | 0.11 | 0.013 | 1.92 | 0. 0110 | 0.13 | 0.010 | 1.48 | 0.0087 | 0.10 |
| 0.25 | 0.011 | 1.62 | 0.0043 | 0.05 | 0.015 | 2.22 | 0. 0031 | 0.04 | 0.014 | 2.07 | 0.0095 | 0.11 |
| 0.50 | 0.021 | 3.10 | 0.0025 | 0.03 | 0.020 | 2.95 | 0. 0110 | 0.13 | 0.016 | 2.36 | 0.0063 | 0.07 |
| 1.0 | 0.035 | 5.17 | 0.0059 | 0.07 | 0.031 | 4.58 | 0. 0150 | 0.17 | 0.030 | 4.43 | 0.0047 | 0.05 |

* Corrosion rate calculated from respectively weight loss

** Corrosion rate calculated from $i_{corr}$

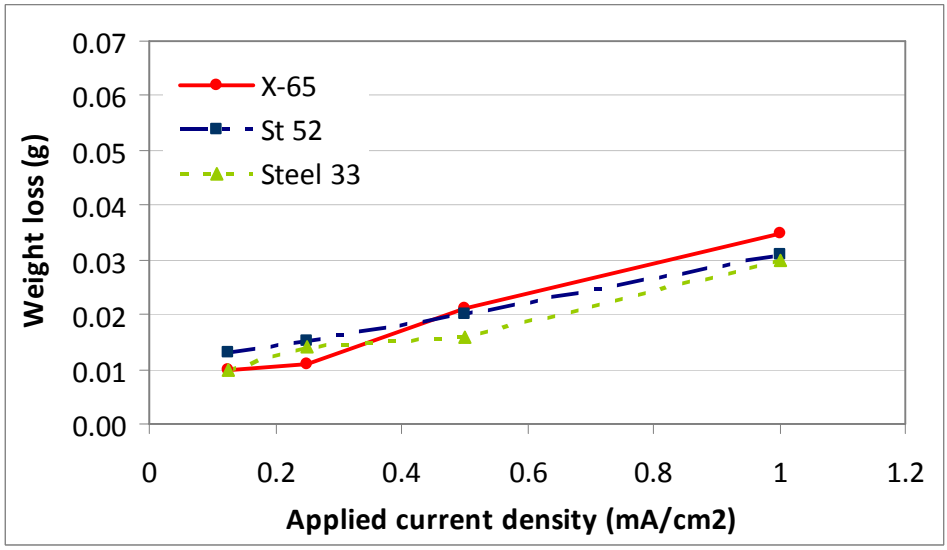


**FIGURE 4.5** Weight losses of the specimens which are applied with different anodic currents for 24 hours

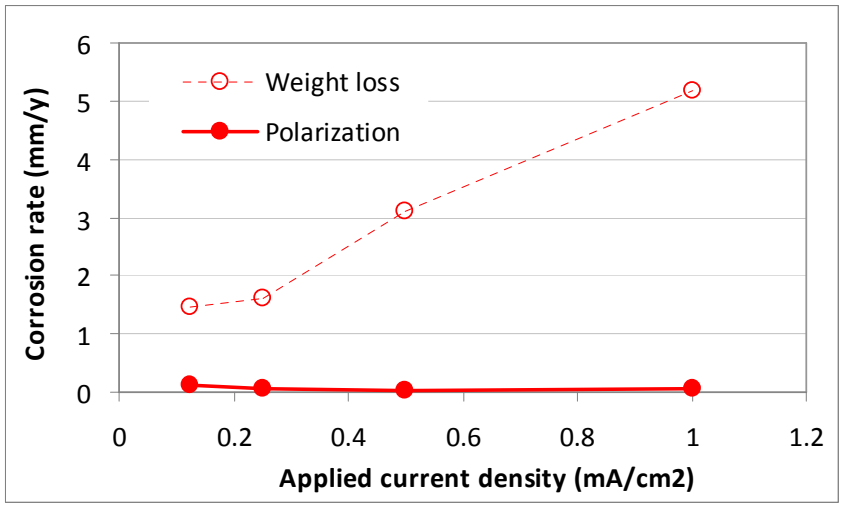


(a) X-65

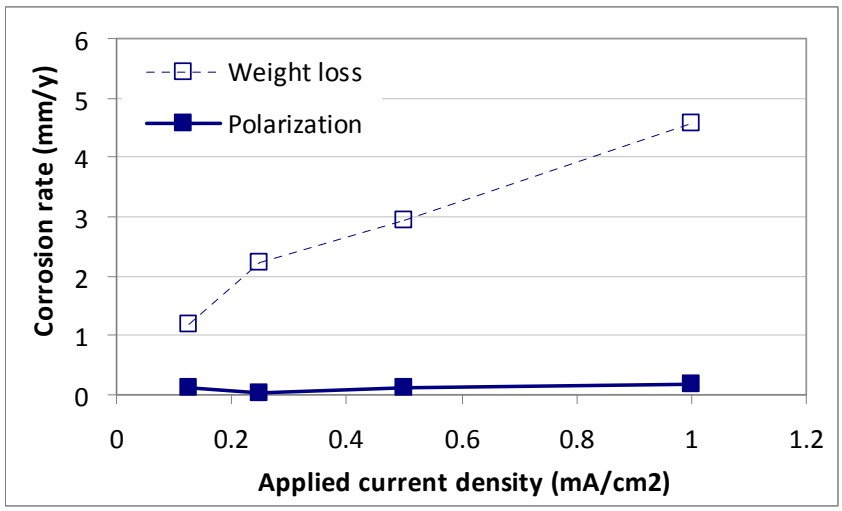


(b) St52

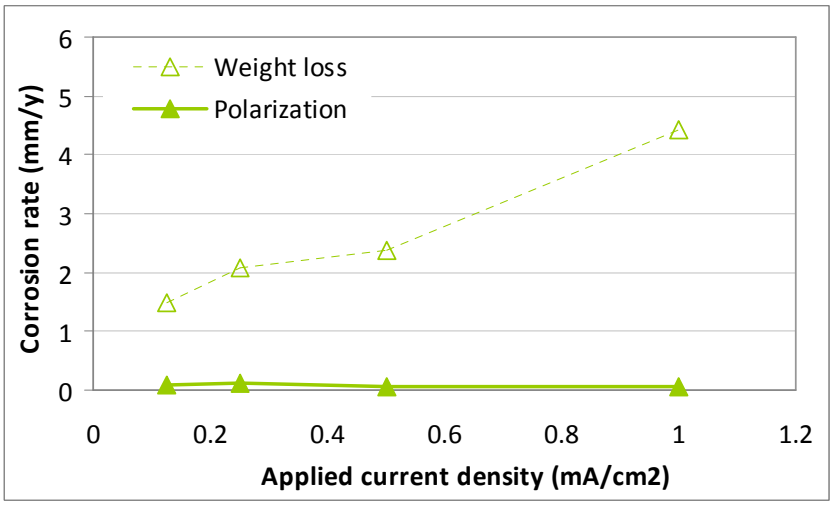


(c) Steel33

**FIGURE 4.6** Corrosion rates of the electrodes applied with different anodic currents for 24 hours

There were two of X-65 samples with different applied anodic currents examined by SEM analysis. The cross-section images of the specimen which is exposed to 0.125 mA/cm$^2$ are shown in Figure 4.7. It can be seen that there was a layer between epoxy used for preserving the surface and steel substrate. The chemical analysis result from EDS reveals that there was $Fe_3C$ contained in the layer, but no $FeCO_3$ was detected. It is as expected that $FeCO_3$ is difficult to form at low pH (<4) and temperature [16].

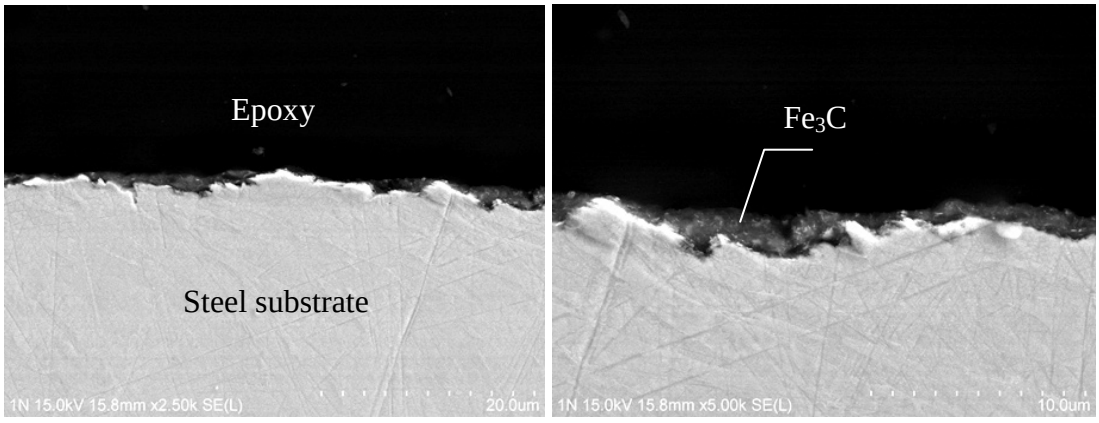


**FIGURE 4.7** SEM images of the X-65 electrode applied with anodic current density of 0.125 mA/cm$^2$ for 24 hours

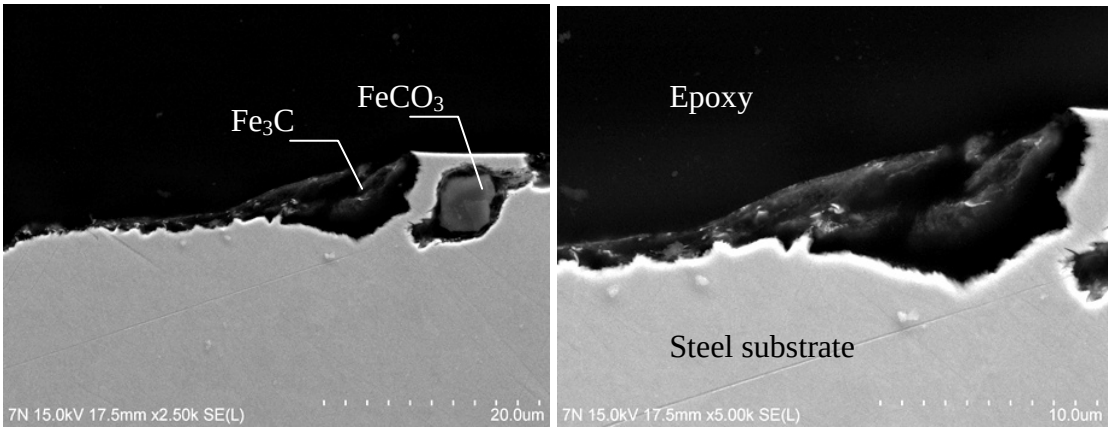


**FIGURE 4.8** SEM images of the X-65 electrode applied with anodic current density of 1.0 mA/cm$^2$ for 24 hours

The images of another X-65 specimen with higher applied current (1.0 mA/cm$^2$) are shown in Figure 4.8. From the pictures, the surface of the steel had more severe damage compared to the electrode with lower applied current. In addition, EDS results show that the film contained both iron carbide and iron carbonate at the locations pointed out in the picture. The formation of the iron carbonate can indicates high $Fe^{2+}$ concentration from the iron dissolution. However, the increase in the corrosion rate at applied current density of 1.0 mA/cm$^2$ showed that $FeCO_3$ formed non-protective layer under this condition.

The results from the electrochemical techniques and SEM/EDS can be summarized that the applied current density had an effect on the corrosion rate and the film formation. The variation of corrosion rates indicated the difference in microstucture of the electrodes with different applied current densities. Severe corrosion was noticed at high applied current. Therefore, it can be concluded that applying the higher current causes more severe damage on the steel surfaces and, as a consequence, more iron carbide is obtained.

## 4.2 Effect of Exposure Time

In these experiments all three kinds of steel were applied with fixed 0.25 mA/cm$^2$ anodic current. The exposure time is the parameter which varied as 12, 24, 48 and 96 hours. Figure 4.9 (a) through (c) shows the responding of the potential during galvanostatic measurements.

St52 specimens still showed faster approaching to equilibrium condition than other two steels. They spent around 15 hours while some electrodes made of X-65 and Steel33 needed more than 20 hours to be at the equilibrium. Furthermore, St52 potentials are very close and more consistent. X-65 and Steel33 have a variation in the potentials and it seemed they did not reach the equilibrium before 20 hours of the corrosion period. The significant variation in potential of X-65 and Steel33 could be due to the difference in the structure of each electrode.

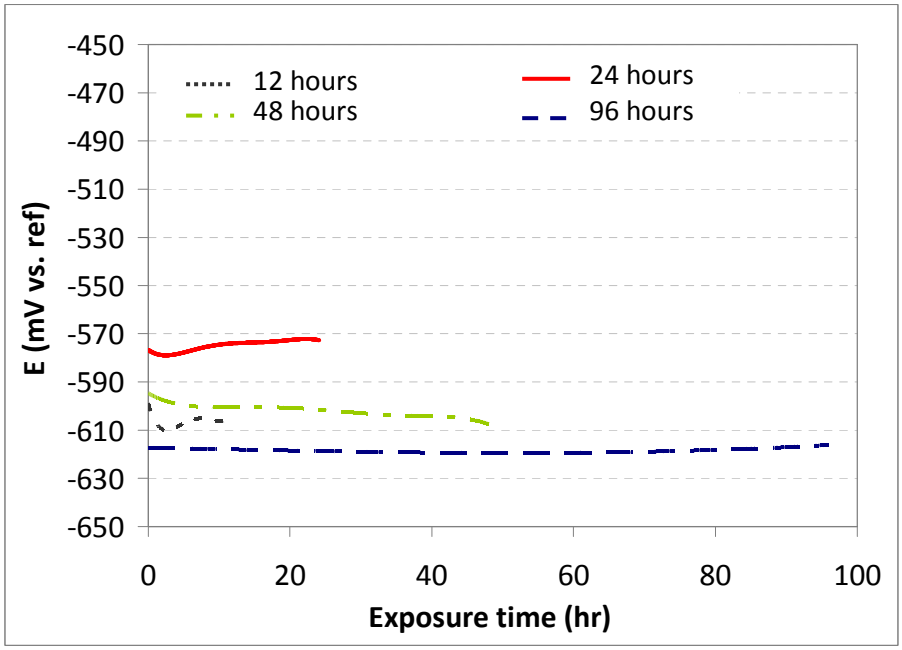


(a) X-65

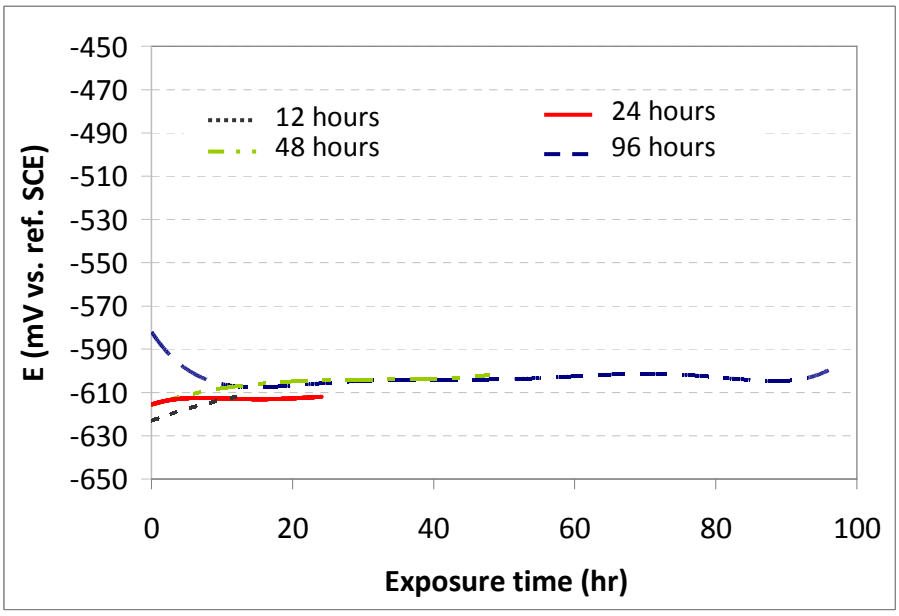


(b) St52

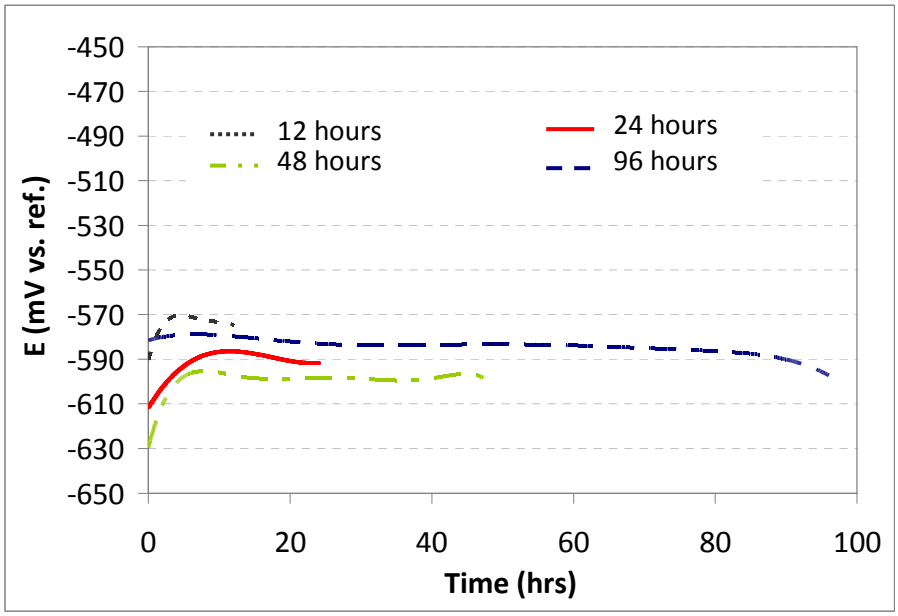


(c) Steel33

**FIGURE 4.9** Responding potentials of the working electrodes which are applied with 0.25 mA/cm$^2$ for different exposure periods

The potentials at the end of the galvanostatic measurements are depicted in Figure 4.10. The figure shows that Steel 33 had the highest potentials for all exposure periods, except at 24 hours. The potential slightly decreased when the electrodes exposed for longer time. X-65 behaved differently as the potential reach the peak at 24 hours and after which it decreased to the lowest compared to other steels at 96 hours. Unlike the others, St52 had increasing potentials, even though its potentials are the lowest for the short period of experiments. All three steels had the potentials very closed when they were corroded for 48 hours. For the longest exposure (96 hour) Steel33 had the highest potential, followed by St52 and X-65, respectively.

The inconsistent results of the potential might caused from many reasons. However, as they were done under the same conditions, the main cause is focused on the structure or surface change during the corrosion process.

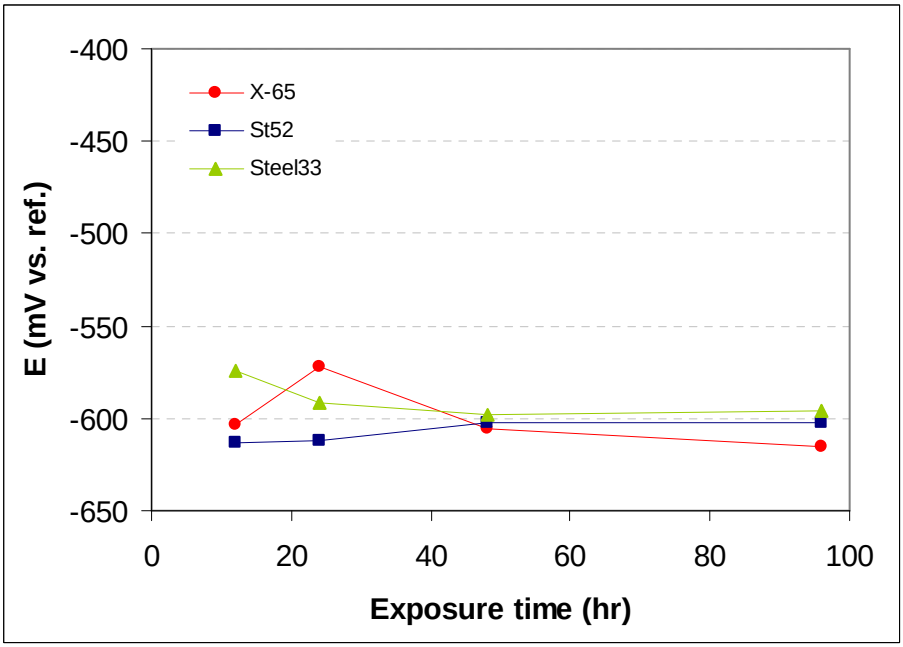


**FIGURE 4.10** Potentials at the end of galvanostatic measurement with fixed applied currents for different exposure time

The weight loss measurement results are shown in Figure 4.11 and Table 4.3. From the figure, it is obviously seen that the weight losses increased proportionally with the exposure time. It also shows general trend that St52 had the highest weight loss followed by Steel33 and X-65. However, the weight loss of X-65 was slightly higher than Steel33 at 96 hours. This increase in weight loss of X-65 was probably from some error in the measurement.

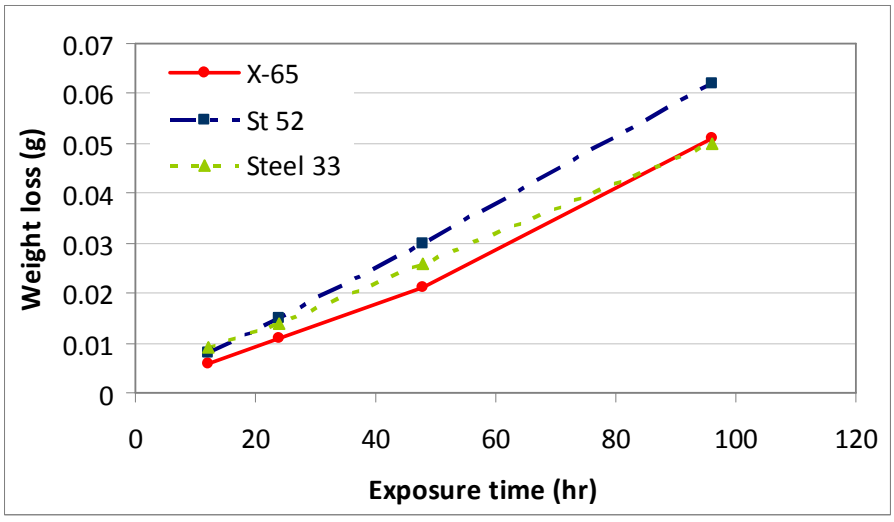


**FIGURE 4.11** Weight losses of the specimens which are applied with 0.25 mA/cm$^2$ for different exposure periods

**TABLE 4.3**

Weight losses, corrosion currents and corrosion rates of the specimens which are applied with current density of 0.25 mA/cm$^2$ for different exposure time

| Exposure Time (hr) | X-65 | | | | St52 | | | | Steel33 | | | |
|---|---|---|---|---|---|---|---|---|---|---|---|---|
| | Weight loss method | | Polarization method | | Weight loss method | | Polarization method | | Weight loss method | | Polarization method | |
| | WL (g) | CR* (mm/y) | $i_{corr}$ (mA/cm$^2$) | CR** (mm/y) | WL (g) | CR* (mm/y) | $i_{corr}$ (mA/cm$^2$) | CR** (mm/y) | WL (g) | CR* (mm/y) | $i_{corr}$ (mA/cm$^2$) | CR** (mm/y) |
| 12 | 0.006 | 1.77 | 0.0031 | 0.04 | 0.008 | 2.36 | 0.0150 | 0.17 | 0.009 | 2.66 | 0.0050 | 0.06 |
| 24 | 0.011 | 1.62 | 0.0043 | 0.05 | 0.015 | 2.22 | 0.0031 | 0.04 | 0.014 | 2.07 | 0.0095 | 0.11 |
| 48 | 0.021 | 1.55 | 0.0073 | 0.08 | 0.030 | 2.22 | 0.0100 | 0.12 | 0.026 | 1.92 | 0.0048 | 0.06 |
| 96 | 0.051 | 1.88 | 0.0100 | 0.12 | 0.062 | 2.29 | 0.0096 | 0.11 | 0.050 | 1.85 | 0.0100 | 0.12 |

* Corrosion rate calculated from respectively weight loss

** Corrosion rate calculated from $i_{corr}$

For the corrosion rate determination, the comparison of the corrosion rates from polarization and weight loss are shown in Figure 4.12. The values calculated from two methods showed the difference which the values from polarization method are lower than the weight loss approach.

According to the figures, the corrosion rates of all steels slightly high in the short-period experiment. It might be from attack in the beginning of the corrosion before the electrodes got stabilized. The corrosion rates of X-65 and St52 from the weight loss are almost constant. Steel33, on the other hand, had decreasing trend in the corrosion rate, but the change is not large. However, this can be implied that the steels corroded with the constant rates over time; therefore, the weight loss is a function of the exposure time.

For polarization, St52 had decreasing trend in corrosion rate. Like the previous experiments, it can be explained by the structure of the steel surfaces. As the steels exposed to the corrosion longer, more iron carbide is left on the surface. Thus, lower corrosion rate is from the less active areas for corrosion.

However, X-65 gave the results in the opposite way as its corrosion rates slightly increased over time while Steel33 showed unpredicted corrosion rates. It is difficult to explain this phenomenon with these limited data as the steel surfaces were not analyzed further. Therefore, the structure of the steel surface after corrosion should be examined in more detail in other study in the future. Nevertheless, it was

noticed again that the difference of the corrosion rate is very low and can be neglected.

In conclusion, it was found that the iron dissolution is proportional to the exposure time. This increase in the weight loss is also in agreement with other studies [4, 16]. As the weight loss increased, hence, the iron carbide is expected to accumulate more on the surface with longer exposure.

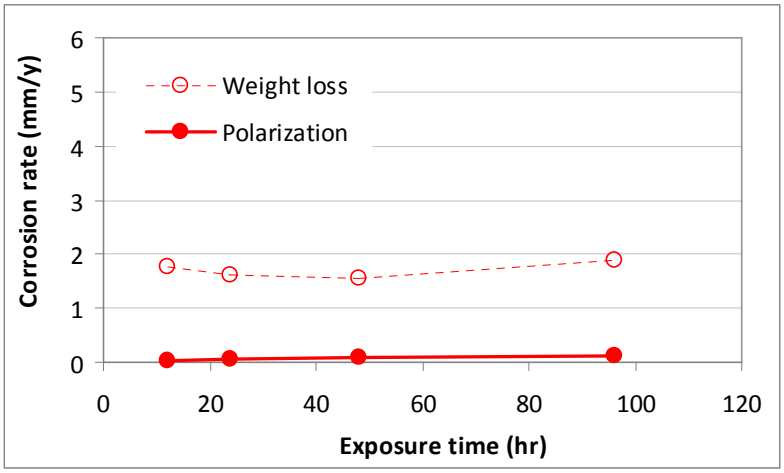


(a) X-65

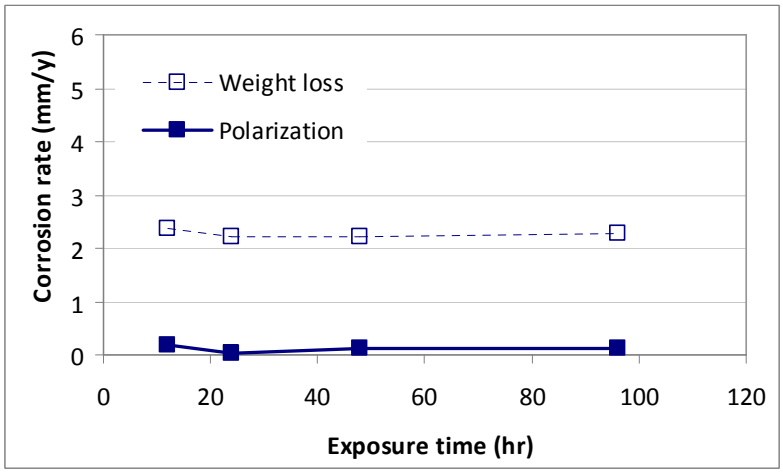


(b) St52

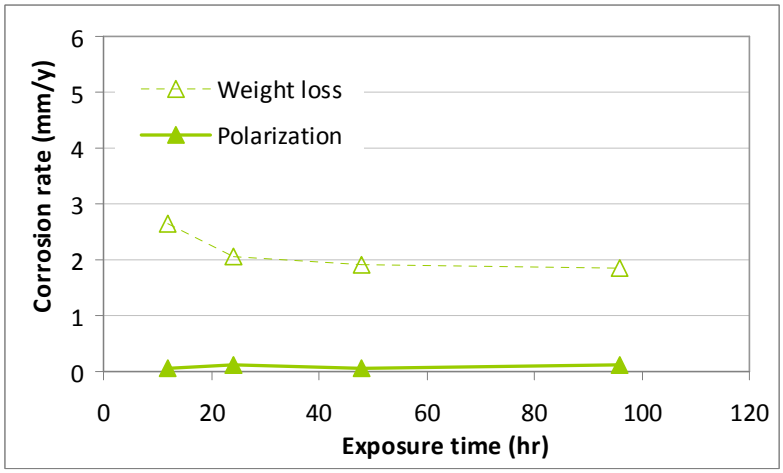


(c) Steel33

**FIGURE 4.12** Corrosion rates of the electrodes applied with current density of 0.25 $mA/cm^2$ for different exposure time

### 4.3 Effect of Applied Current Density and Exposure Time

As it is seen that weight losses were dependent on the applied anodic current and exposure time, the idea of the present experiments, therefore, is to reduce the duration of corrosion by applying higher current density. To study the relationship of the applied current density and exposure time, electrodes would be applied with the high current for a short time and vice versa. If these two parameters are proportional to the corrosion reactions, the weight losses of electrodes made from the same material should be equal, since the current is lowered halfway while the exposure time is doubled. According to the proposed correlation, the corrosion process is possibly accelerated in shorter time by applying higher current.

The electrodes were corroded by using galvanostatic method same as the previous experiments. The trend lines of the potentials during the measurements are shown in Figure 4.13.

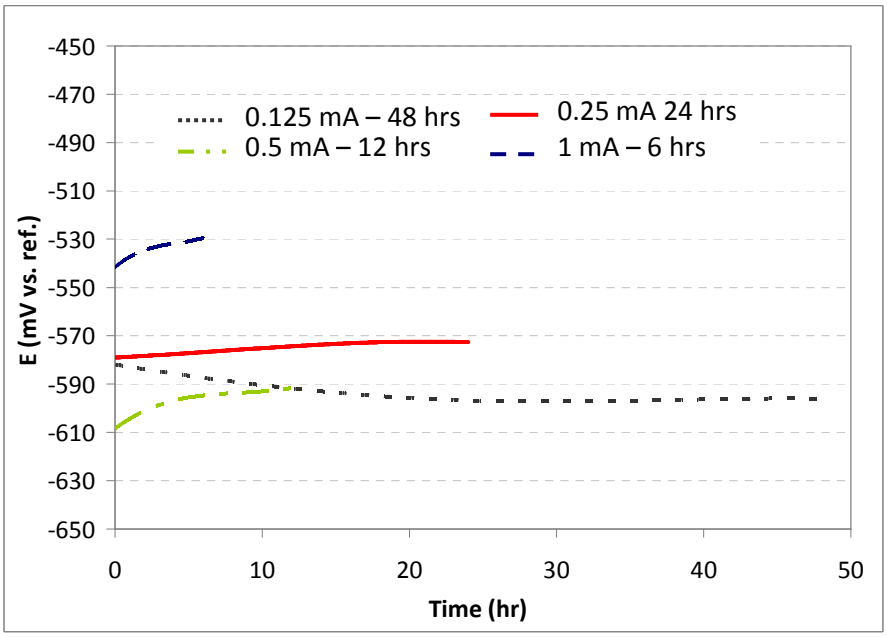
-450
-470
-490
-510
-530
-550
-570
-590
-610
-630
-650
E (mV vs. ref.)
0.125 mA – 48 hrs
0.25 mA 24 hrs
0.5 mA – 12 hrs
1 mA – 6 hrs
0
10
20
30
40
50
Time (hr)

(a) X-65

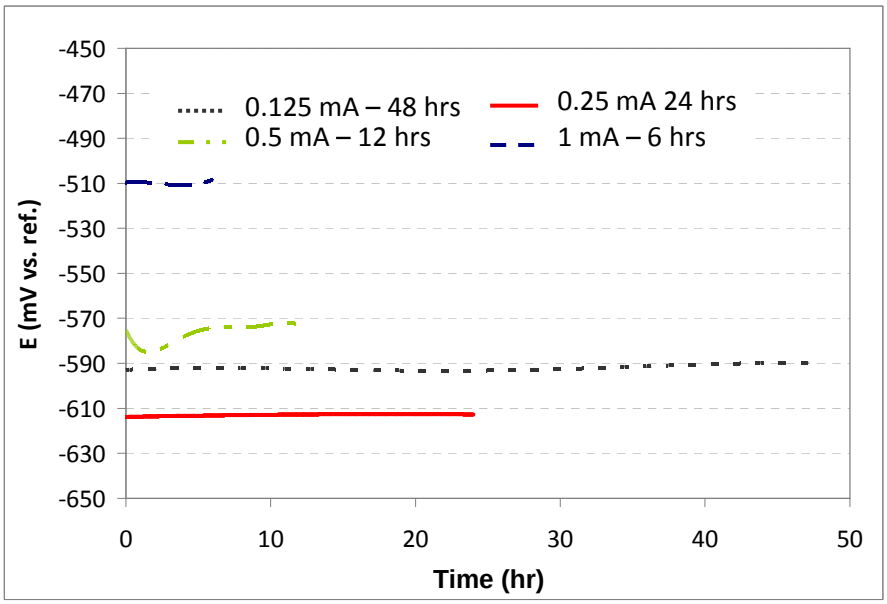
-450
-470
-490
-510
-530
-550
-570
-590
-610
-630
-650
E (mV vs. ref.)
0.125 mA – 48 hrs
0.25 mA 24 hrs
0.5 mA – 12 hrs
1 mA – 6 hrs
0
10
20
30
40
50
Time (hr)

(b) St52

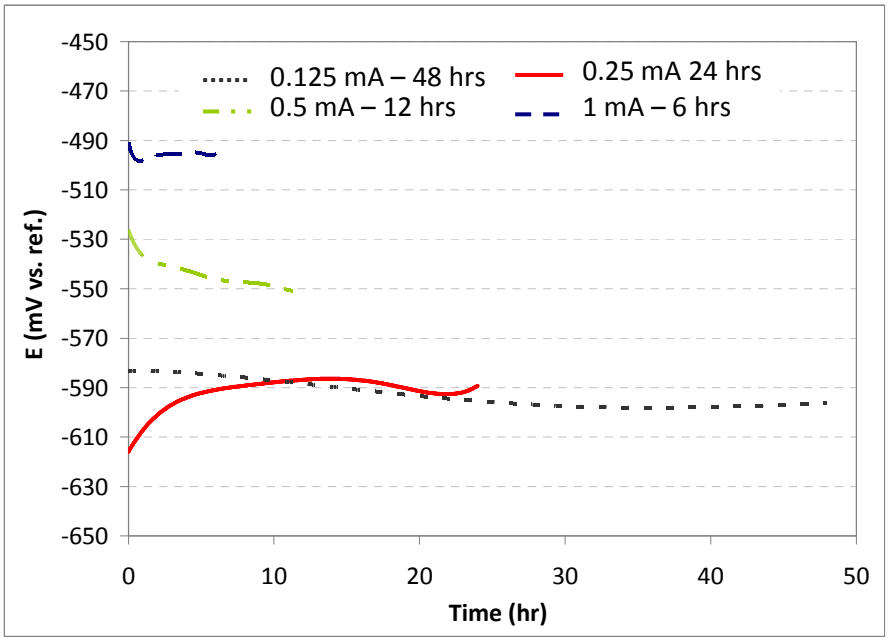


(c) Steel33

**FIGURE 4.13** Responding potentials of the working electrodes which are applied with different current densities for different exposure times

For the short periods with high applied current, it seemed that X-65 and Steel33 electrodes were still not in the equilibrium conditions. It probably needs at least 15 to 20 hours for stabilization. This is also found in the previous experiments.

High applied currents shifted the potentials to be at higher levels as expected. However, the X-65 electrode applied with 0.5 mA/cm$^2$ and St52 with 0.25 mA/cm$^2$ showed significant deviation as their potentials were too low and high, respectively. This could be due to some defects on the surface caused from the surface treatment because it was observed at the starting of the experiments.

The potentials at the end of each condition are shown in Figure 4.14. The figure shows that the potentials declined when decreasing applied currents and prolonging the exposure, except for X-65 which 0.25 mA/cm$^2$ is applied for 24 hours which its potential was surprisingly high. However, it is difficult to get the accurate results of the short-period experiments for the short-period since they did not reach the stabilized state. Comparing the results of different steels shows that the trends going randomly as also experienced in the previous experiments. With high current density of 1 and 0.5 mA/cm$^2$, steel33 had the highest potential followed by St52 and X-65. Lowering the current to 0.25 mA/cm$^2$, the potential of X-65 increased higher

than Steel33 and St52. At the lowest current with the longest exposure time, their potentials are very close. The disagreement is shown when comparing with the results in 4.1 (Figure 4.3). Hence, it cannot draw the general conclusion of the behavior of three steels influenced by the anodic current under these conditions.

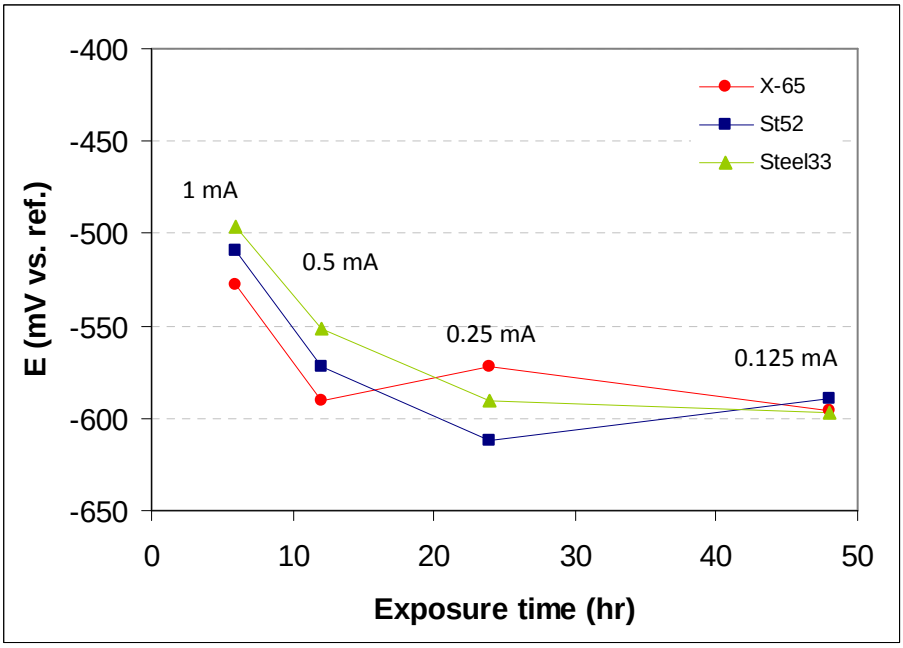


**FIGURE 4.14** Potentials at the end of galvanostatic measurement of the electrodes which are applied with different currents for different exposure time

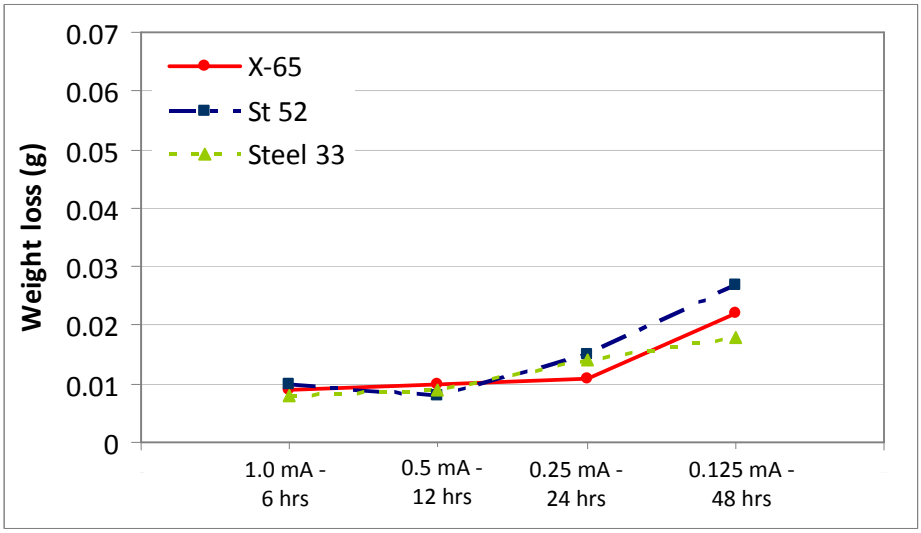


**FIGURE 4.15** Weight losses of specimens which are applied with different anodic current and exposure times

The weight losses of the specimens are listed in Table 4.4. For an overview shown in Figure 4.15, they increased over time in non-linear manner. The weight losses of three steels were closed when applying the highest current 1.0 $mA/cm^2$ for 6 hours and 0.5 $mA/cm^2$ for 12 hours. The significant increase was observed when the steels exposed to the lower current densities for the longer periods.

**TABLE 4.4**

Weight losses, corrosion currents and corrosion rates of the specimens which are applied with different current density and exposure time

| **Applied current (mA/cm2) - Exposure time (hr)** | **X-65** | | | | **St52** | | | | **Steel33** | | | |
|---|---|---|---|---|---|---|---|---|---|---|---|---|
| | **Weight loss method** | | **Polarization method** | | **Weight loss method** | | **Polarization method** | | **Weight loss method** | | **Polarization method** | |
| | WL (g) | CR* (mm/y) | $i_{corr}$ ($mA/cm^2$) | CR** (mm/y) | WL (g) | CR* (mm/y) | $i_{corr}$ ($mA/cm^2$) | CR** (mm/y) | WL (g) | CR* (mm/y) | $i_{corr}$ ($mA/cm^2$) | CR** (mm/y) |
| 1 - 6 | 0.009 | 5.32 | 0.0056 | 0.06 | 0.010 | 5.91 | 0.0100 | 0.12 | 0.008 | 4.73 | 0.0027 | 0.03 |
| 0.5 - 12 | 0.010 | 2.95 | 0.0040 | 0.05 | 0.008 | 2.36 | 0.0110 | 0.13 | 0.009 | 2.66 | 0.0091 | 0.11 |
| 0.25 - 24 | 0.011 | 1.62 | 0.0043 | 0.05 | 0.015 | 2.22 | 0.0031 | 0.04 | 0.014 | 2.07 | 0.0095 | 0.11 |
| 0.125 - 48 | 0.022 | 1.62 | 0.0080 | 0.09 | 0.027 | 1.99 | 0.0056 | 0.06 | 0.018 | 1.33 | 0.0042 | 0.05 |

* Corrosion rate calculated from respectively weight loss

** Corrosion rate calculated from $i_{corr}$

The corrosion rates from both methods are shown in Figure 4.16. The rates obtained from weight loss conversion significantly decreased when reduced the applied current density and increased the exposure time. Based on the fact that the corrosion rate calculated from the weight loss is the average corrosion rate of the specimen over the exposure time, with high applied current densities, the steels corroded very fast resulting in high rates. On the other hand, low applied currents resulted in low corrosion rates.

For polarization, it is difficult to make a conclusion as the values varied in unpredictable manner and also the magnitude is very small. The small differences could be due to the uncertainty of the measurements. Like the previous experiment, the investigation on the surfaced in more detail should be performed.

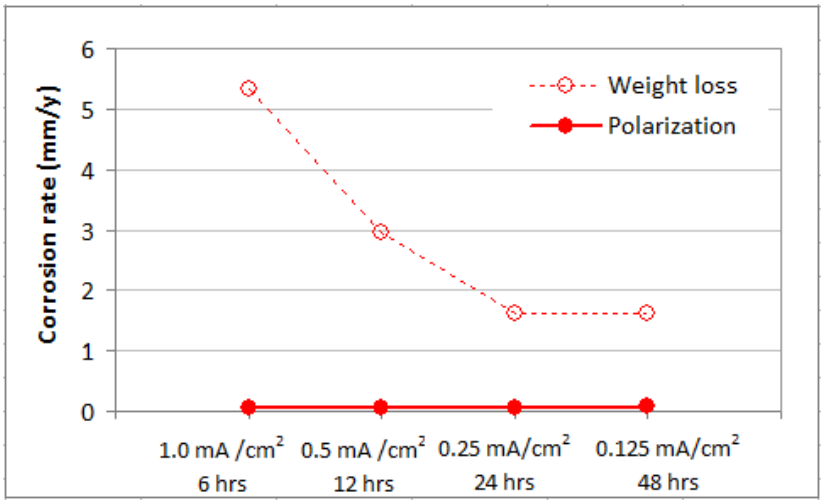


(a) X-65

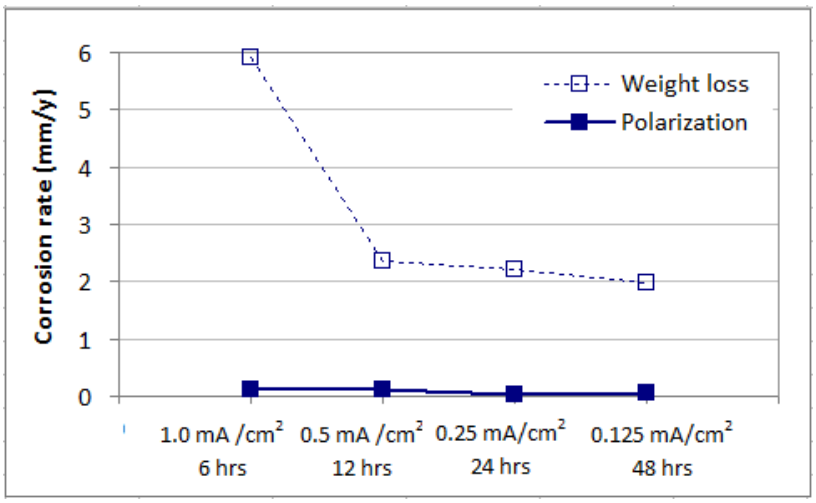


(b) St52

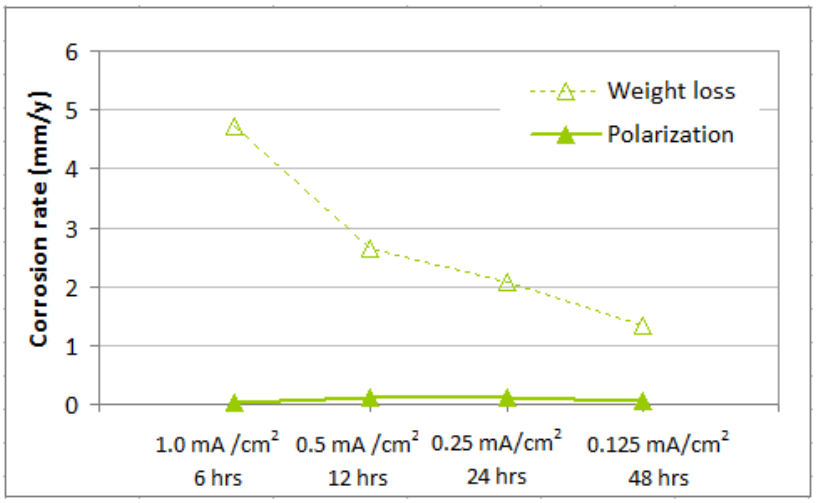


(c) Steel33

**FIGURE 4.16** Corrosion rates of the electrodes applied with different current density for different exposure time

In principle, the metal losses of each kind of steel should be equal except in case over corrosion occurs. As the results in Figure 4.15 showed increasing weight losses, it could probably due to the over corrosion from kinetic reasons that made non-linear relationship between corrosion rate and exposure time.

From the discussion above, it cannot be clarified exactly that if reducing exposure time can be compensated directly by applying the higher current density. It is due to non-linear behavior affected by applied current and exposure time. Therefore, studying the relationship of both parameters and the corrosion behavior should be extended further.

### 4.3 Effect of Chemical Composition and Structure of Steels

Comparison of corrosion behavior of three different steels, in term of weight loss, had been shown in Figure 4.5, 4.11 and 4.15 in the previous sections. Those figures illustrate the metal loss trend of three different steels under different conditions.

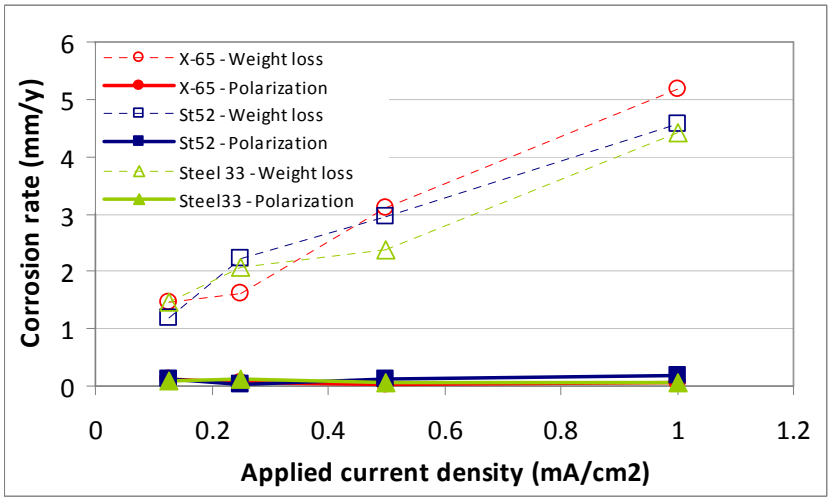


(a) Different current is applied for 24 hours

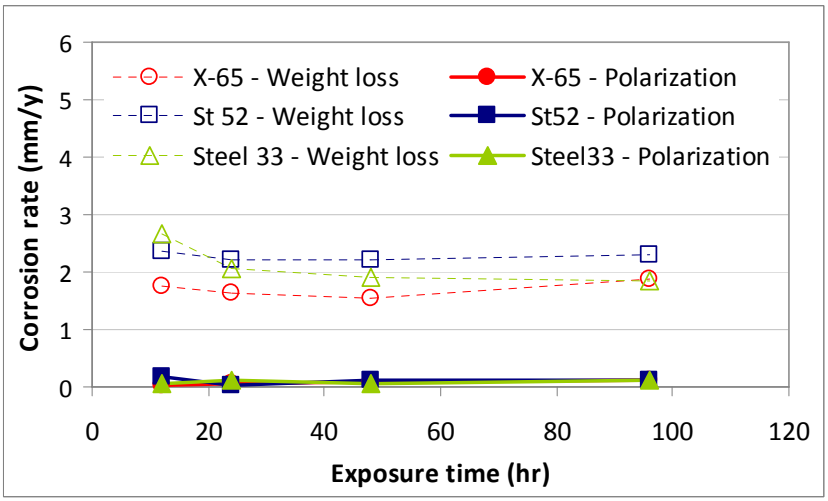


(b) Fixed 0.25 mA/cm$^2$ is applied with different exposure time

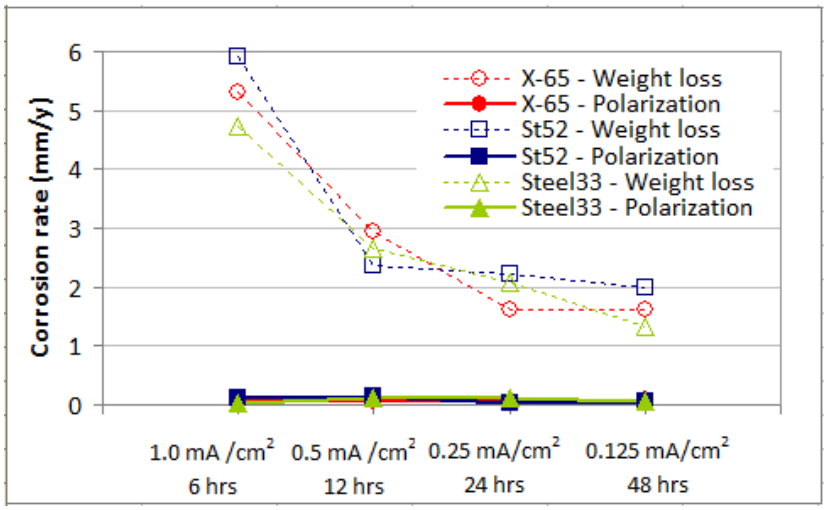


(c) Different current is applied for different exposure time

**FIGURE 4.17** Corrosion rates of the three steels in the different conditions

Figure 4.17 shows the comparison of the corrosion rates of the three steels under different conditions. It is evident that the corrosion rates from polarization of three steels under different conditions are very close and the difference can be neglected. Thus the discussion would be mainly on the results from weight loss.

In figure 4.17 (a) where the electrodes exposed to varied applied anodic current for fixed corrosion periods, three steels had the corrosion rates close to each other. Higher weight losses of St52 than Steel33 were observed. X-65 had low corrosion rate when applying low currents, however the rate increased faster than two other steels when high current (1.0 mA/cm$^2$) is applied.

For Figure 4.17 (b) when the fixed currents is applied for different corrosion periods, St 52 corroded faster than other steels while X-65 seemed to corrode with the lowest rate. In the last case (Figure 4.17 (c)) which both applied current and exposure time are varied, the corrosion rate of Steel33 remained lower than St52. For X-65, its corrosion rates in almost all conditions are also lower than St52 and higher than Steel33.

It is evident that St52 had higher corrosion rate than Steel33 for almost every conditions. It can be explained by the difference of composition of the steels. As listed in Table 3.1, St52 contains higher carbon than Steel33 while Steel33 has much more chromium than St52. This compostion leads to high corrosion rate in St52 and low corrosion rate in Steel33 as it is also observed from many studies [17].

In case of X-65, it can be seen that the corrosion rates of X-65 did not show the general trend compared to the others. Comparing the results of X-65 with St52 which has the same ferritic-pearlitic microstructure, it was expected that St52 would corroded faster than X-65 due to its higher carbon content. However, the corrosion rates of X-65 results showed the inconsistency. Including the results of galvanostatic method, the corrosion of X-65 seemed to be sensitive when the electrodes exposed to the corrosion less than 20 hours where they probably did not reach the equilibrium condition.

Comparing the results from SEM/EDS analysis of the samples applied with the current density of 1.0 $mA/cm^2$ for 24 hours, it was found that the iron carbonate scales was observed on the X-65 specimen only (Figure 4.8). Furthermore, it seemed that the surface of X-65 got more severe damage than the others. The analysis of St52 and Steel33 is shown in Figure 4.18. For St52, there is $Fe_3C$ detected on the surface, but no $FeCO_3$ was observed. The results of Steel33 showed that Cr is contained in the corrosion layer which confirmed the effect of Cr content on the corrosion rate reduction.

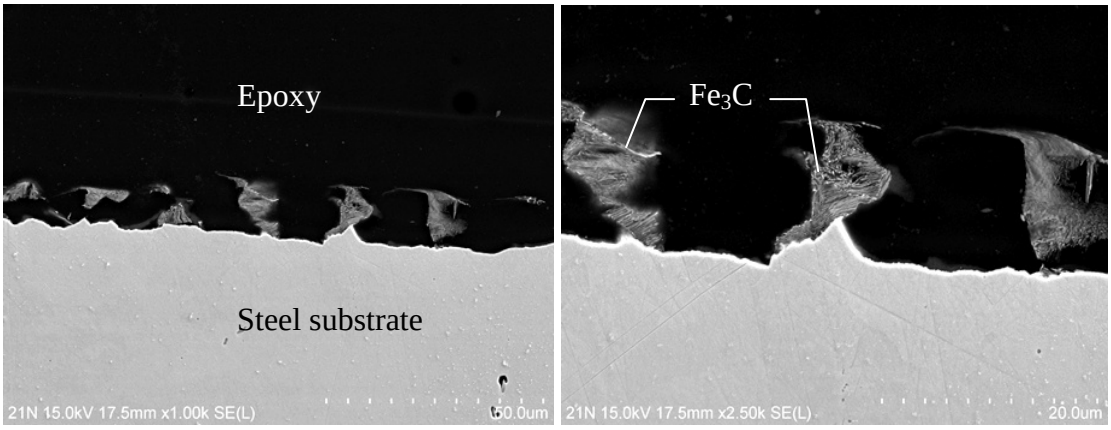


(a) St52

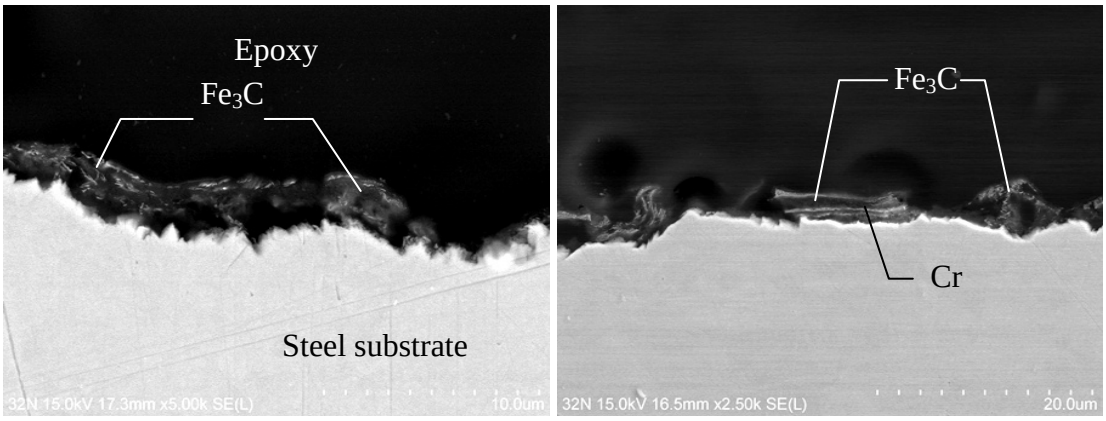


(b) Steel33

**FIGURE 4.18** SEM images of the electrodes which are applied with the anodic current density of 1.0 mA/cm$^2$ for 24 hours

From the discussion above, it can be concluded that Steel33 has lower corrosion rate than St52 due to the addition of carbon and chromium. The behavior of X-65 remains in doubt as its unpredictable weight loss is shown. Therefore, like other researches [17], it is difficult to speculate the exact effects of microstructure and composition of the carbon steels on $CO_2$ corrosion process.

## 5 CONCLUSION

The corrosion behaviors of X-65, St52 and Steel33 specimens under $CO_2$-saturated-NaCl solution are concluded as follow:

1. The applied anodic current density influences the corrosion rate X-65, St52 and Steel33 steels. The corrosion rates increased when applying higher current density.

2. The weight losses of the metals increased with the exposure time.

3. Steel33 has higher corrosion resistance than St52 due to high Cr and low C content. However, the corrosion behavior of X-65 can not be stated clearly compared to St52 and Steel33.

4. Accelerating the corrosion in order to obtain carbide structure in $CO_2$ corrosion can be done by galvanostatically applying anodic current to an electrode.

## REFERENCES


1. Nesic, S., et al., *Mechanistic Modeling for CO2 Corrosion with Protective Iron Carbonate Films*, in *CORROSION 2001*. 2001, NACE International: Houston, Tx.
2. Nesic, S., J. Postlethwaite, and S. Olsen, *An Electrochemical Model for Prediction of Corrosion of Mild Steel in Aqueous Carbon Dioxide Solutions.* Corrosion, 1996. **52**(04).
3. Nesic, S., J. Lee, and V. Ruzic, *A Mechanistic Model of Iron Carbonate Film Growth and the Effect on CO2 Corrosion of Mild Steel*, in *CORROSION 2002*. 2002, NACE International: Denver, Co.
4. Gulbrandsen, E., et al., *Effect of Precorrosion on the Performance of Inhibitors for CO2 Corrosion of Carbon Steel*, in *CORROSION 98*. 1998, NACE International: San Diego Ca.
5. Sun, W., K. Chokshi, and S. Nesic, *Iron Carbonate Scale Growth and the Effect of Inhibition in CO2 Corrosion of Mild Steel*, in *CORROSION 2005*. 2005, NACE International: Houston, Tx.
6. Gao, M., X. Pang, and K. Gao, *The Growth Mechanism of CO2 Corrosion Product Films.* Corrosion Science, 2010.
7. López, D.A., et al., *The Influence of Carbon Steel Microstructure on Corrosion Layers: An XPS and SEM characterization.* Applied Surface Science, 2003. **207**(1-4): p. 69-85.
8. Tretheway, K. and J. Chamberlain, *Corrosion for Science and Engineering*. 2nd ed. 1995, Eastbourne: Pearson Education.
9. Kermani, M.B. and A. Morshed, *Carbon Dioxide Corrosion in Oil and Gas ProductionA Compendium.* Corrosion, 2003. **59**(08).
10. Groysman, A., *Corrosion for Everybody*. 2009: Springer.
11. Ueda, M. and H. Takabe, *Effect of Environmental Factor and Microstructure on Morphology of Corrosion Products in CO2 Environments*, in *CORROSION 99*. 1999, NACE International: San Antonio, Tx.
12. Crolet, J.L., N. Thevenot, and S. Nesic, *Role of Conductive Corrosion Products in the Protectiveness of Corrosion Layers.* Corrosion, 1998. **54**(03).

13. Dugstad, A., H. Hemmer, and M. Seiersten, *Effect of Steel Microstructure on Corrosion Rate and Protective Iron Carbonate Film Formation.* Corrosion, 2001. **57**(04).
14. Pourbaix, M., *Atlas of Electrochemical Equilibria in Aqueous Solutions*. 2nd ed. 1974, Texas.
15. Muralidharan, S., et al., *Influence of Alternating, Direct and Superimposed Alternating and Direct Current on the Corrosion of Mild Steel in Marine Environments.* Desalination, 2007. **216**(1-3): p. 103-115.
16. Mora-Mendoza, J.L. and S. Turgoose, *Fe3C Influence on the Corrosion Rate of Mild Steel in Aqueous CO2 Systems Under Turbulent Flow Conditions.* Corrosion Science, 2002. **44**(6): p. 1223-1246.
17. López, D.A., T. Pérez, and S.N. Simison, *The Influence of Microstructure and Chemical Composition of Carbon and Low Alloy Steels in CO2 Corrosion. A State-of-the-Art Appraisal.* Materials & Design, 2003. **24**(8): p. 561-575.
18. Craig, B.D., D.S. Anderson, and A. International, *Handbook of Corrosion Data*. 1995: ASM International.
19. Korb, P.L.J. and ASM, *ASM Handbook Volume 13: Corrosion*. 1987: ASM International(OH).
20. Al-Hassan, S., et al., *Effect of Microstructure on Corrosion of Steels in Aqueous Solutions Containing Carbon Dioxide.* Corrosion, 1998. **54**(06).
21. Prentice Hall India Pvt., L., *Engineering Materials: Properties and Applications of Metals and Alloys*. 2004: Prentice-Hall of India.
22. Schmitt, G. and M. Horstemeier, *Fundamental Aspects of CO2 Metal Loss Corrosion - Part II: Influence of Different Parameters on CO2 Corrosion Mechanisms*, in *CORROSION 2006*. 2006, NACE International: San Diego Ca.
23. Revie, R.W. and H.H. Uhlig, *Corrosion and Corrosion Control: an Introduction to Corrosion Science and Engineering*. 2008: Wiley-Interscience.
24. Dugstad, A., *Mechanism of Protective Film Formation During CO2 Corrosion of Carbon Steel*, in *CORROSION 98*. 1998, NACE International: San Diego Ca.
25. Zhao, Y.T., et al., *The Mechanical Properties and Corrosion Behaviors of Ultra-Low Carbon Microalloying Steel.* Materials Science and Engineering: A, 2007. **454-455**: p. 695-700.

26. Kateřina, K. and R. Gubner, *Development of Standard Test Method for Investigation of Under-deposit Corrosion in Carbon Dioxide Environment and Its Application in Oil and Gas Industry*, in *CORROSION 2010*. 2010, NACE International: San Antonio, TX.
27. Orden, A.C.V., *Applications and Problem Solving Using the Polarization Technique*, in *CORROSION 98*. 1998, NACE International: San Diego Ca.
28. Aagotnes, N.O., et al., *Comparison of Corrosion Measurements by Use of AC-Impedance, LPR, and Polarization Methods on Carbon Steel in CO2 Purged NaCl Electrolytes*, in *CORROSION 99*. 1999, NACE International: San Antonio, Tx.
29. Roberge, P.R., *Corrosion Inspection and Monitoring*. 2007: Wiley-Interscience.
30. Baboian, R., *Corrosion Tests and Standards: Application and Interpretation*. 2005: ASTM International.
31. ASTM International, *ASTM G102 Standard Practice for Calculation of Corrosion Rates and Related Information from Electrochemical Measurements*. 1999: West Conshohocken, PA.
32. Skoog, D.A., F.J. Holler, and S.R. Crouch, *Principles of Instrumental Analysis*. 2007: Thomson Brooks/Cole.

# APPENDIX

## APPENDIX A Determination of Corrosion Rate

Specimen: X-65 with 1.0 mA/cm$^2$ current density and 24-hour exposure

*Weight loss measurement:*

Using equation (20),

$$CR = \frac{K_1 \bullet W}{A \bullet T \bullet D}$$

when

$K_1 = 8.76 \times 10^4$

$T = 24$ hours

$A = 3.14$ cm$^2$

$W = 0.035$ g, and

$D = 7.87$ g/cm$^3$

thus

$$CR = \frac{8.76 \bullet 10^4 \bullet 0.035}{3.14 \bullet 24 \bullet 7.87}$$

$$= 5.17 \text{ mm/y}$$

*Polarization curve*:

According to ASTM G102 standard, the linear area selected to find the corrosion current should be ±20 mV from the free-corrosion potential. Therefore, the tangent lines are placed as shown in the below figure.

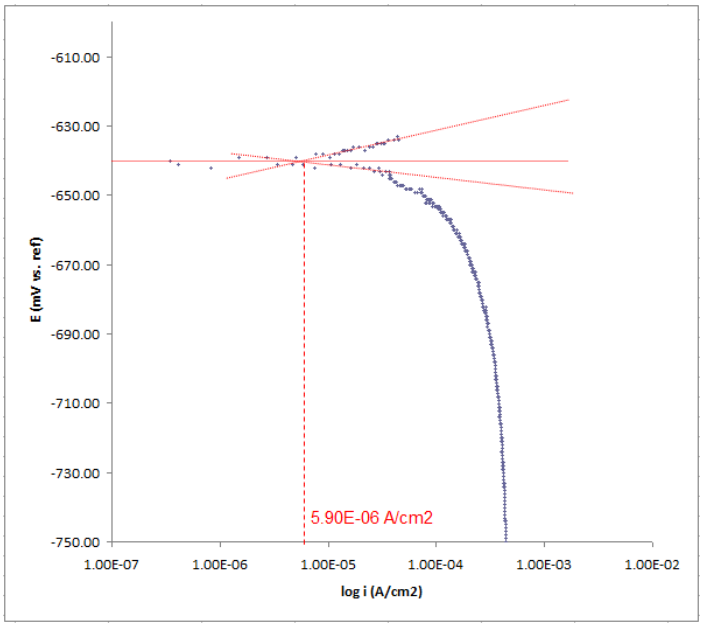


substitute the values of each variable in equation (21)

$$CR = \frac{i_{corr} \cdot K_2 \cdot EW}{D}$$

$i_{corr}$ = 5.9 x $10^{-6}$ A/$cm^2$

$K_2$ = 3.27 x $10^{-3}$

EW = 27.92, and

D = 7.87 g/$cm^3$

thus,

$$CR = \frac{5.9 \cdot 10^{-6} \cdot 3.27 \cdot 10^{-3} \cdot 27.92}{7.87}$$

$$= 0.07 \text{ mm/y}$$

## APPENDIX B SEM/EDS Analysis

### B.1 SEM/EDS analysis of X-65 specimen which is applied 0.125 mA/cm$^2$ current density for 24 hours

Accelerating voltage: 15.0 kV

Magnification: 5000

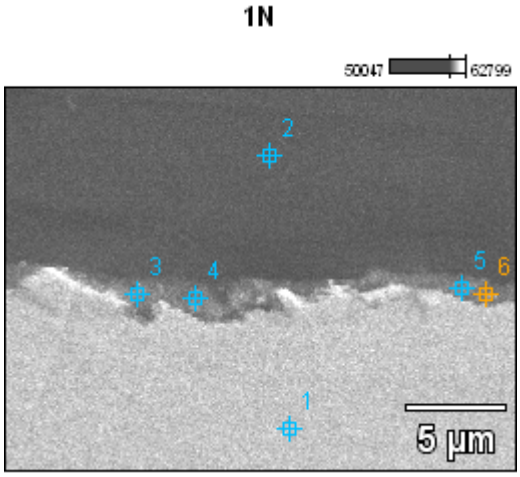


**SEM image**

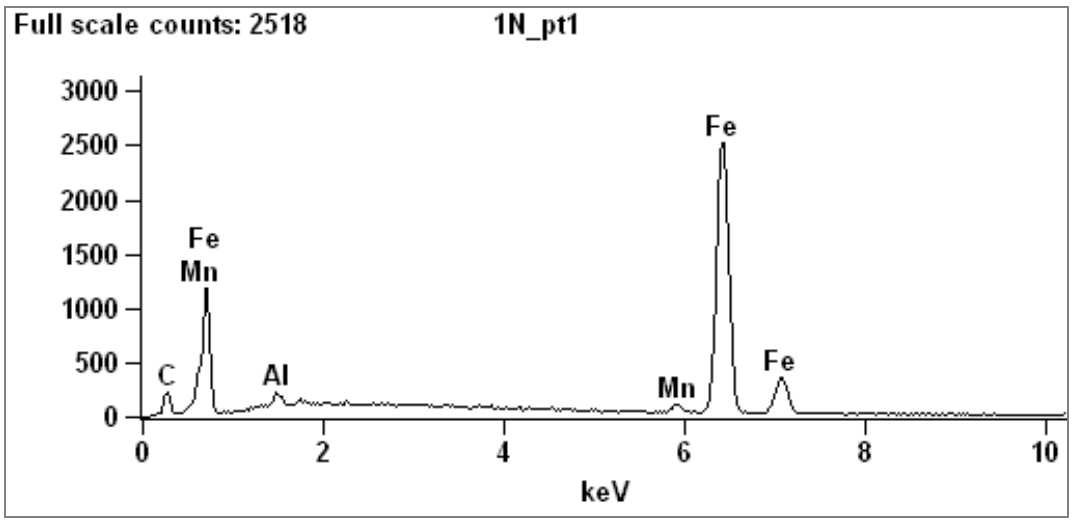

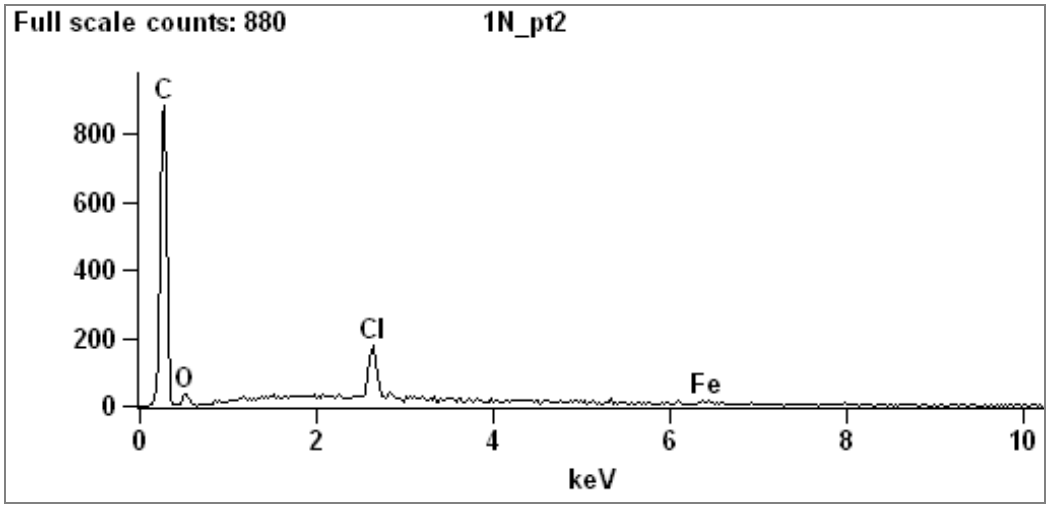
Full scale counts: 880
1N_pt2
C
O
Cl
Fe
800
600
400
200
0
0
2
4
6
8
10
keV

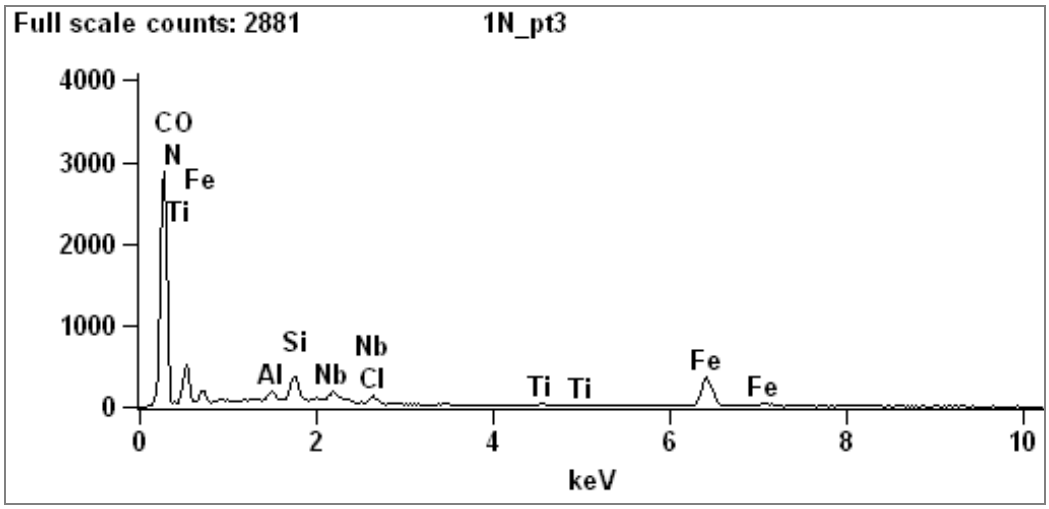
Full scale counts: 2881
1N_pt3
CO
N
Fe
Ti
Si
Al
Nb
Nb
Cl
Ti
Ti
Fe
Fe
4000
3000
2000
1000
0
0
2
4
6
8
10
keV

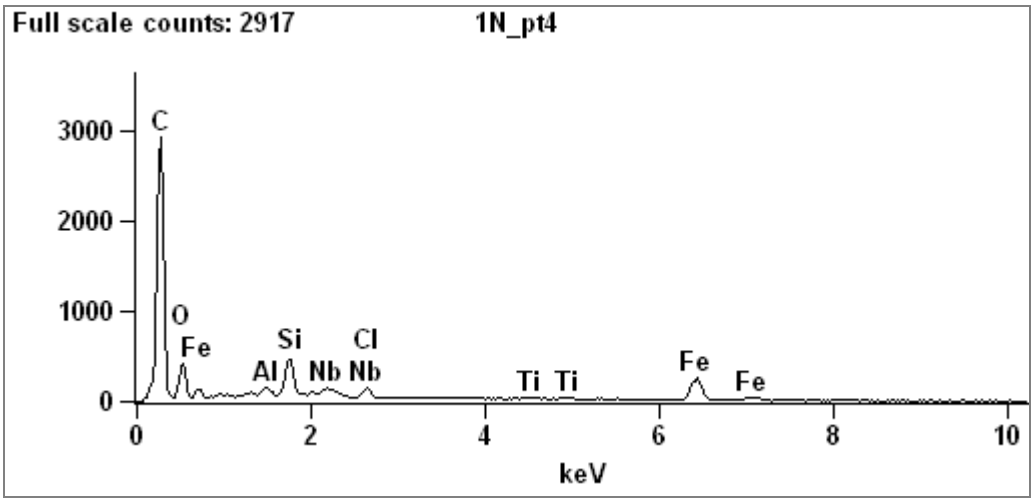
Full scale counts: 2917
1N_pt4
C
O
Fe
Si
Al
Cl
Nb
Nb
Ti
Ti
Fe
Fe
3000
2000
1000
0
0
2
4
6
8
10
keV

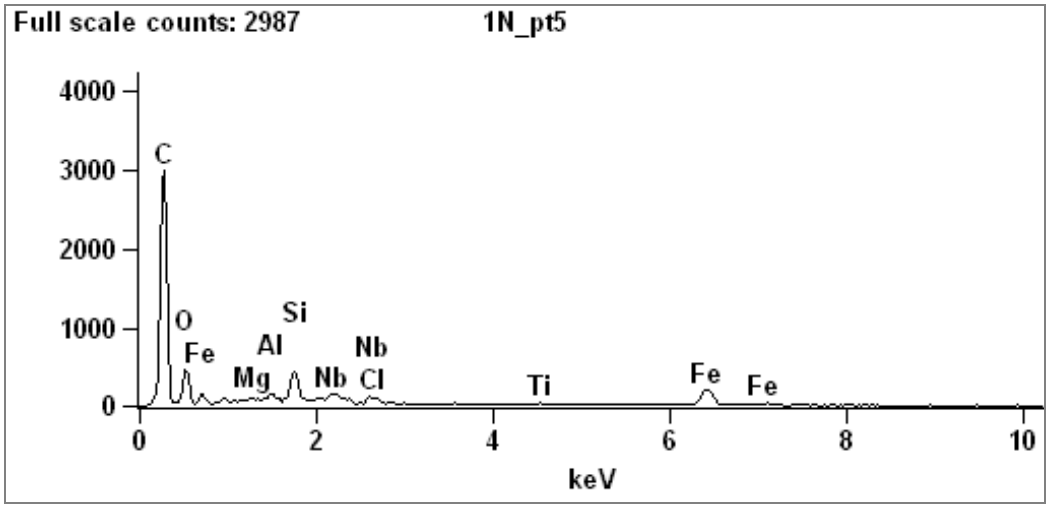


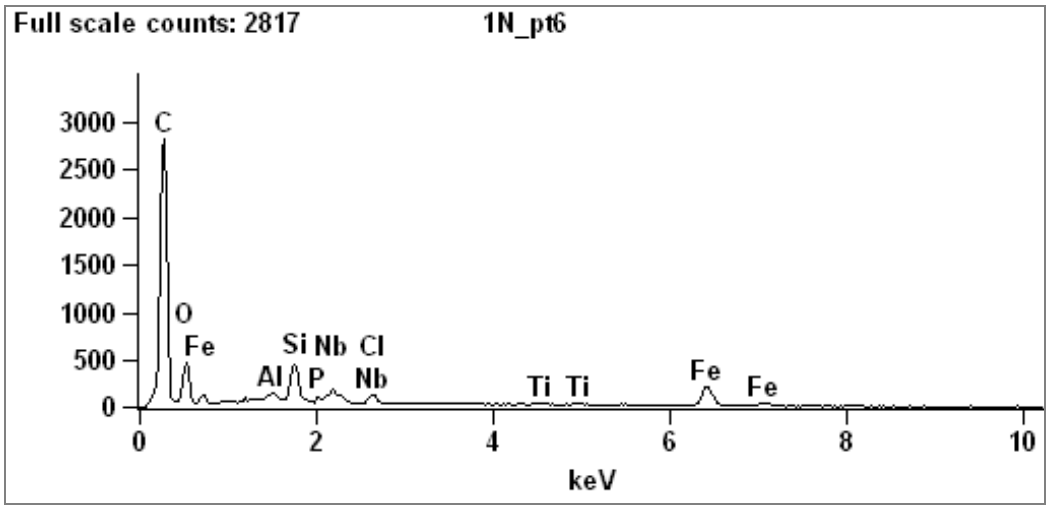


**Atom %**

| | *C-K* | *N-K* | *O-K* | *Mg-K* | *Al-K* | *Si-K* | *P-K* | *Cl-K* | *Ti-K* | *Mn-K* | *Fe-K* | *Nb-L* |
|---|---|---|---|---|---|---|---|---|---|---|---|---|
| ***1N_pt1*** | 36.30 | | | | 1.42 | | | | | 1.15 | 61.12 | |
| ***1N_pt2*** | 92.14 | | 6.00 | | | | | 1.56 | | | 0.30 | |
| ***1N_pt3*** | 66.15 | 10.68 | 19.58 | | 0.21 | 0.53 | | 0.19 | 0.11 | | 2.43 | 0.13 |
| ***1N_pt4*** | 80.07 | | 16.34 | | 0.17 | 0.83 | | 0.26 | 0.06 | | 2.14 | 0.13 |
| ***1N_pt5*** | 78.54 | | 18.10 | 0.05 | 0.16 | 0.78 | | 0.25 | 0.11 | | 1.88 | 0.15 |
| ***1N_pt6*** | 78.70 | | 18.14 | | 0.17 | 0.80 | 0.04 | 0.21 | 0.07 | | 1.66 | 0.21 |

**B.2 SEM/EDS analysis of X-65 specimen which is applied 1.0 mA/cm$^2$ current density for 24 hours**

Accelerating voltage: 15.0 kV

Magnification: 2500

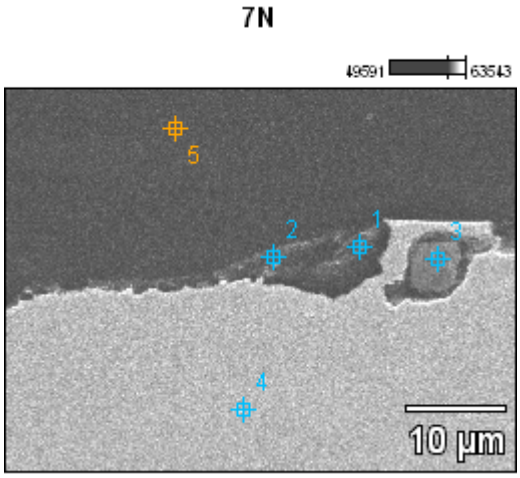


**SEM image**

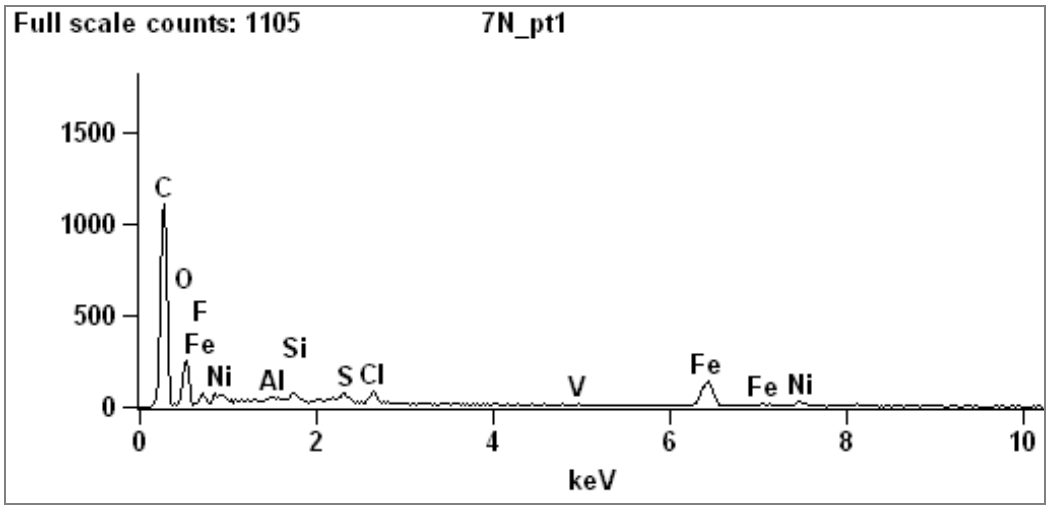

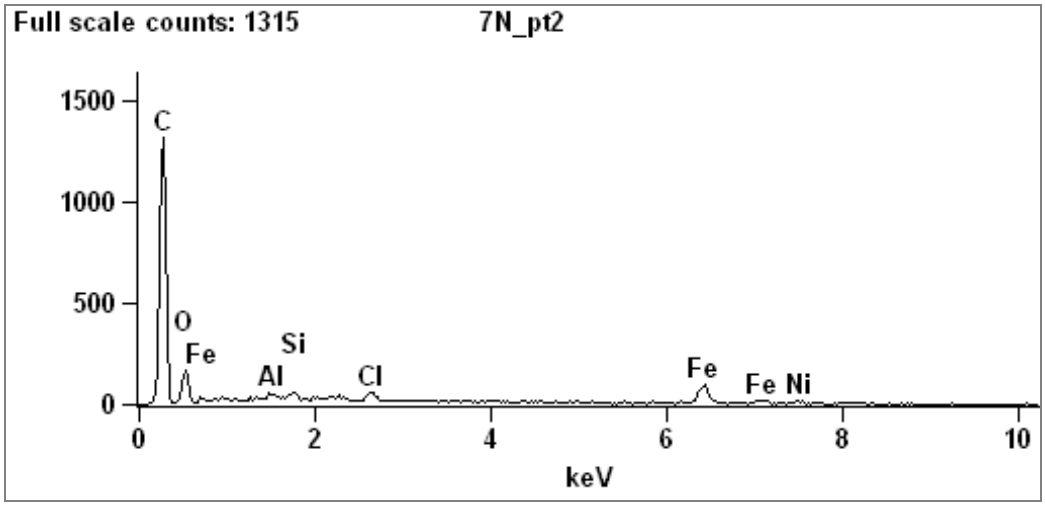
Full scale counts: 1315
7N_pt2
1500
1000
500
0
C
O
Fe
Al
Si
Cl
Fe
Fe Ni
0
2
4
6
8
10
keV

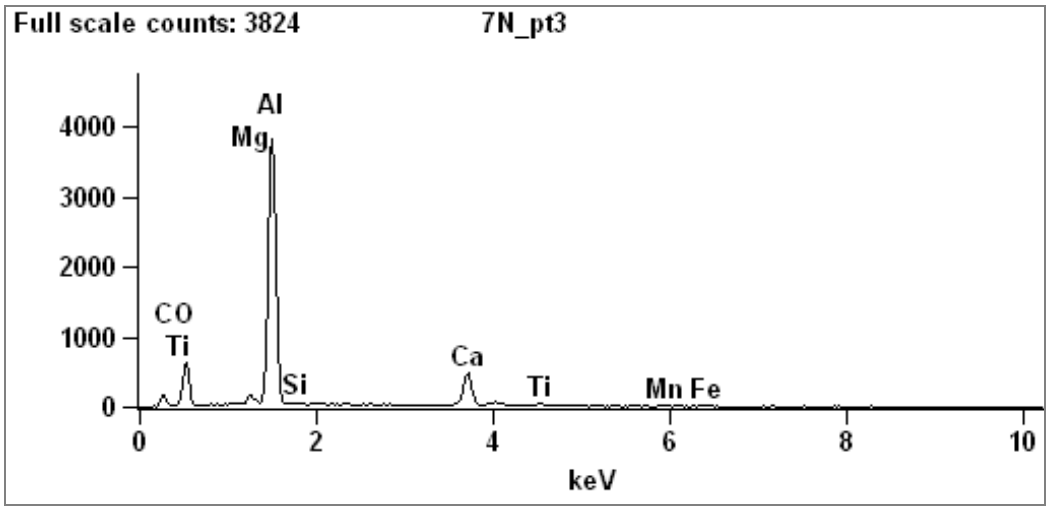
Full scale counts: 3824
7N_pt3
4000
3000
2000
1000
0
Al
Mg
CO
Ti
Si
Ca
Ti
Mn Fe
0
2
4
6
8
10
keV

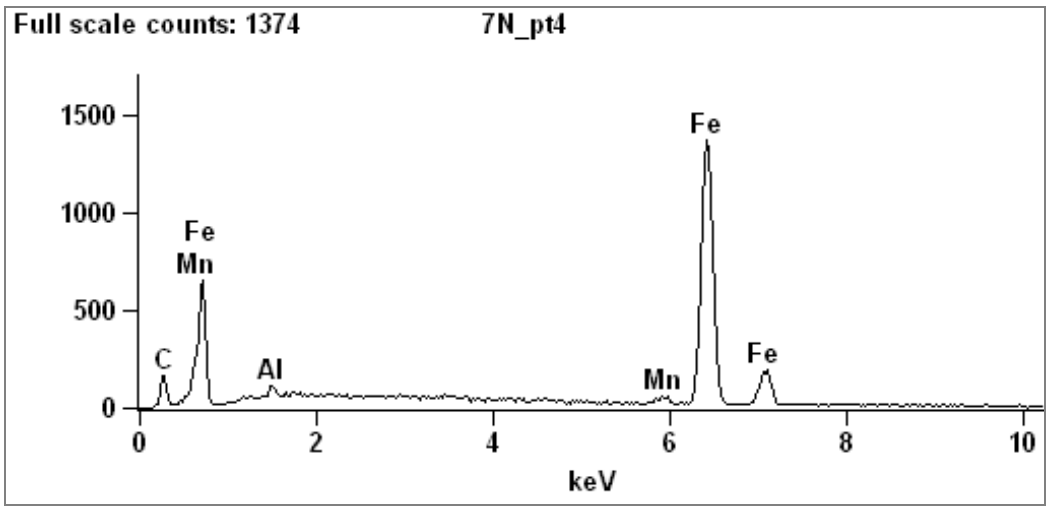
Full scale counts: 1374
7N_pt4
1500
1000
500
0
Fe
Mn
C
Al
Mn
Fe
0
2
4
6
8
10
keV

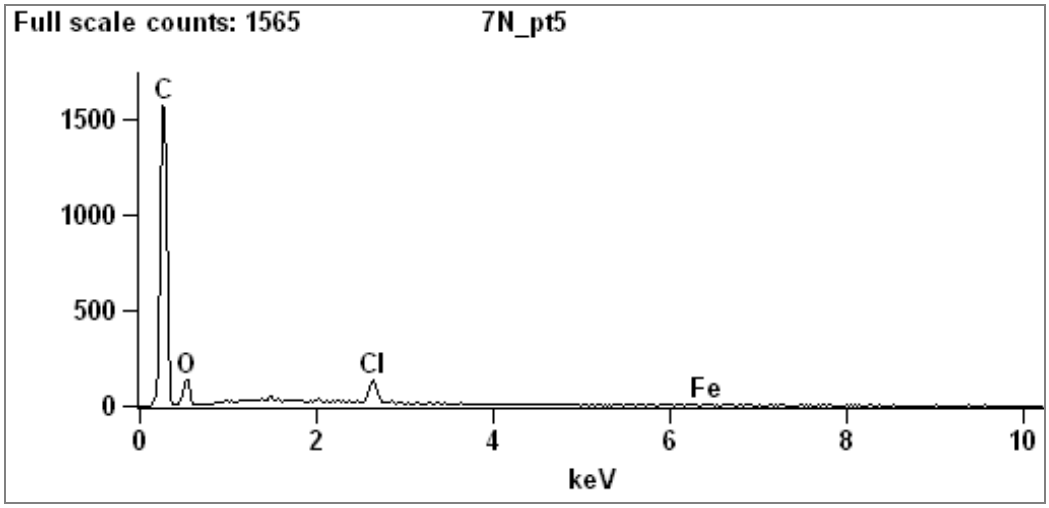


Atom %

| | C-K | O-K | F-K | Mg-K | Al-K | Si-K | S-K | Cl-K | Ca-K | Ti-K | V-K | Mn-K | Fe-K | Ni-K |
|---|---|---|---|---|---|---|---|---|---|---|---|---|---|---|
| ***7N_pt1*** | 72.88 | 22.02 | 0.65 | | 0.14 | 0.20 | 0.23 | 0.33 | | | 0.08 | | 2.69 | 0.79 |
| ***7N_pt2*** | 79.40 | 17.94 | | | 0.08 | 0.11 | | 0.37 | | | | | 1.82 | 0.27 |
| ***7N_pt3*** | 27.82 | 45.54 | | 0.69 | 21.16 | 0.23 | | | 3.78 | 0.29 | | 0.09 | 0.40 | |
| ***7N_pt4*** | 43.06 | | | | 1.11 | | | | | | | 1.03 | 54.80 | |
| ***7N_pt5*** | 83.77 | 15.34 | | | | | | 0.73 | | | | | 0.16 | |

**B.3 SEM/EDS analysis of St52 specimen which is applied 1.0 mA/cm$^2$ current density for 24 hours**

Accelerating voltage: 15.0 kV

Magnification: 2500

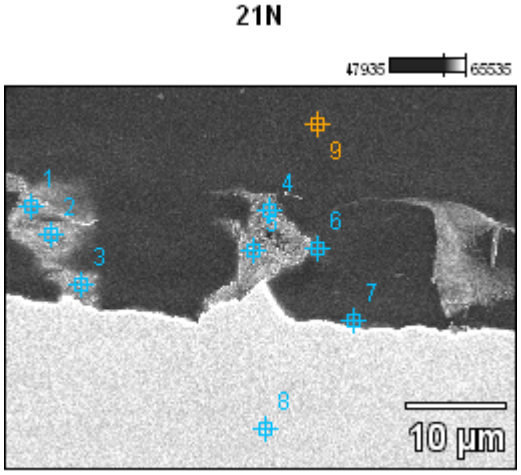


**SEM image**

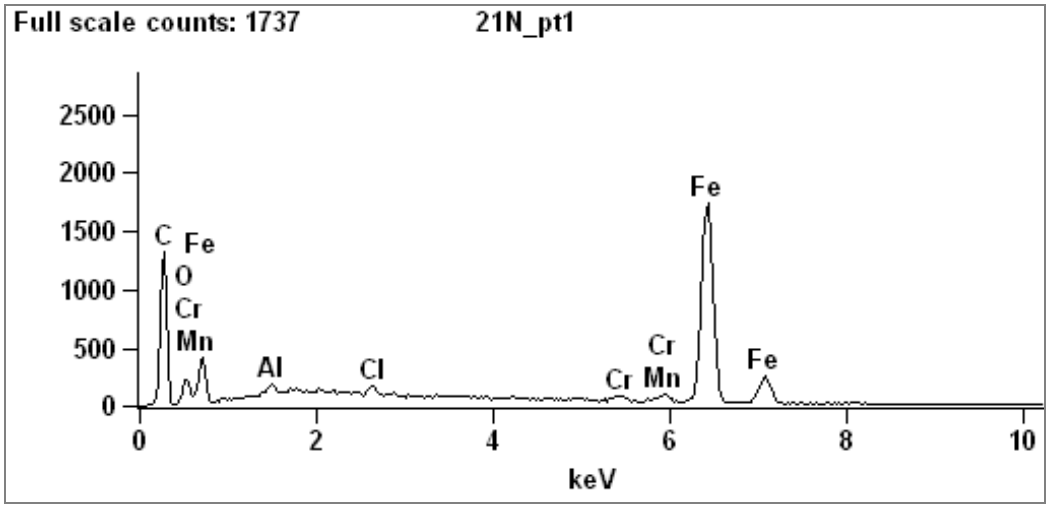
Full scale counts: 1737
21N_pt1
2500
2000
1500
1000
500
0
C
Fe
O
Cr
Mn
Al
Cl
Cr
Cr
Mn
Fe
Fe
0
2
4
6
8
10
keV

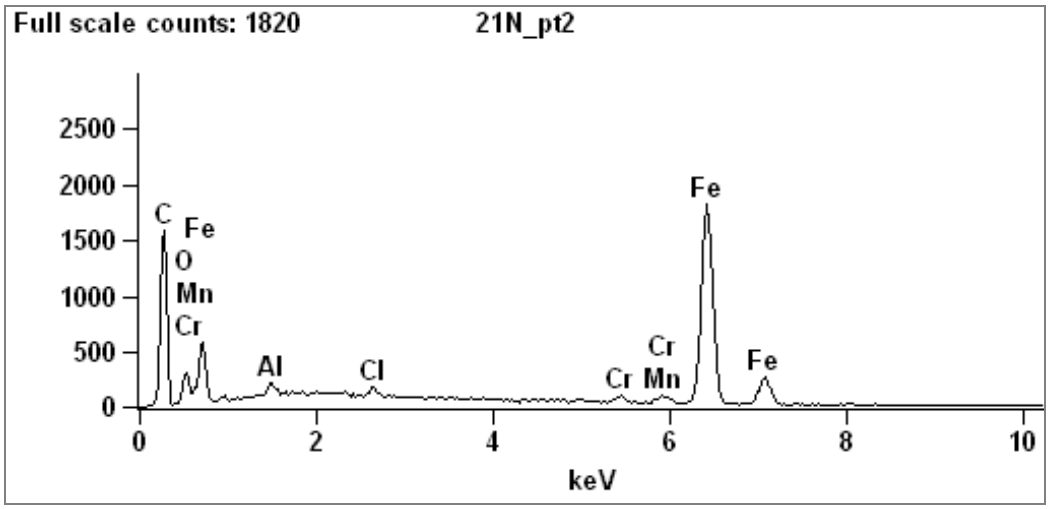
Full scale counts: 1820
21N_pt2
2500
2000
1500
1000
500
0
C
Fe
O
Mn
Cr
Al
Cl
Cr
Cr
Mn
Fe
Fe
0
2
4
6
8
10
keV

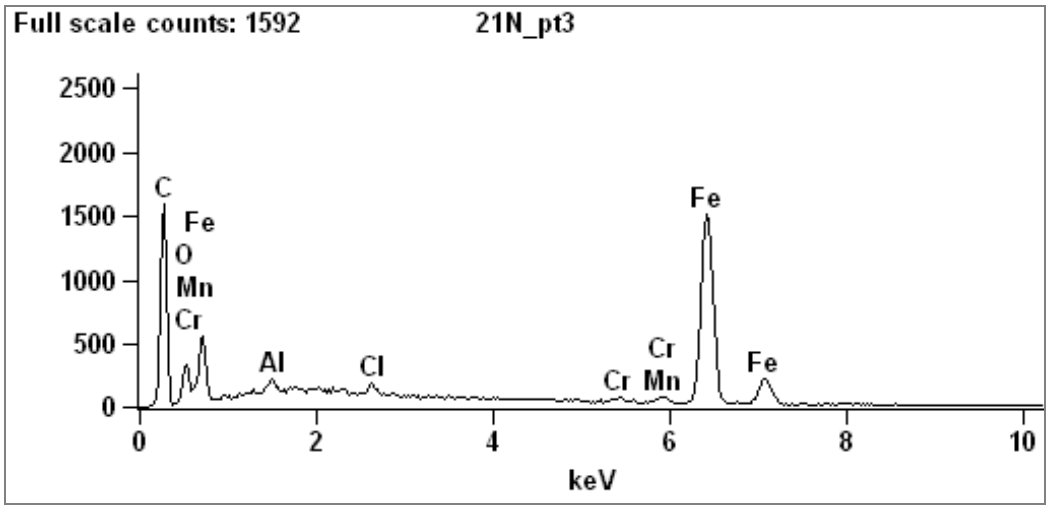
Full scale counts: 1592
21N_pt3
2500
2000
1500
1000
500
0
C
Fe
O
Mn
Cr
Al
Cl
Cr
Cr
Mn
Fe
Fe
0
2
4
6
8
10
keV

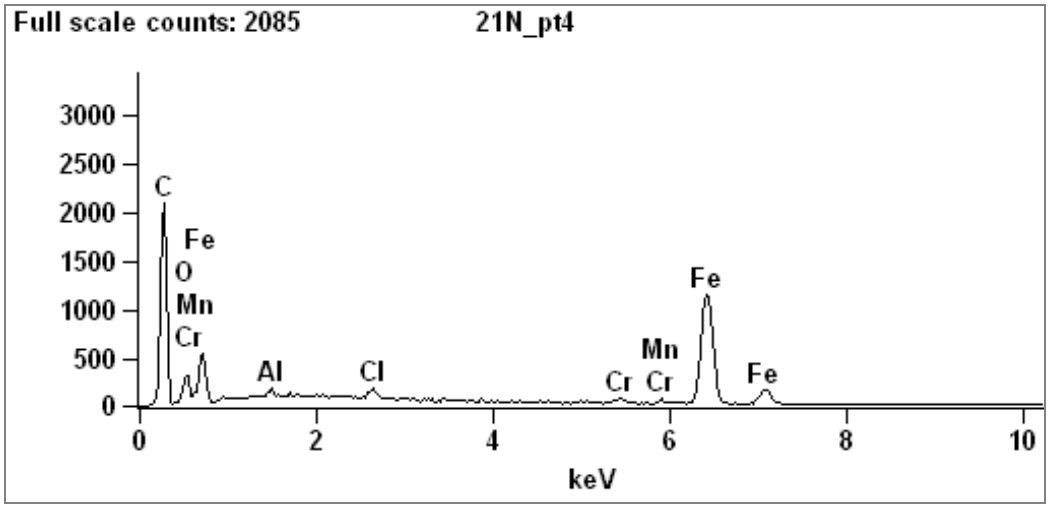
Full scale counts: 2085
21N_pt4
3000
2500
2000
1500
1000
500
0
C
Fe
O
Mn
Cr
Al
Cl
Cr
Mn
Cr
Fe
Fe
0
2
4
6
8
10
keV

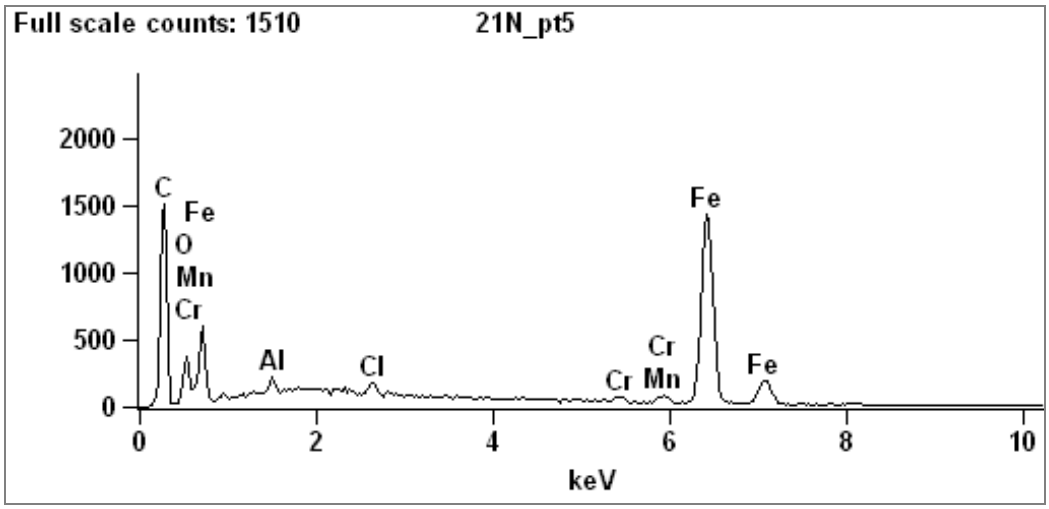
Full scale counts: 1510
21N_pt5
2000
1500
1000
500
0
C
Fe
O
Mn
Cr
Al
Cl
Cr
Cr
Mn
Fe
Fe
0
2
4
6
8
10
keV

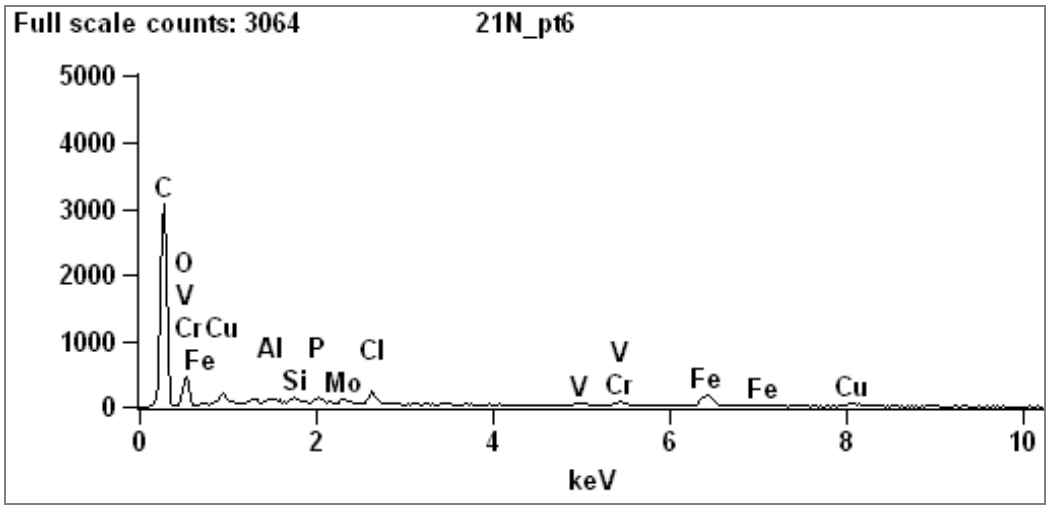
Full scale counts: 3064
21N_pt6
5000
4000
3000
2000
1000
0
C
O
V
Cr
Cu
Fe
Al
Si
P
Mo
Cl
V
V
Cr
Fe
Fe
Cu
0
2
4
6
8
10
keV

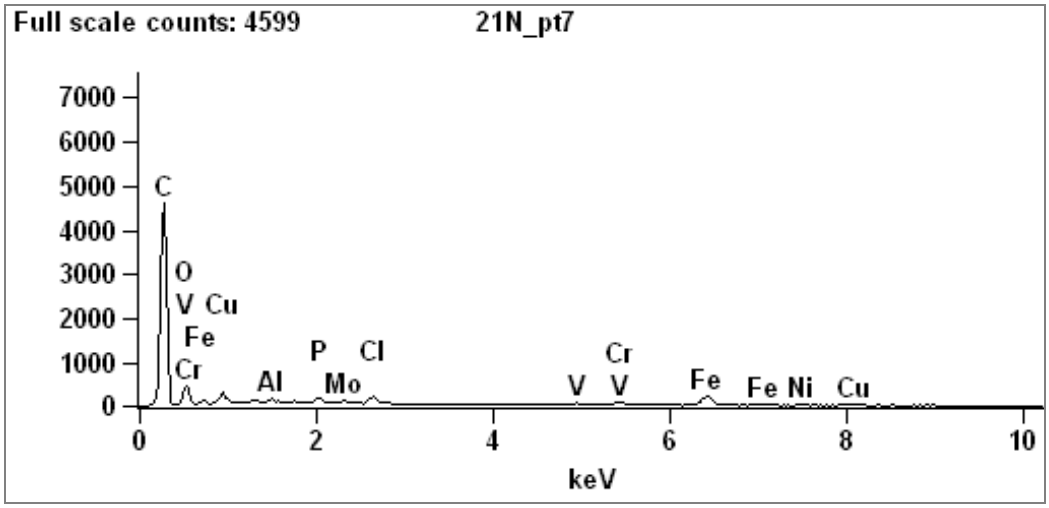
Full scale counts: 4599
21N_pt7
7000
6000
5000
4000
3000
2000
1000
0
C
O
V Cu
Fe
Cr
Al
P
Mo
Cl
V
Cr
V
Fe
Fe Ni
Cu
0
2
4
6
8
10
keV

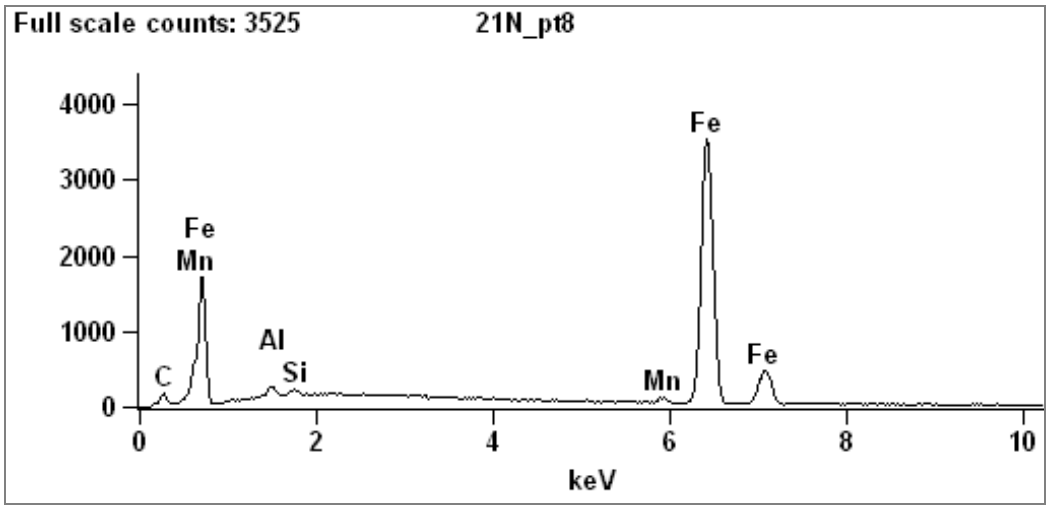
Full scale counts: 3525
21N_pt8
4000
3000
2000
1000
0
Fe
Mn
C
Al
Si
Mn
Fe
Fe
0
2
4
6
8
10
keV

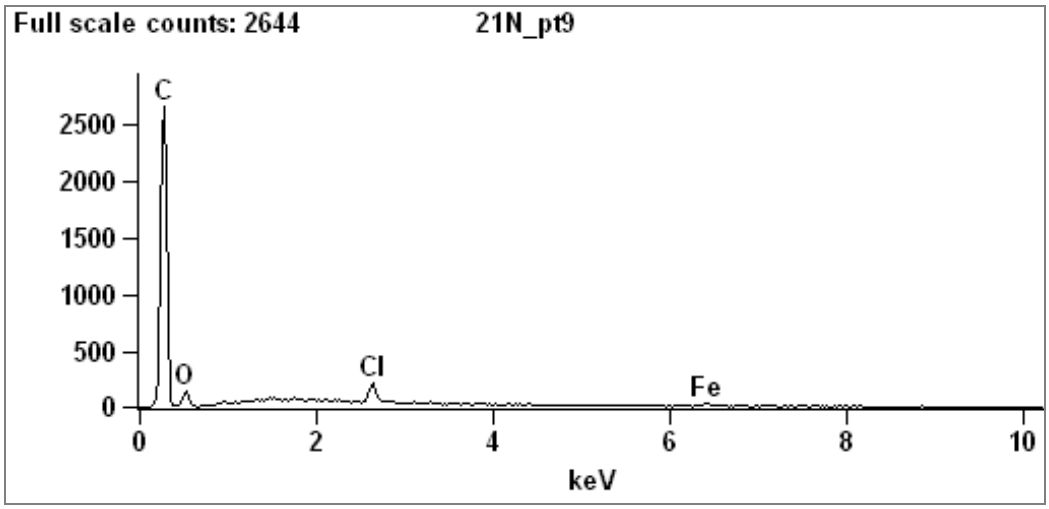
Full scale counts: 2644
21N_pt9
2500
2000
1500
1000
500
0
C
O
Cl
Fe
0
2
4
6
8
10
keV

Atom %

| | C-K | O-K | Al-K | Si-K | P-K | Cl-K | V-K | Cr-K | Mn-K | Fe-K | Ni-K | Cu-K | Mo-L |
|---|---|---|---|---|---|---|---|---|---|---|---|---|---|
| ***21N_pt1*** | 70.70 | 8.75 | 0.25 | | | 0.24 | | 0.31 | 0.76 | 19.01 | | | |
| ***21N_pt2*** | 71.17 | 10.26 | 0.35 | | | 0.17 | | 0.26 | 0.51 | 17.27 | | | |
| ***21N_pt3*** | 70.92 | 12.00 | 0.31 | | | 0.28 | | 0.16 | 0.47 | 15.86 | | | |
| ***21N_pt4*** | 76.35 | 11.59 | 0.18 | | | 0.31 | | 0.28 | 0.27 | 11.01 | | | |
| ***21N_pt5*** | 70.98 | 13.20 | 0.24 | | | 0.22 | | 0.25 | 0.51 | 14.60 | | | |
| ***21N_pt6*** | 78.77 | 17.59 | 0.09 | 0.10 | 0.12 | 0.38 | 0.30 | 0.34 | | 1.59 | | 0.66 | 0.07 |
| ***21N_pt7*** | 82.44 | 14.36 | 0.07 | | 0.13 | 0.29 | 0.21 | 0.33 | | 1.38 | 0.12 | 0.57 | 0.09 |
| ***21N_pt8*** | 24.90 | | 1.04 | 0.44 | | | | | 1.13 | 72.48 | | | |
| ***21N_pt9*** | 88.58 | 10.50 | | | | 0.68 | | | | 0.23 | | | |

**B.4 SEM/EDS analysis of Steel33 specimen which is applied 1.0 mA/cm$^2$ current density for 24 hours**

Accelerating voltage: 15.0 kV

Magnification: 5000

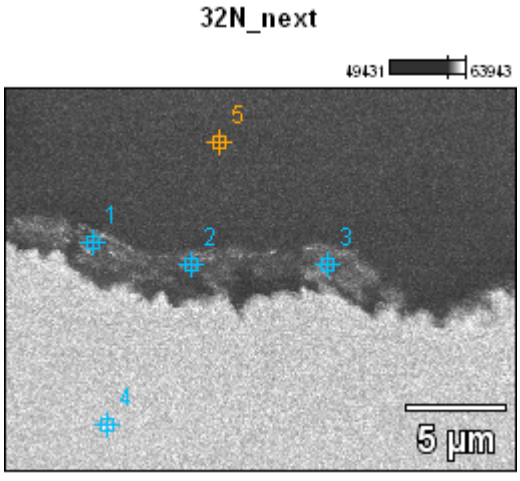


**SEM image**

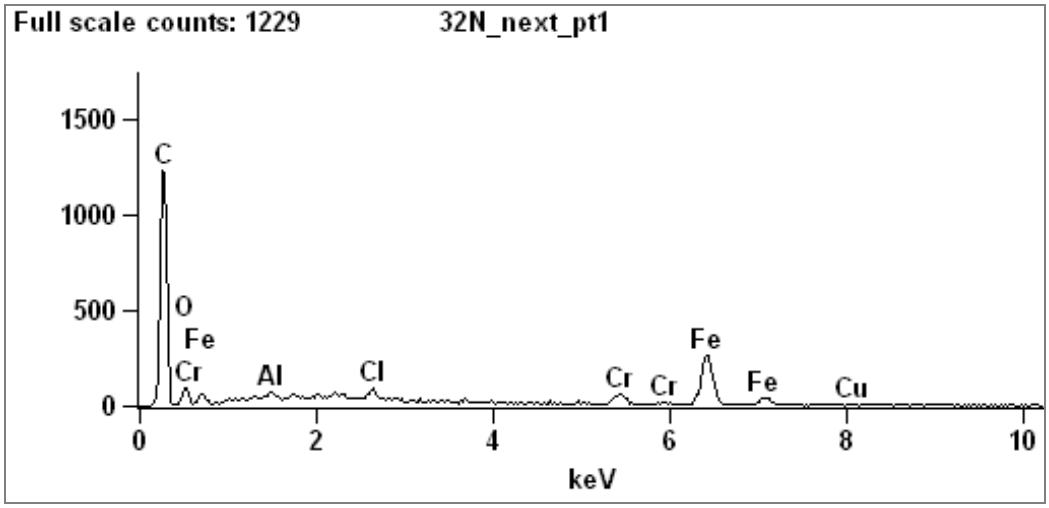
Full scale counts: 1229
32N_next_pt1
1500
1000
500
0
C
O
Fe
Cr
Al
Cl
Cr
Cr
Fe
Fe
Cu
0
2
4
6
8
10
keV

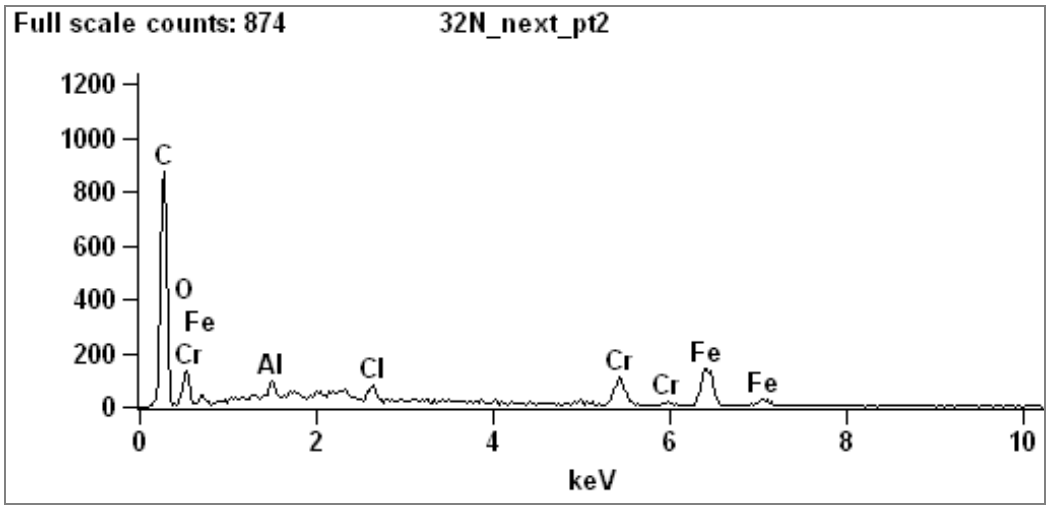
Full scale counts: 874
32N_next_pt2
1200
1000
800
600
400
200
0
C
O
Fe
Cr
Al
Cl
Cr
Cr
Fe
Fe
0
2
4
6
8
10
keV

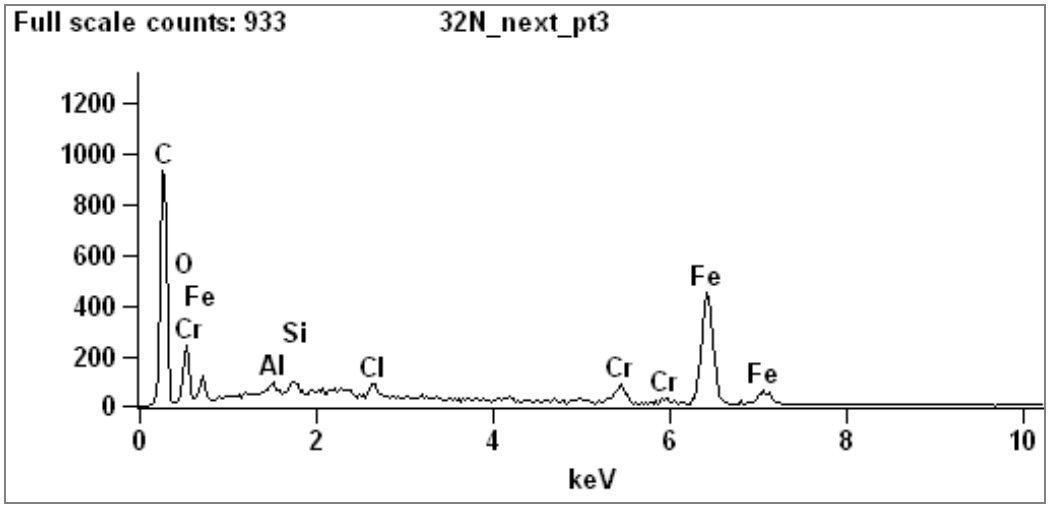
Full scale counts: 933
32N_next_pt3
1200
1000
800
600
400
200
0
C
O
Fe
Cr
Si
Al
Cl
Cr
Cr
Fe
Fe
0
2
4
6
8
10
keV

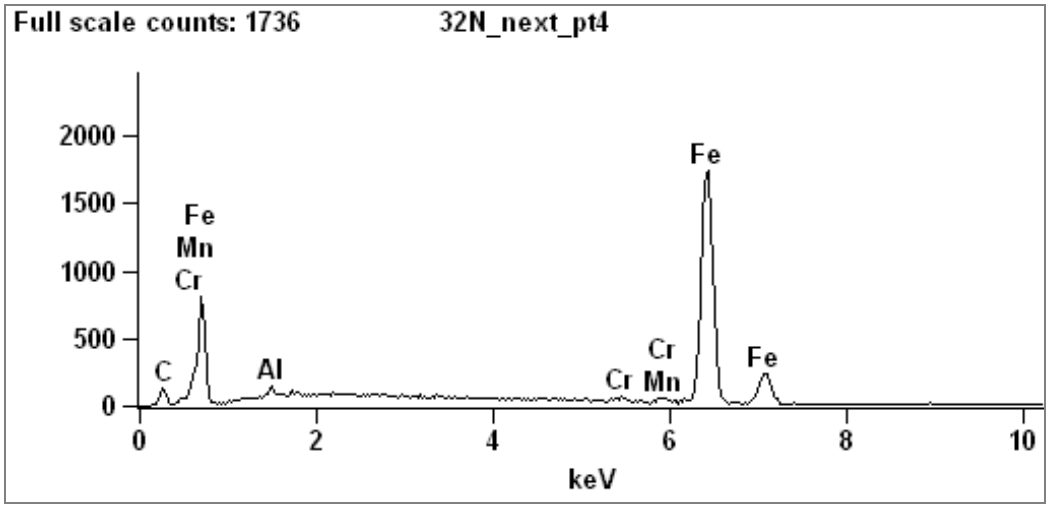


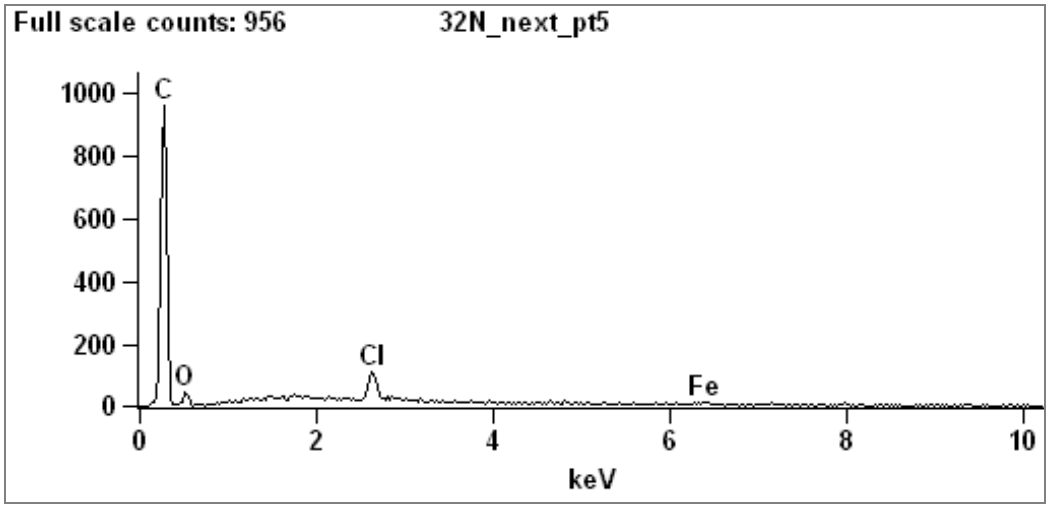


Atom %

| | C-K | O-K | Al-K | Si-K | Cl-K | Cr-K | Mn-K | Fe-K | Cu-K |
|---|---|---|---|---|---|---|---|---|---|
| ***32N_next_pt1*** | 84.72 | 8.58 | 0.18 | | 0.39 | 0.63 | | 5.33 | 0.16 |
| ***32N_next_pt2*** | 79.54 | 13.90 | 0.32 | | 0.60 | 1.57 | | 4.08 | |
| ***32N_next_pt3*** | 74.03 | 15.71 | 0.25 | 0.26 | 0.33 | 0.79 | | 8.63 | |
| ***32N_next_pt4*** | 30.71 | | 1.14 | | | 0.58 | 1.11 | 66.47 | |
| ***32N_next_pt5*** | 90.79 | 7.82 | | | 1.16 | | | 0.23 | |

Accelerating voltage: 15.0 kV

Magnification: 5000

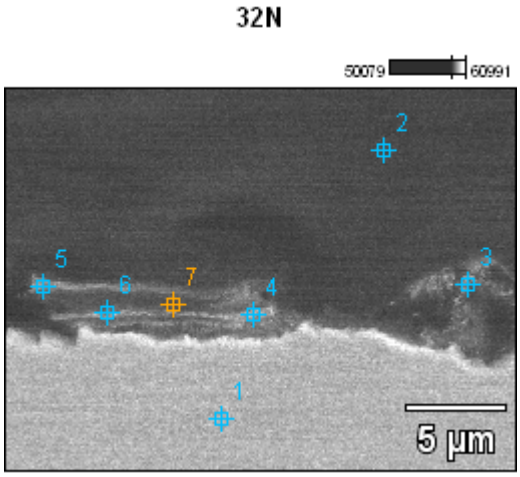


**SEM image**

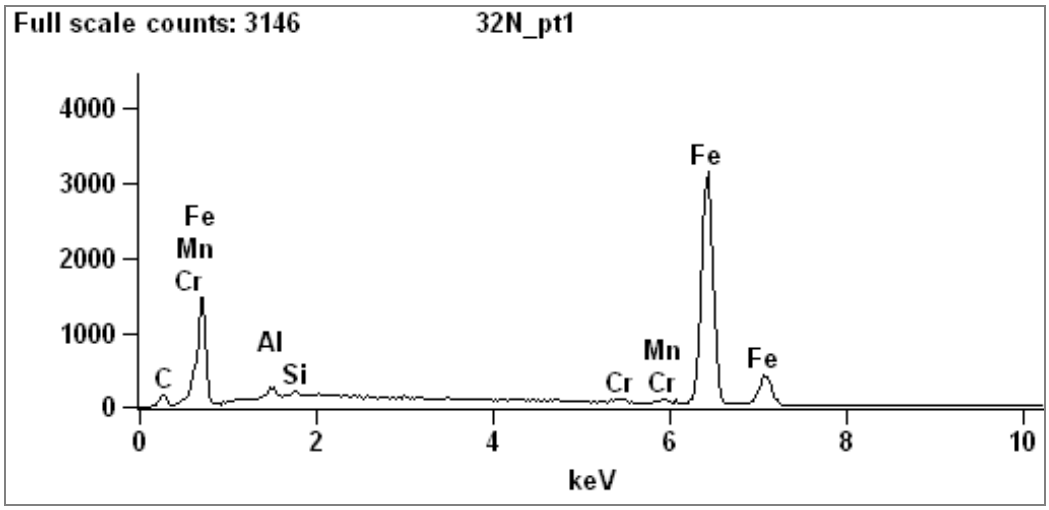


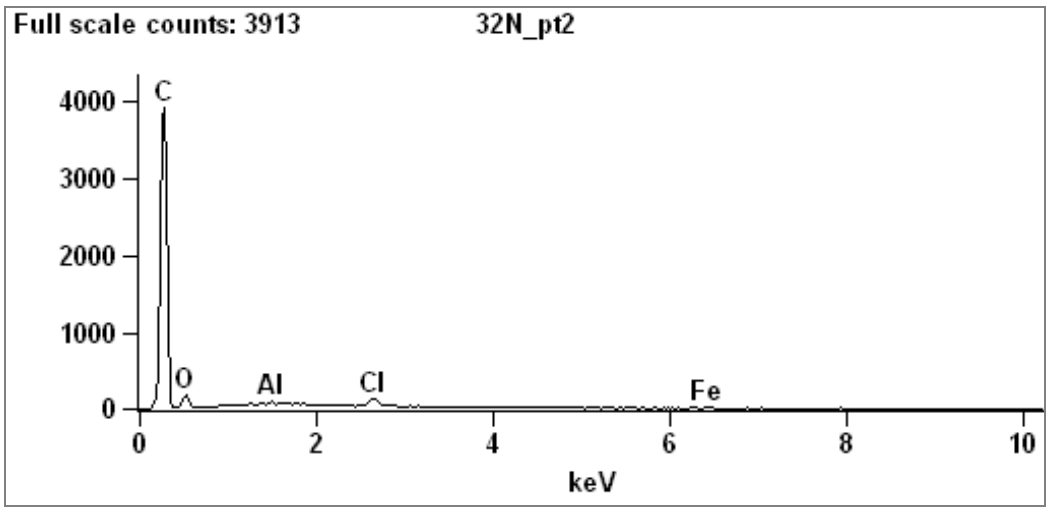

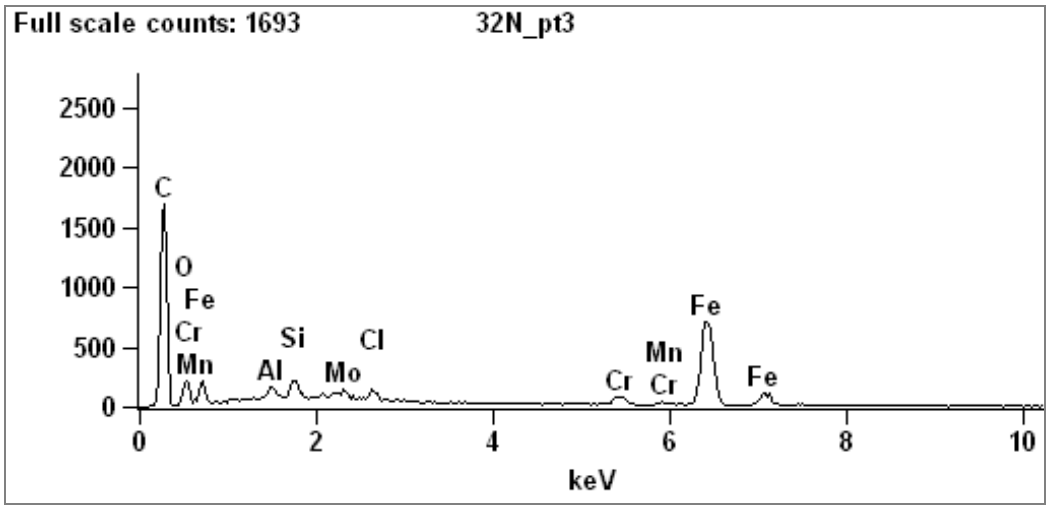
Full scale counts: 1693
32N_pt3
2500
2000
1500
1000
500
0
C
O
Fe
Cr
Mn
Al
Si
Mo
Cl
Cr
Mn
Cr
Fe
Fe
0
2
4
6
8
10
keV

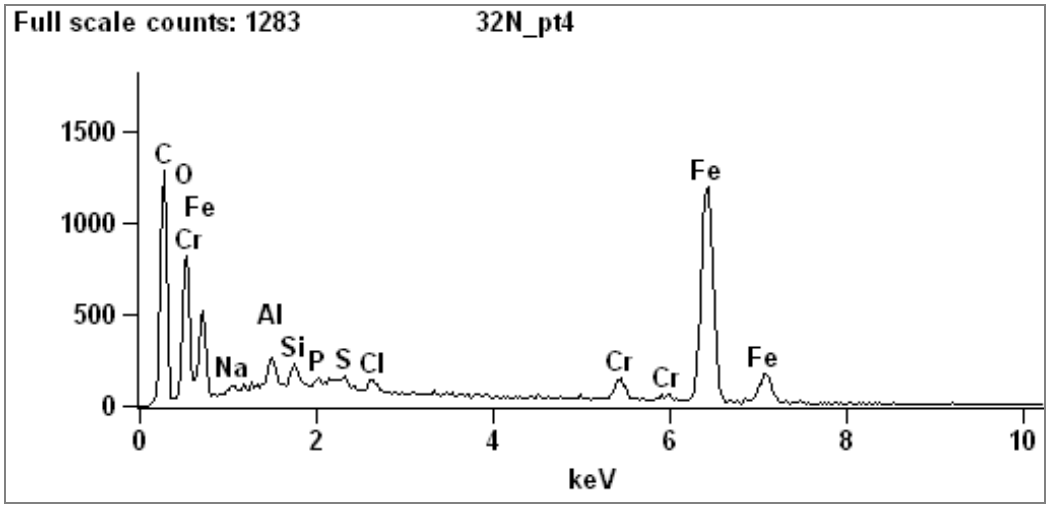
Full scale counts: 1283
32N_pt4
1500
1000
500
0
C
O
Fe
Cr
Na
Al
Si
P
S
Cl
Cr
Cr
Fe
Fe
0
2
4
6
8
10
keV

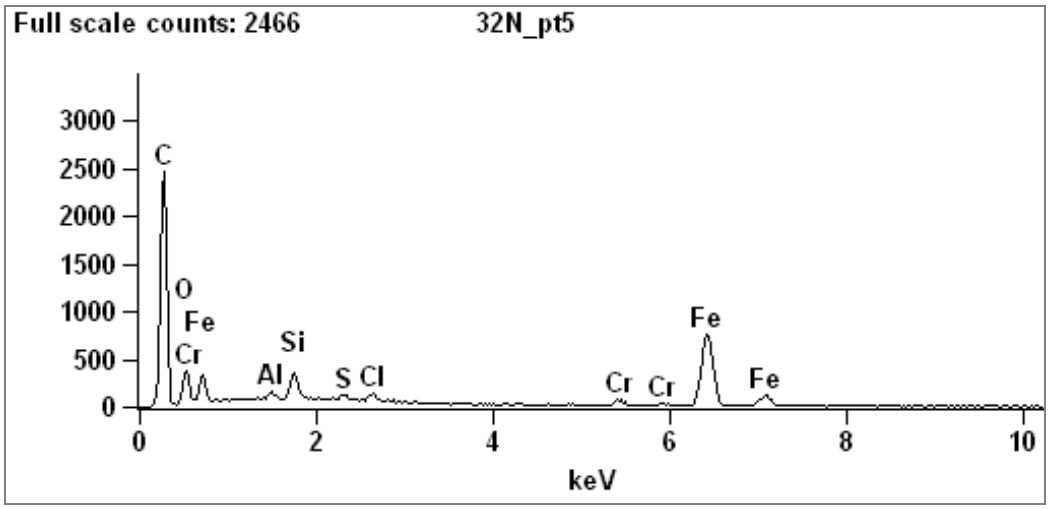
Full scale counts: 2466
32N_pt5
3000
2500
2000
1500
1000
500
0
C
O
Fe
Cr
Al
Si
S
Cl
Cr
Cr
Fe
Fe
0
2
4
6
8
10
keV

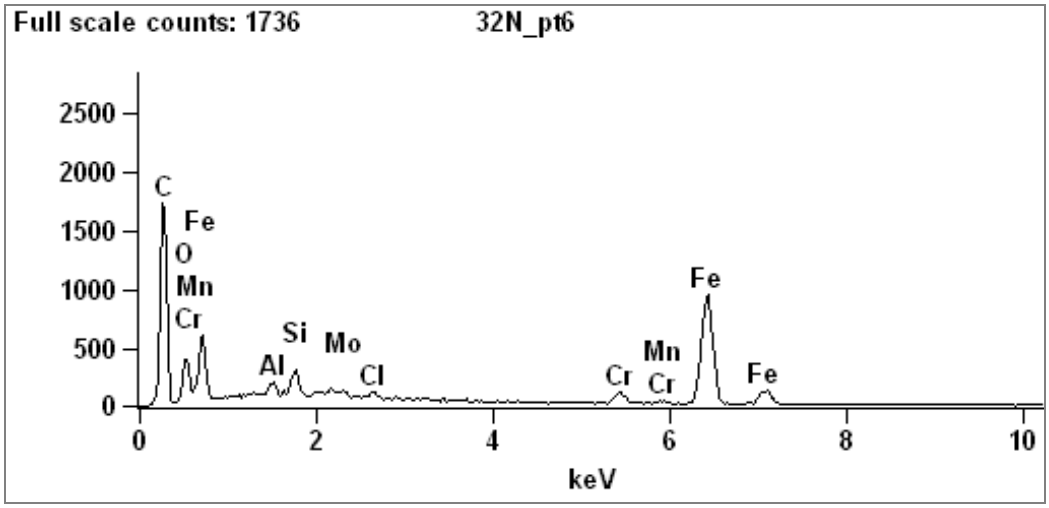


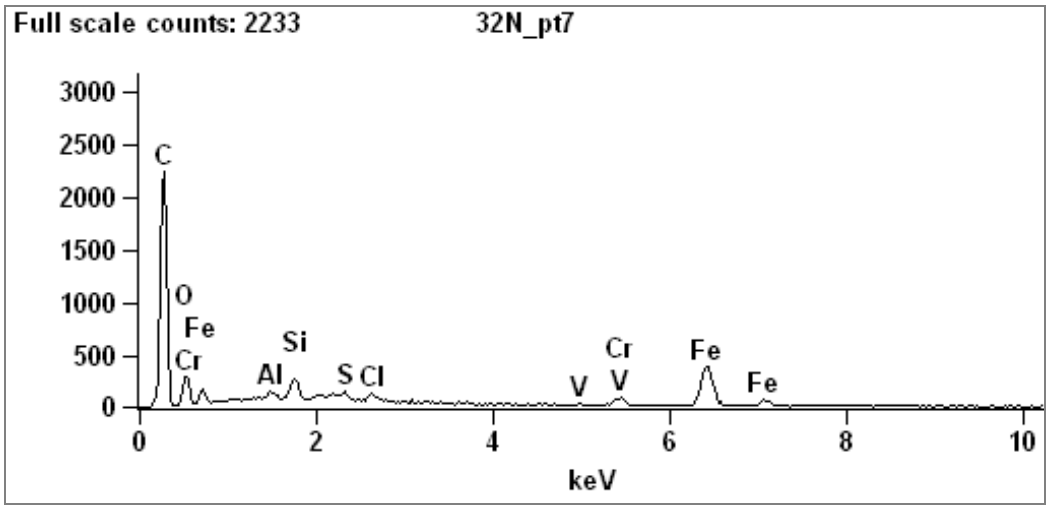


Atom %

| | C-K | O-K | Na-K | Al-K | Si-K | P-K | S-K | Cl-K | V-K | Cr-K | Mn-K | Fe-K | As-L | Mo-L |
|---|---|---|---|---|---|---|---|---|---|---|---|---|---|---|
| ***32N_pt1*** | 27.93 | | | 1.15 | 0.40 | | | | | 0.59 | 0.94 | 68.99 | | |
| ***32N_pt2*** | 88.83 | 10.65 | | 0.04 | | | | 0.35 | | | | 0.14 | | |
| ***32N_pt3*** | 79.06 | 10.54 | | 0.31 | 0.47 | | | 0.35 | | 0.48 | 0.18 | 8.46 | 0.01 | 0.13 |
| ***32N_pt4*** | 60.91 | 24.75 | 0.15 | 0.50 | 0.31 | 0.03 | 0.07 | 0.20 | | 0.68 | | 12.41 | | |
| ***32N_pt5*** | 78.89 | 12.94 | | 0.17 | 0.65 | | 0.14 | 0.22 | | 0.22 | | 6.77 | | |
| ***32N_pt6*** | 73.65 | 15.15 | | 0.27 | 0.54 | | | 0.23 | | 0.56 | 0.19 | 9.37 | | 0.05 |
| ***32N_pt7*** | 80.53 | 13.65 | | 0.14 | 0.59 | | 0.13 | 0.25 | 0.06 | 0.43 | | 4.20 | | |

## APPENDIX C Polarization Curves

The polarization curves measured from the experiments are shown by following figures.

### C.1 Polarization curves of the specimens which are applied with different applied anodic currents for 24 hours.

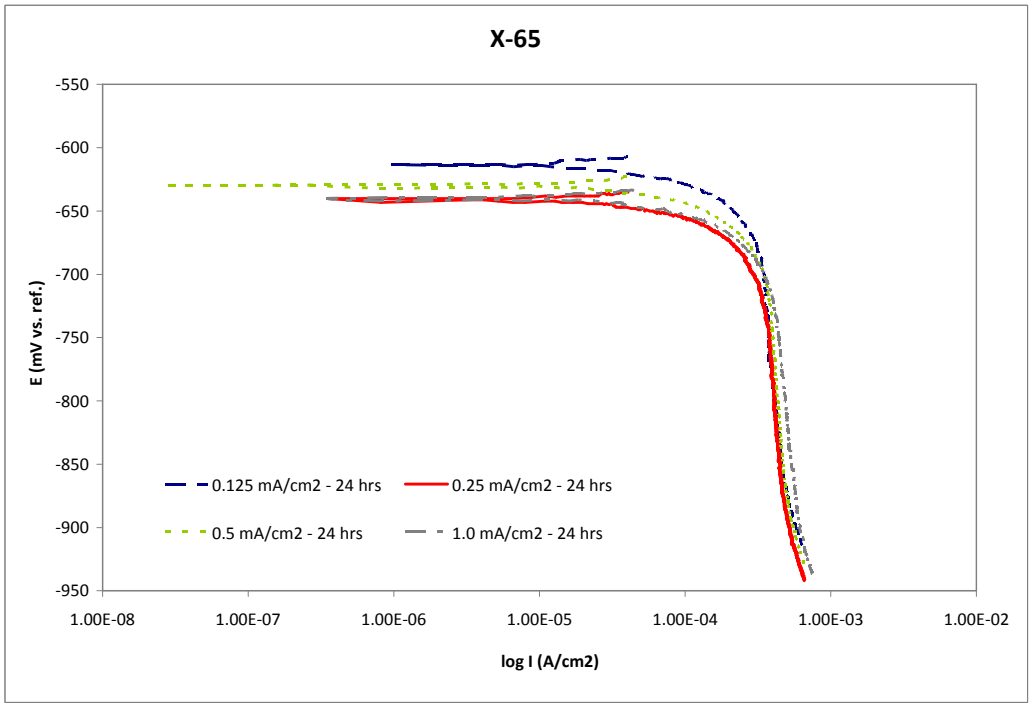


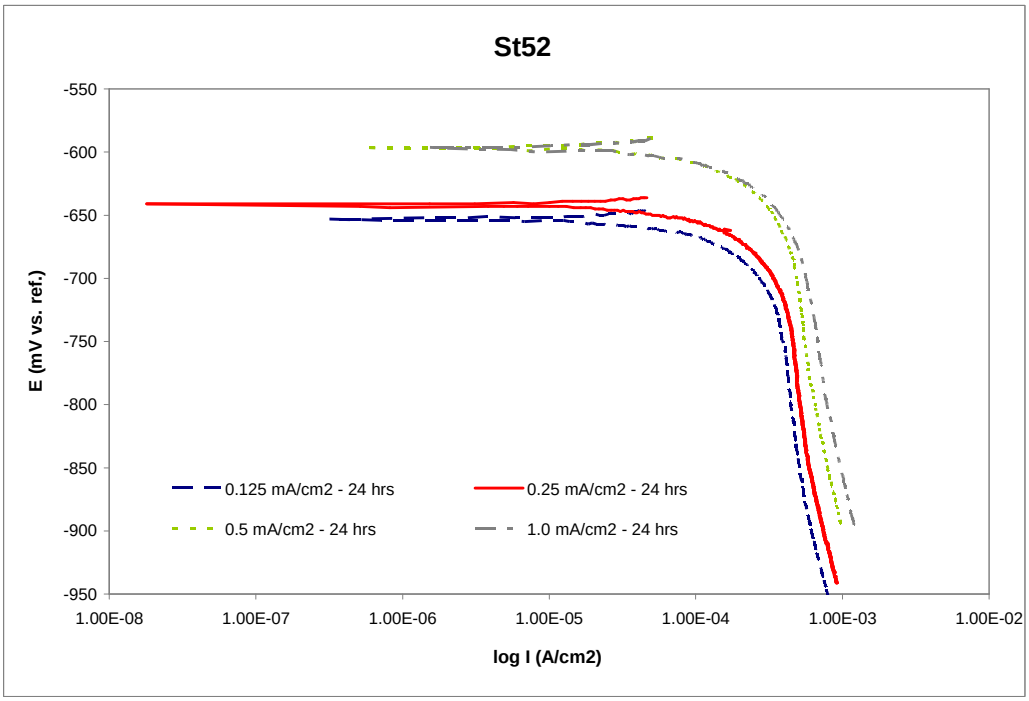

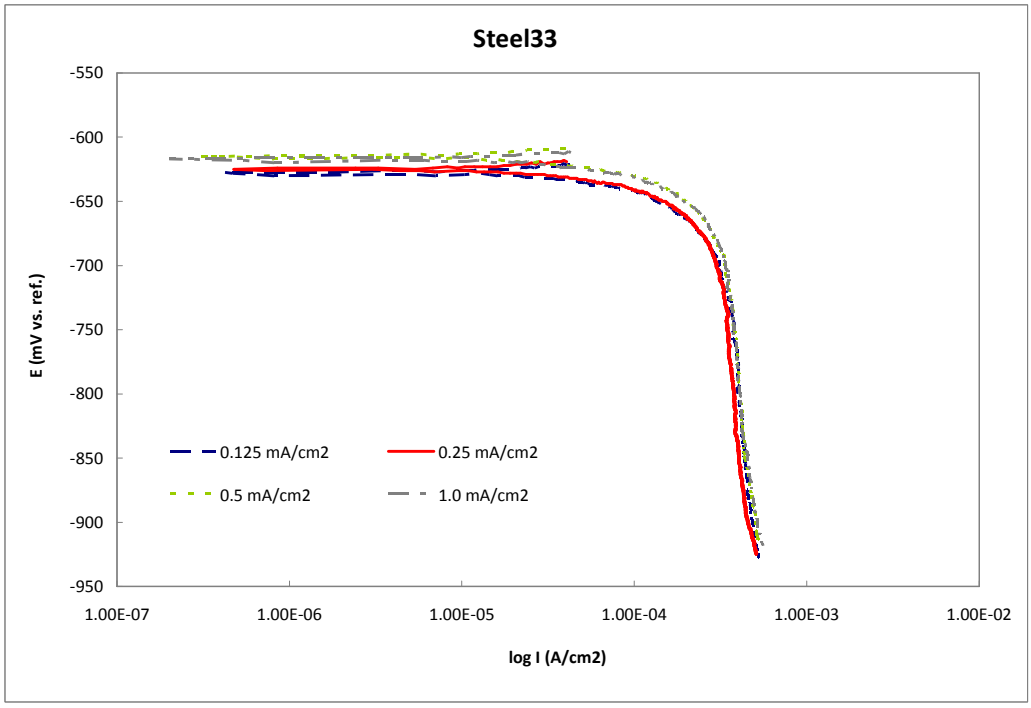


## C.2 Polarization curves of the specimens which are applied with 0.25 mA/cm$^2$ for different exposure time

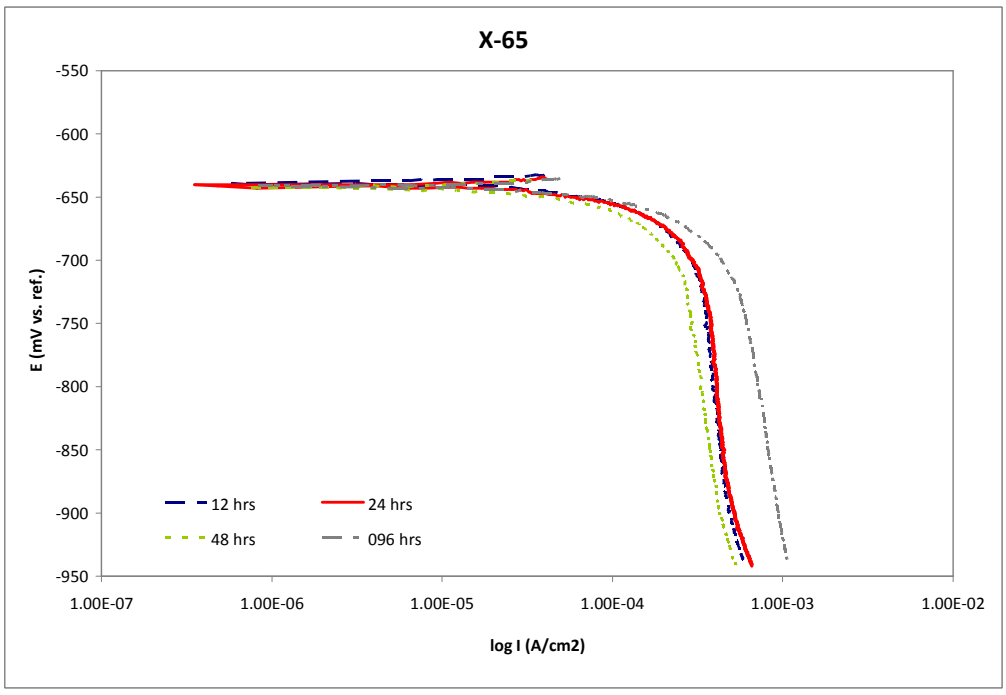

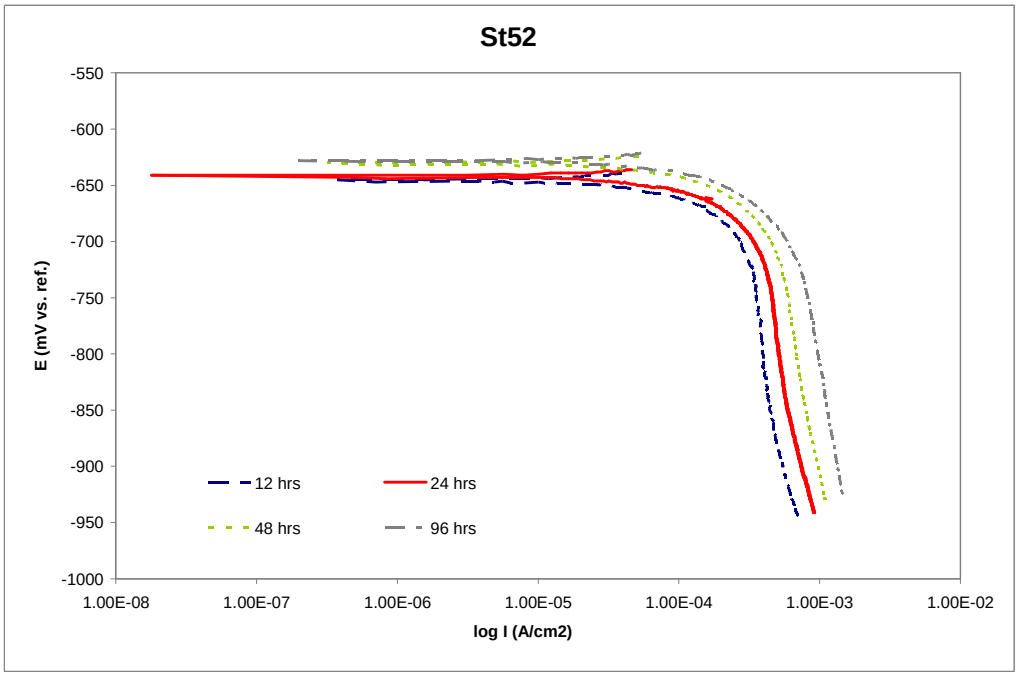
St52
-550
-600
-650
-700
-750
-800
-850
-900
-950
-1000
E (mV vs. ref.)
12 hrs
24 hrs
48 hrs
96 hrs
1.00E-08
1.00E-07
1.00E-06
1.00E-05
1.00E-04
1.00E-03
1.00E-02
log I (A/cm2)

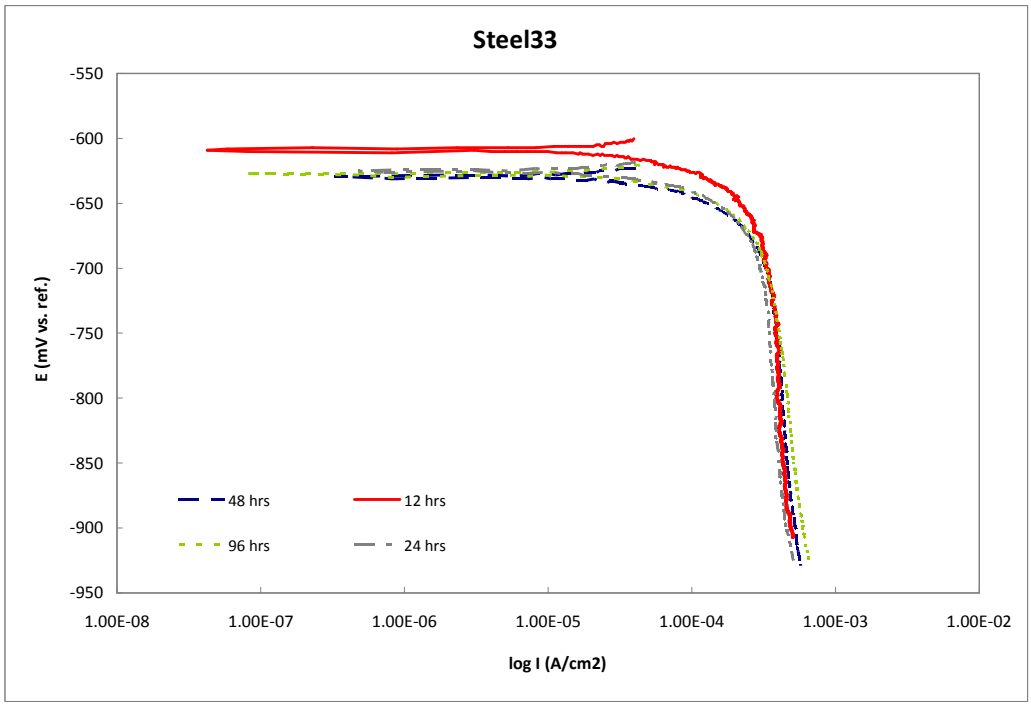
Steel33
-550
-600
-650
-700
-750
-800
-850
-900
-950
E (mV vs. ref.)
48 hrs
12 hrs
96 hrs
24 hrs
1.00E-08
1.00E-07
1.00E-06
1.00E-05
1.00E-04
1.00E-03
1.00E-02
log I (A/cm2)

## C.3 Polarization curves of the specimens which are applied with different applied anodic current for different exposure time

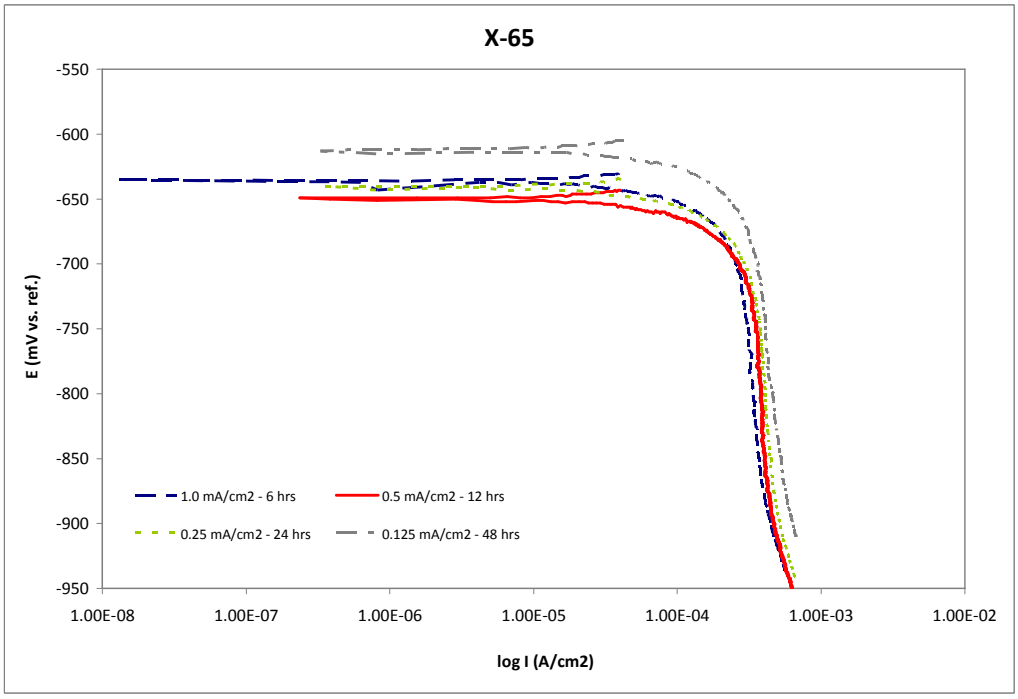


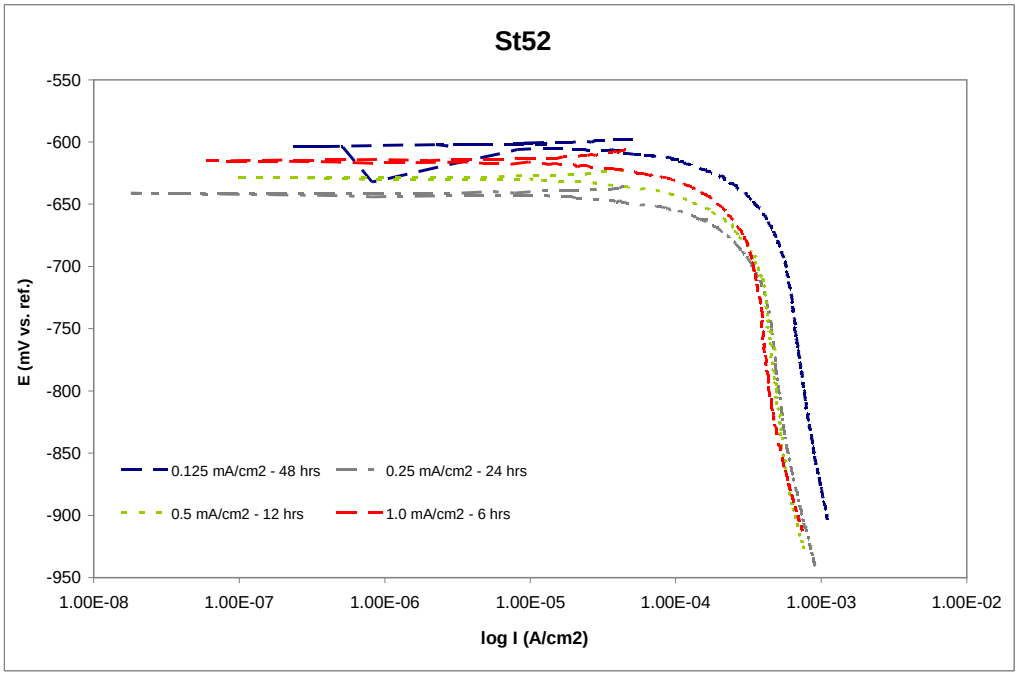

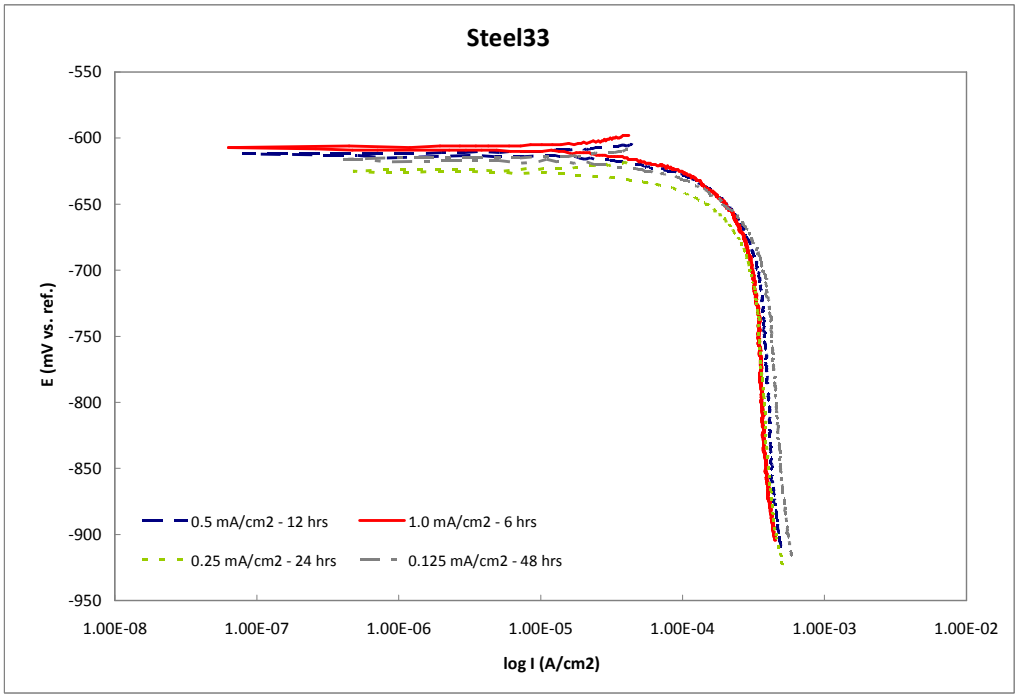
Steel33
-550
-600
-650
-700
-750
-800
-850
-900
-950
E (mV vs. ref.)
0.5 mA/cm2 - 12 hrs
1.0 mA/cm2 - 6 hrs
0.25 mA/cm2 - 24 hrs
0.125 mA/cm2 - 48 hrs
1.00E-08
1.00E-07
1.00E-06
1.00E-05
1.00E-04
1.00E-03
1.00E-02
log I (A/cm2)